Novel protein biomarkers for advanced pseudarthrosis treatment revealed by mass spectrometry

Inauguraldissertation

zur Erlangung des Grades eines Doktors der Medizin (Humanbiologie)

des Fachbereiches Medizin

der Justus-Liebig-Universität Gießen

vorgelegt von

Stefanie Kern

aus Frankfurt am Main

Gießen (2021)

Novel protein biomarkers for advanced pseudarthrosis treatment revealed by mass spectrometry

Inauguraldissertation

zur Erlangung des Grades eines Doktors der Medizin (Humanbiologie)

des Fachbereiches Medizin

der Justus-Liebig-Universität Gießen

vorgelegt von

Stefanie Kern

aus Frankfurt am Main

Gießen (2021)

Aus dem Fachbereich Medizin der Justus-Liebig-Universität Gießen
Labor für Experimentelle Unfallchirurgie der Klinik und Poliklinik für
Unfall-, Hand- und Wiederherstellungschirurgie

Gutachter: Prof. Dr. rer.nat. Thaqif El Khassawna
Gutachter: Prof. Dr. med. Till Keller
Tag der Disputation: 07.03.2022

Contents

1. Introduction

Bone regeneration after fracture is a crucial issue in clinic practice and research [1]. Despite advanced surgical methods, about 5-10 % of all fractures show delayed healing and pseudarthrosis development. Up to 50 % of open fractures of the tibia result in non-healing [2]. Pseudarthrosis development leads to prolonged pain and reduced functionality of the affected bone. Long and complicated treatment causes increased socioeconomic costs [3]. Treatment costs for an established pseudarthrosis of long bones was over $11,800 in Canada and $11,333 in the USA in 2014 [4, 5]. Therefore, an early diagnosis of pseudoarthrosis is essential from a medical point of view as well as from an ecological point of view and last but not least especially from the patient's point of view. Diagnosing a delay in fracture healing and the start of a possible pseudarthrosis development at an early stage would be a cornerstone for trauma treatment. Clinicians wait for at least 6 months before diagnosing pseudarthrosis. Recent pseudarthrosis treatment involves surgical procedures, including the application of bone graft substitutes and implantation of osteoconductive bone substitute materials [5]. Furthermore, surgeons often try to improve fracture healing by implantation of osteoinductive molecules [7]. Osteoinductive factors like bone morphogenetic proteins (BMP) induces differentiation of mesenchymal stem cells (MSC) into osteoblasts, the bone-building cells [7]. Other osteoinductive factors are transforming growth factor-beta 1 (TGF-β1) [8], alkaline phosphatase (ALP) [9], collagen III amino-terminal propeptide (PIIINP) [10], vascular endothelial growth factor (VEGF) [11] or macrophage colony stimulating factor (M-CSF) [11]. The aim of using bone substitute materials osteoinductive factors is improved fracture healing. While osteoconductive materials provide a scaffold needed for bone cells to attach and grow on, osteoinductive materials provide more promising osteogenic stimulation.

However, there are some serious drawbacks in pseudarthrosis treatment with osteogenic factors because of their diverse functions in regulatory systems [6]. The same growth factors that induce differentiation of MSCs to osteoblasts are also able to enhance unwanted proliferation of fibroblasts. Thereby, instead of the desired osteogenic stimulation of bone-forming osteoblasts, fibroblasts are increasingly formed, which often lead to pronounced pseudarthroses [12]. Fibroblasts are the abundant cell type in pseudarthrosis, which also have osteoblast-like functions [7, 13, 14]. The resulting fibrous tissue that forms prevents the growth of new bone tissue and provides insufficient

mechanical support, therefore leading to impaired bone fracture healing [7, 13, 14]. Therefore, the feasibility and plausibility of using common osteoconductive growth factors in pseudarthrosis treatment as a rule of thumb is questionable [12]. However, to date it has not been identified why the addition of osteogenic growth factors in some cases does not lead to accelerated and improved fracture healing. Thus, analysis of MSCs and fibroblast response to osteogenic stimulation can assist in understanding pseudarthrosis development. Analysis of possible differences in the proteomes of stimulated MSCs and fibroblasts is of great interest, as proteins can serve as important biomarkers. Mass spectrometry-based proteomics is an indispensable tool in the analysis of proteins [15]. Hence, it is used in this work to reveal novel biomarker for pseudarthrosis diagnosis and prediction.

Another critical point in the treatment of pseudarthrosis is the correct classification. Pseudarthroses are classified clinically into different types. First, pseudoarthroses are classified as aseptic or septic. Furthermore, a distinction is made between atrophic or hypertrophic pseudoarthroses. Depending on the type of pseudarthrosis, the type of treatment differs [16]. Treatment of hypertrophic pseudarthrosis usually aims at improving mechanical stability whereas atrophic pseudarthrosis treatment involves improvement of the biological environment [17]. Atrophic pseudarthrosis often show no to very little callus formation and damage to the vascularization at the fracture site [18]. To find out which systemic factors lead to atrophic pseudarthrosis or to hypertrophic pseudarthrosis, a retrospective clinical study was performed. In this study characteristics of patients with hypertrophic pseudarthrosis were compared to atrophic pseudarthrosis patients. A second retrospective study was conducted to examine the influence of infection on fracture healing. Overall, this part of the work shows the importance of retrospective clinical studies and further basic research in fracture healing to assess effectiveness of current surgical and pharmacological treatment approaches.

1.1. Bone Structure

The skeleton, the supportive structure of the body, consists of two different tissues, the bone or osseous tissue and the cartilage. Cartilage is a semi-rigid form of connective tissue which provides flexibility for movement. Bone is a hard, dense connective tissue which gives the structural support. Calcium phosphate in form of hydroxyapatite ($Ca_5(PO_4)_3(OH)$ hardens bone by mineralization [19]. Critical functions of the skeletal

system are movement, locomotion, protection of vital internal organs like heart and lung as well as providing of mineral and fat homeostasis. Furthermore, the skeletal system serves as a reservoir of growth factors and cytokines. It also produces blood cells within the bone marrow niches [20-22].

The adult human skeleton has 206 bones, without sesamoid bones, which can be divided into four categories based on their shapes: long, short, flat, and irregular bones. Bone function is directly linked to their shape. Long bones, e.g., femur or humerus, are crucial for skeletal mobility and move under muscle contraction. Short bones, including the carpals in the hand and the tarsals in the foot, provide stability and support with only little to no movement. Flat bones, like ribs, scapulae and cranial bones, function as protectors of internal organs and points of attachment for muscles. Vertebrae, as example for irregular bones, support the spinal cord [21, 22].

Morphologically, bone tissue can be differentiated into compact/cortical bone or cancellous bone. Cancellous bone is also called spongy or trabecular bone (**Figure 1 A**). Compact and cancellous bone have the same chemical composition and only differ in their microstructure. Compact bone is dense and solid to withstand compressive forces and surrounds the bone marrow space. Trabecular bone is composed of a honeycomb-like network of trabecular plates and rods. This allows trabecular bone to support differences and changes in weight distribution. Distribution of both types of bone tissue depends on the function of the bone [22, 23]. Overall, the mass of adult human skeleton consists of 80 % cortical and 20 % trabecular bone [21].

Cortical bone is build up by so-called osteons as basic units [23, 24] (**Figure 1 B**). Osteons comprise concentric rings of calcified matrix, the lamellae, which surround a central canal, the Haversian canal. This canal contains blood vessels, nerves, and lymphatic vessels. Haversian canals are connected to each other by transverse Volkmann's canals. Furthermore, central Haversian canals are linked to embedded osteocytes, which are located inside lacunae, via a canalicular network. Canaliculi allow the transport of nutrients to the embedded osteocytes [22, 24].

Cancellous or trabecular bone also contains osteocytes in lacunae which are found in the trabeculae. Those trabeculae form a lattice-like network of rods and spikes providing mechanical strength [22, 25] (**Figure 1 C+D**).

The periosteum and the endosteum are bone membranes. The endosteum covers the inner bone surface. Osteoblasts and osteoclasts are present in the endosteum. The periosteum

covers the outer surface of all bones. It consists of two layers, an outer fibrous layer and an inner cambial layer. The fibrous layer consists mainly of fibroblasts and collagen. The cambial layer contains osteoprogenitor cells, MSCs, osteoblasts, fibroblasts, microvasculature, and nerves. The periosteum is therefore a central mediator of bone healing [26-29].

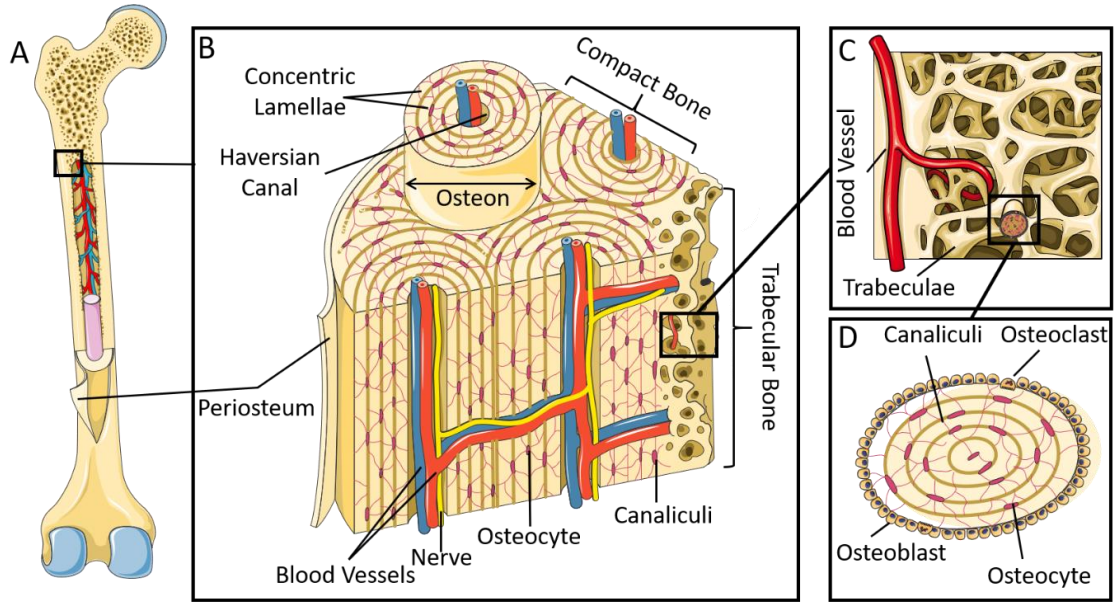

Figure 1: Illustration of typical long bone structure. A) Long bone, in this case the femur, consists of a tubular shaft, the so-called diaphysis, which runs between the proximal and distal ends of the bone. The hollow region in the diaphysis, the medullary cavity, contains yellow bone marrow as well as blood vessels. The walls of the diaphysis are composed of dense compact bone forms the shell of the diaphysis with the periosteum as outer layer of bone. B) A detailed image of the microstructure of compact bone. The basic structural unit of compact bone is the osteon which contains Haversian canal in its center. Haversian canals contain nerves and blood vessels and are connected via transverse Volkmann canals. C) Trabecular bone is composed of trabeculae which are covered by the endosteum. Red bone marrow which contains hematopoietic cells and fat fills the spaces between the trabeculae. D) Cross-section of trabecular bone shows osteocytic network. Canaliculi connect the adjacent cavities for blood and nutrient supply. Furthermore, osteoblasts and osteoclasts are located in the endosteum. (This figure was created using Servier Medical Art templates, which are licensed under a Creative Commons Attribution 3.0 Unported License; https://smart.servier.com [30].)

Another important element in bone structure is the collagen network. In compact and trabecular bone, collagen fibers are orientated parallel, resulting in so-called lamellar bone. In the growing skeleton and during the healing phases after fractures, woven bone

is formed initially. In this microscopic bone structure, collagen fibers are arranged anisotropically which results in mechanically weaker bone compared with lamellar bone. During healing as well as growing process, woven bone gets replaced by lamellar bone [19, 22, 23].

Lamellar bone consists of 35 % organic and 65 % inorganic matrix. Around 95 % of the organic matrix is type I collagen. Collagen fibers provide a surface for inorganic salt crystals like hydroxyapatite to adhere. Hydroxyapatite is the key for bone hardness and strength. Therefore, collagen fibers provide the flexibility and elasticity of bones [22]. The remaining 5 % of bone matrix consists of proteoglycans, non-collagenous proteins and several bone cell types. Non-collagenous proteins are osteopontin (OPN), osteonectin (ONC), osteocalcin (OCN), bone sialoprotein (BSP) and alkaline phosphatases (ALP) [31]. Bone cells are crucial for bone function and bone remodeling, despite their small amount of the total bone volume. Different types of cells are found within bone tissue. Among them are osteoblasts, osteoclasts, osteocytes, chondrocytes, osteogenic cells, and bone-lining cells [21, 22, 32].

1.2. Bone Remodeling

Bone remodeling is crucial for maintenance and adaptation of a healthy skeleton. It involves multicellular processes including cell-cell interactions, biochemical signalling and mechanical stimuli [33]. Every year, about 10 % of the adult human skeleton is remodelled, i.e. repaired and renewed [25, 33]. Remodeling of bone tissue depends on the dynamic balance between two major processes: bone formation and bone resorption. For bone homeostasis, regulation of those processes is essential. Most bone diseases occur as the result of an imbalance in bone remodeling [25]. Remodeling requires different cell types, among them are osteoblast, osteoclasts, and osteocytes. In addition, several factors originating from immune cells, including B- and T-cells, are also involved in bone remodeling [34, 35] (**Figure 2**).

Beginning of bone remodeling is hallmarked by attraction of osteoclast progenitors to the remodeling site. Osteoclasts are derived from hematopoietic stem cells. Osteocytes share precursors with monocytes, macrophages and B-cells [25]. Several factors regulate osteoclast differentiation. The most important ones are macrophage colony-stimulating factor (M-CSF), receptor activator of nuclear factor kappa B (RANK) and its ligand (RANKL), and osteoprotegerin (OPG) [25, 36]. Activation of RANK by its ligand

RANKL promotes osteoclastogenesis. Mesenchymal stromal cells produce RANKL. Osteoblasts, osteocytes, and T-cells produce RANKL as well [37]. Interaction of RANK and RANKL is in turn inhibited by OPG, which is a decoy receptor for RANKL [25].

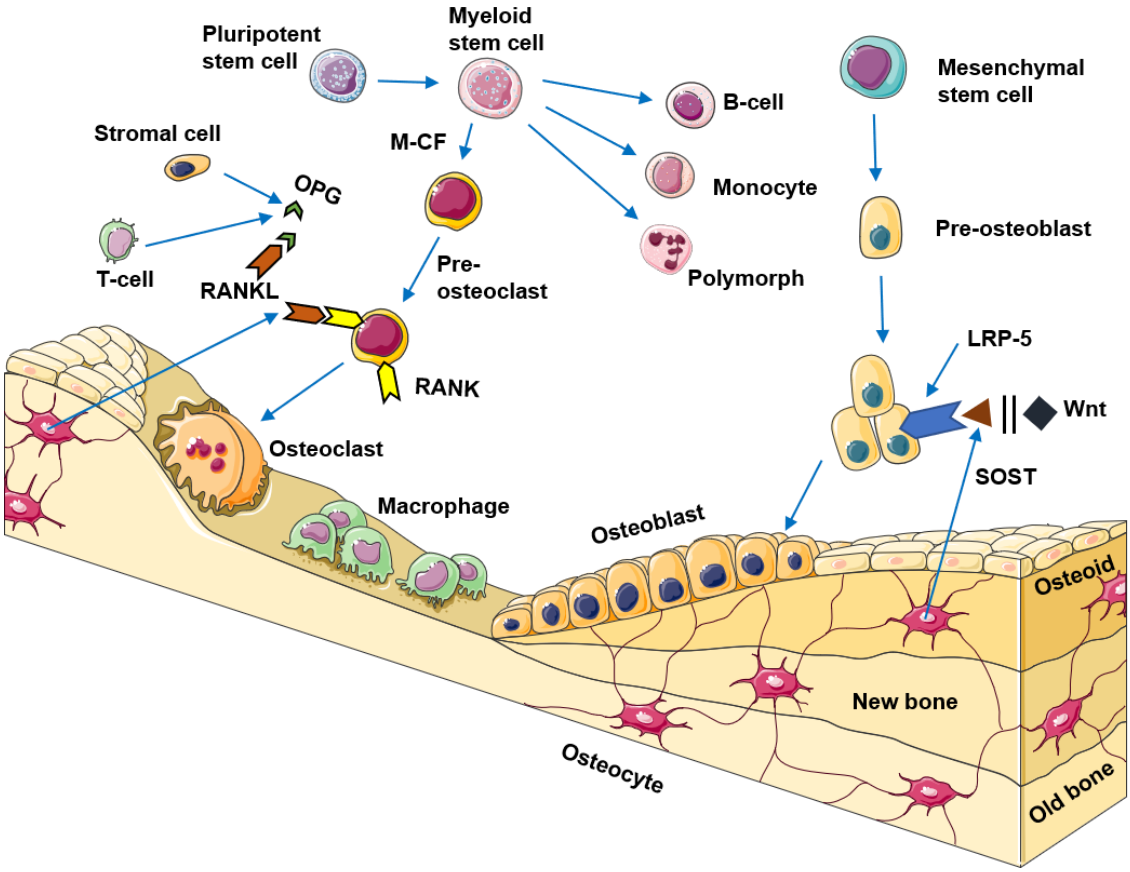

Figure 2: Lineage of osteoblasts and osteoclasts, the major cells responsible for bone remodeling. Bone remodeling takes place to renew bone tissue and to repair small injuries and micro-damages. During the remodeling process, bone tissue is resorbed by osteoclasts while osteoblasts form new bone tissue. In both processes, multicellular signaling pathways regulate bone formation and resorption. Activation of osteoclasts is controlled through the RANK/RANKL/OPG pathway. Wnt-LRP5–SOST pathway is one of the major differentiation pathways of osteoblasts. Imbalance in cellular events of bone remodeling lead to systemic bone diseases like osteoporosis. (RANK= receptor activator of nuclear factor kappa B, RANKL= RANK ligand, OPG= osteoprotegerin, LRP5= low-density lipoprotein receptor-related protein, SOST= sclerostin, Wnt= Wingless-type) (This figure was created using Servier Medical Art templates, which are licensed under a Creative Commons Attribution 3.0 Unported License; https://smart.servier.com. [13],[19])

Mature osteoclasts attach to the bone surface by forming a sealing zone and a ruffled border. Afterwards, osteoclasts resorb bone matrix by secreting hydrochloric acid, which dissolves hydroxyapatite, and proteolytic enzymes. This enables proteolytic enzymes to access bone matrix for degradation of bone matrix proteins. Cathepsin K, one of the most

important proteolytic enzymes expressed by osteoclasts, degrades bone collagen. After completion of bone resorption, osteoclasts move away from bone surface and undergo apoptosis [25, 38]. Dysregulation in osteoclast differentiation and activity lead to several bone diseases like osteopetrosis [25, 34], and osteoporosis [38, 39].

Bone formation process begins with migration of osteoblast progenitor cells to the site that has undergone bone resorption. Cells of osteoblast lineage are stromal cells, bone lining cells, osteoprogenitors, pre-osteoblasts, osteoblasts, and osteocytes. They all derive from mesenchymal stromal cells (MSCs) which have also the ability to differentiate into chondrocytes, myoblasts, and adipocytes [25, 40-43]. Primary function of osteoblasts is the synthesis of osteoid, a matrix mainly composed of type 1 collagen, and the subsequent mineralization of osteoid. Differentiation of MSCs to osteoprogenitor cells, pre-osteoblasts and finally mature osteoblast takes place in response to complex signalling pathways of interaction between transcriptional regulators, growth factors, hormones and signalling-molecules [23]. Among those factors are bone morphogenic proteins (BMP), platelet-derived growth factor (PDGF), and transforming growth factor beta (TGF-β). TGF-β promotes osteoblastogenesis through extracellular signal-regulated kinases (ERK) and Wnt signaling. ERK is part of mitogen activated protein kinases (MAPK) signaling that promotes osteoblast proliferation [44, 45]. Osterix (Osx) is another essential factor for osteoblast differentiation and proliferation. Osx binds to the promotor of several osteoblast specific genes such as OCN, type 1 collagen and ALP [19, 25]. Downstream of Osx, lipoprotein-receptor-related protein 5 (LRP5) stimulates bone formation when activated by Wnt proteins. An antagonist of Wnt and inhibitor of bone formation is sclerostin (SOST). SOST is secreted by osteocytes [25, 46]. Dysfunction of those signalling pathways leads to several diseases, such as osteoarthritis, neurodegenerative diseases, osteoporosis [13, 25, 35, 39, 46-48].

Osteoblasts trapped within bone matrix differentiate into osteocytes. Osteocytes are the most abundant and long-living cells in bone tissue, presenting 90-95% of total bone cells. They interact with one another and with cells on the bone surface by cell processes that run through canaliculi inside the bone matrix [49]. In response to mechanical loading, osteocytes produce signalling molecules such as prostaglandins. Thus, they are acting as mechanical sensors in bone tissue [50-52]. In addition, osteocytes express proteins such as matrix extracellular phosphoglycoprotein (MEPE) and SOST. Therefore, they are important for bone remodeling and bone homeostasis [53].

1.3. Fracture Healing

Fracture healing is a complex biological process. It involves a series of overlapping healing phases and processes that recaps many events which take place during embryonical development of the skeleton [54]. Cellular recruitment, changes in gene expression of several thousand genes, and compound synthesis are part of fracture healing [55] (**Figure 3**). Bone healing is unique, since bone is the only tissue which heals without scar tissue formation. Native tissue is regenerated, and mechanical integrity is restored in normal bone fracture healing [54, 56]. However, 10-15 % of all fractures result in delayed union, non-union or pseudarthrosis. Successful fracture healing is associated with many factors such as fracture location, infection, and patient's characteristics [57]. For therapeutic development it is crucial to understand the cellular and molecular events undergoing in fracture healing in detail.

Fracture healing can take place directly, which is called primary fracture healing, or indirectly, which is called secondary fracture healing. The most common form is indirect fracture healing, where anatomical reduction or rigidly stable conditions are not required. Direct fracture healing involves only intramembranous ossification. Indirect fracture healing consists of both, endochondral and intramembranous ossification [55]. In endochondral ossification, cartilage is formed as a precursor or template and bone develops by replacing this cartilage tissue, forming mineralized bone tissue. In intramembranous ossification intermediate cartilage is not involved and MSCs are directly differentiated into osteoblasts [55, 58]. Direct fracture healing only involves intramembranous ossification.

Overall, bone repair can be divided into different phases: reactive phase (involves inflammation and hematoma formation), reparative phase (formation of soft cartilaginous and hard bony callus), and bone remodeling phase [59].

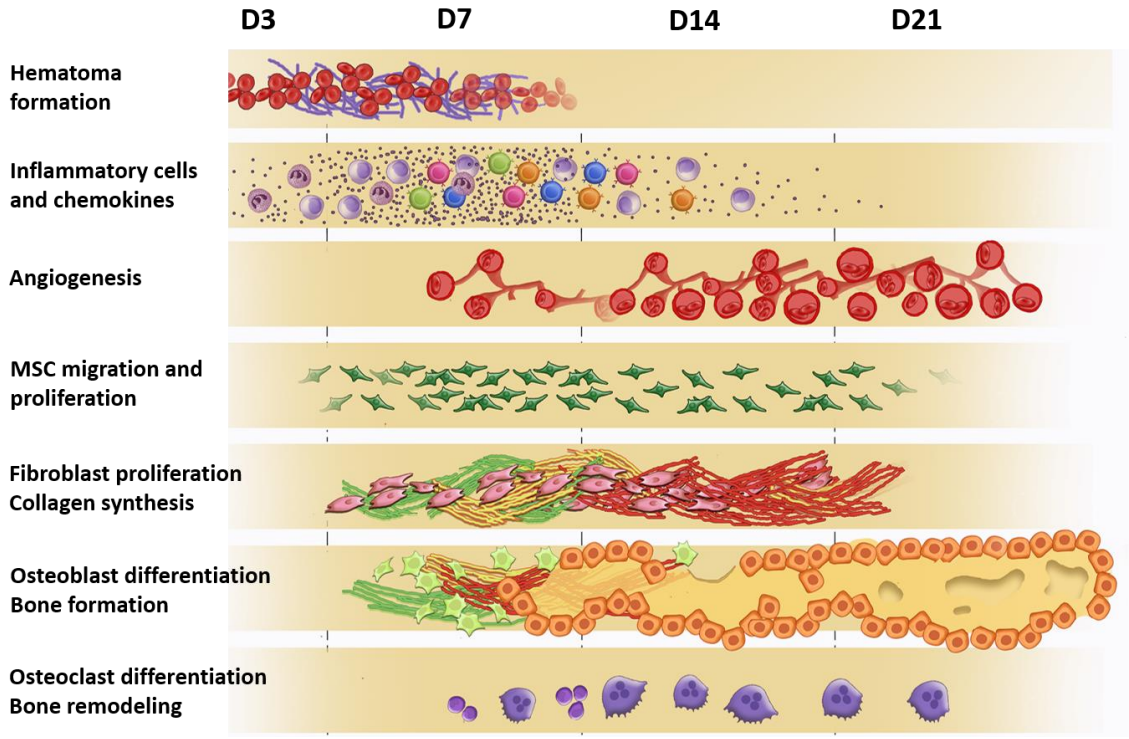

Figure 3: Inflammatory response and healing processes in a wild type mouse model. Bone healing is characterized by different phases which are overlapping. Hematoma formation, which starts at D3 (D=Day), initiates response of inflammatory cells. This leads to fibrocartilaginous callus formation characterized by fibroblast proliferation, MSC differentiation to chondrocytes, and collagen synthesis from D7 onwards. Migration and proliferation of MSCs, angiogenesis, and osteoblast differentiation hallmark the beginning of ossification at D14. In a final phase, bone formation is followed by subsequent remodeling. (Modified after Roberts, J.L., et al, 2018 [59])

1.3.1. Reactive Phase

Immediately after fracture injury, a hematoma is formed as result of disrupted blood vessels and surrounding tissue. Hematoma formation then initiates the early inflammatory reaction to induce the subsequent repair of the destroyed tissue [59, 60]. The inflammatory phase can further be divided into the pro- and anti-inflammatory phase [61]. The cellular composition of that phase consists of lymphocytes, macrophages and monocytes which migrate into fracture hematoma [62, 63] (**Figure 3**). Reactive oxygen species (ROS) promote the activation and recruitment of those inflammatory cells. The role of ROS is not only to clear cellular debris and combat infection. They also trigger recruitment of fibroblasts to the callus and vascularization [64]. Therefore, inflammatory cells produce pro- and anti-inflammatory cytokines, growth factors and mediators like interleukin 1 (IL-1), IL-6, tumour necrosis factor (TNF) and prostaglandins (PG) [64, 65].

Dysregulation of the inflammatory phase can impair healing or even cause non-unions. Both can be observed in patients with diabetes mellitus or alcohol abuse [59].

1.3.2. Reparative phase

As response to the inflammatory event, MSCs and fibroblasts are recruited to the fracture site (**Figure 3**). MSCs undergo differentiation into cartilage-producing chondrocytes. Fibroblasts and chondrocytes produce a semi-rigid soft callus. This callus serves as a template for the bony callus and is also able to provide mechanical stability to the fracture [55, 59, 63]. Fibrous tissue is produced by fibroblasts, mainly in areas where cartilage production by chondrocytes is deficient. Fibroblasts secrete collagen fibres to connect bone ends. Thus, a fibrocartilaginous callus is formed [63]. Fibroblasts and chondrocytes proliferation are stimulated by several growth factors such as fibroblast growth factor 1 (FGF-1) and Runx1. Chondrogenesis is also stimulated by BMPs [59, 63]. After chondrocytes proliferation, they become hypertrophic followed by apoptosis. This triggers vascularization and ossification of cartilaginous extracellular matrix. The fibrocartilaginous callus gets replaced by woven bone [55, 59]. In addition to this endochondral ossification, intramembranous ossification occurs in local areas that have sufficient blood supply and mechanical stability, typically in the inner layer of periosteum. Osteoprogenitor cells and MSCs differentiate into osteoblasts that directly layout woven bone [62].

1.3.3. Remodeling phase

The final phase of bone fracture healing process is the removal of the immature woven bone and the underlying cartilage matrix by osteoclasts by remodeling into lamellar bone. Remodeling restores osteon structures as well as Haversian system. It also restores the biomechanical properties of the fractured bone [59, 62]. In humans, the remodeling of a bone defect can take several months to years to completely restore the bone structure [62]. The most important cell types in this phase of bone healing are osteoclasts and osteoblasts (**Figure 3**). Woven bone resorption by osteoclasts creates so-called cutting cones on the bone surface. In this eroded area, osteoblasts can subsequently build new bone [63]. Crucial for successful bone remodeling is not only a balance between osteoclasts and osteoblasts. Adequate vascularization and mechanical stability are also important. Otherwise, atrophic fibrous pseudarthrosis or hypertrophic pseudarthrosis can occur [55].

1.4. Signalling pathways in fracture healing

Understanding the underlying cellular and subcellular processes in fracture healing is essential for treatment approaches. Important signalling pathways and factors involved in bone healing are: Wnt-pathways, transforming growth factor-β/ bone morphogenetic proteins (BMP/TGF-β), mitogen-activated protein kinase (MAPK) pathway, insulin-like growth factor (IGF), fibroblast growth factor (FGF), and the calcium (Ca^{2+}) pathway [66].

Wnt pathways play an important role in cell processes including cell proliferation, growth, differentiation, migration, and apoptosis [67, 68]. In fracture healing, Wnt signalling is important for osteoblast differentiation and mineralization. There are two prominent signalling cascades activated by Wnt: the Wnt/β-catenin-pathway (canonical) and the Wnt/Ca^{2+}-pathway (noncanonical) [67].

The BMP/TGF-β signaling pathway plays an important regulatory role in bone fracture healing. BMPs and TGF-βs are both growth factors. Their interaction initiate non-canonical and canonical signaling cascades [68]. The non-canonical BMP/TGF-β signaling pathway is involved in osteoblast differentiation, osteoprogenitor proliferation, and bone formation. It includes signaling molecules which are belonging to the mitogen-activated protein kinase family, MAPKs [67].

MAPKs are cytoplasmic serine/threonine kinases. MAPKs transduce signals by activating extracellular signal-regulated kinases (ERKs) through the Ras/MAPK pathway [69]. Ras/MAPK pathway is a link between cell surface and nucleus to regulate cell proliferation, cell death, and cell migration [66]. Besides, MAPK pathway is a key pathway in Neurofibromatosis type 1 (NF1) patients. Patients with NF1 present recalcitrant bone healing and pseudarthrosis development [14]. Neurofibromin is absent in NF1 patients, which activates the MAPK pathway constitutively, leading to osteogenesis inhibition [70].

The FGF signal pathway contributes to the regulation of osteogenesis and angiogenesis. Those complex processes, which also includes cell-cell communication between blood vessel cells and bone cells, play a key role in fracture healing [68]. FGFs bind to FGF receptors (FGFRs), which are afterwards phosphorylated and activated. They further activate intracellular substrates such as Ras, initiating the Ras/MAPK pathway [71].

IGF signaling pathway is also an important signaling pathway in osteoblast differentiation and bone formation [68].

In osteoblast differentiation, Ca^{2+} plays a crucial role. Ca^{2+} as part of the bone mineral is continuously released into the extracellular matrix in form of free ions during bone remodeling process. However, the mechanism of Ca^{2+} signaling is not yet completely understood [66].

1.5. Delayed fracture healing and pseudarthrosis development

Fracture healing depends on various endogenous and exogenous factors. In summary, fracture healing encompasses osteoconduction (scaffold formation), osteoinduction (timed recruitment of different cell types and regulatory factors), and osteogenesis (new bone formation) [72]. If this well-orchestrated physiological process is out of balance, healing is impaired or even failed. Results are non-unions and pseudarthrosis. The American Food and Drug Administration (FDA) determined a minimum of 9 months to define a pseudarthrosis [17]. In clinical routine, pseudarthrosis are usually defined 6 months after fracture, when no progressive signs of bone healing occur and normal bone union without surgical intervention is not to be expected [73]. Despite important developments of treatment of impaired fracture healing, it is still a significant issue in clinical practice. In the United States alone, 5-10 % of all fractures develop into non-unions, pseudarthrosis or delayed healing. Thus, advanced treatment approaches and diagnostic tools are needed [5, 72].

Pseudarthrosis can be divided into different groups according to their radiological and histological characteristics. They can be either aseptic or septic. In addition, they are classified as hypertrophic or atrophic. Septic non-unions are characterized by local infections at the fracture site and in surrounding tissues. In atrophic pseudarthrosis, fracture stabilization is satisfactory, but biological activity is impaired. For example, dysvascular bone ends occur, only little callus tissue is formed, and the fracture gap is filled with fibrous tissue. In hypertrophic pseudarthrosis, bone ends are viable, but fracture stabilization is inadequate. This leads to extensive callus formation [5, 72, 74]. However, evidence exists that the difference between hypertrophic and atrophic pseudarthrosis is not as distinguished as assumed [17]. Previous studies showed similar macroscopically appearance in atrophic and hypertrophic pseudarthrosis. Those appearance include fibrous and fibrocartilaginous tissue [17].

Risk factors for pseudarthrosis development can be either patient dependent or independent (**Figure 4**). Patient independent factors are for example location of fracture,

severity of soft tissue, mechanical stability, degree of bone loss, infection, and surgical treatment [4, 75-78]. Among patient dependent risk factors are age, obesity, gender, smoking, alcohol abuse, and non-steroidal anti-inflammatory drug (NSAID) use. Deficiencies of calcium, vitamin D, or vitamin C are also associated with non-union risk [79-84]. In addition, various genetic and metabolic disorders are risk factors for pseudarthrosis development. Comorbidities with increased inflammation, including diabetes and ageing, can also lead to impaired bone healing [65, 85-89].

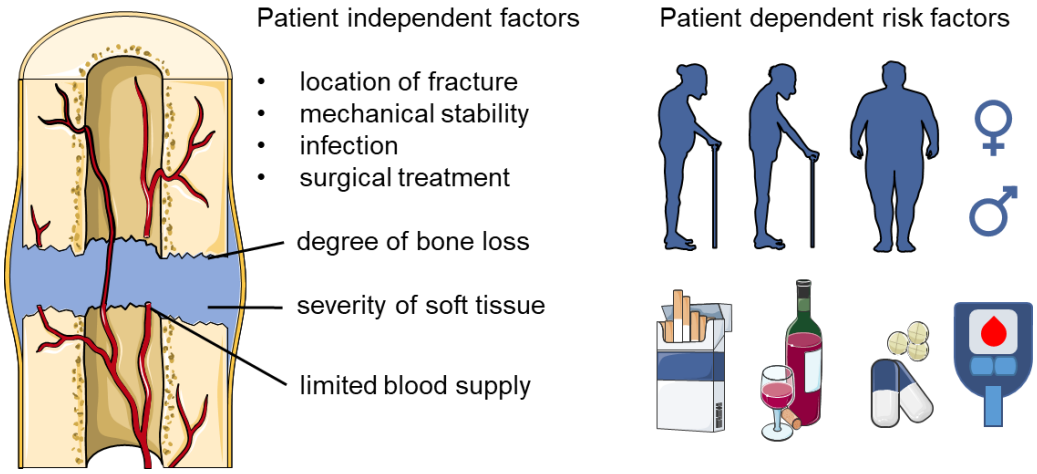

Figure 4: Risk factors for pseudarthrosis development. Among the patient independent risk factors are fracture localization (left panel), mechanical stability and infection. Obesity, age, gender and use of medical drugs, alcohol or nicotine are patient dependent risk factors (right panel)**.** (This figure was created using Servier Medical Art templates, which are licensed under a Creative Commons Attribution 3.0 Unported License; https://smart.servier.com. [13],[19])

1.6. Treatment strategies for pseudarthrosis

Pseudarthrosis treatment basically aims at providing adequate mechanical support and biological environment to the pseudarthrosis site. Therefore, several biological and biophysical approaches for pseudarthrosis treatment are applied by surgeons. In 2007, Giannoudis introduced the “diamond concept” of fracture healing. This concept describes four main elements which are required for successful fracture repair: osteogenic cells, osteoconductive scaffolds, mechanical environment, and growth factors. Successful bone regeneration depends on preservation of the soft tissue and on vascularization of the fracture site combined with stability fixation [90, 91].

The clinical "gold standard" for bone regeneration is the implantation of autologous bone transplant. The aim of this use of bone replacement material is osteoconduction through direct bone binding as well as osteoinduction by promoting the differentiation of stromal

cells into bone cells. Fresh cortical and/or trabecular bone are transplanted from one site of the patient's body (e.g. iliac crest) to the fracture site of the same patient [92]. Nevertheless, there are some drawbacks of this method, e.g., limited availability of bone material and postoperative complications such as pain, haematoma, or infection at the surgery site [92, 93]. Therefore and due to the complex procedure of autologous bone transplantation, it is necessary to develop and improve alternative methods for successful bone regeneration [5].

Application of biofactors (i.e. BMPs) for bone regeneration is another therapeutically approach in fracture healing. Bone morphogenic proteins are such factors. BMPs belong to the transforming growth factor β (TGF-β) superfamily. They stimulate MSCs to differentiate into bone-forming cells. The two most used BMPs for bone injury treatments are BMP-2 (used in tibia shaft fractures) and BMP-7 (treatment of long bone non-unions) [5, 94]. Some clinical trials and studies have proved that BMP-7 treatment of tibial non-unions is efficient [7, 94-97]. However, other studies reported side effects like local infection and wound complication after BMP application [5]. Cho et al. showed 2008 in their study of congenital pseudarthrosis that fibrous tissue and fibroblasts isolated at the site of non-union did not undergo osteoblastic differentiation in response to BMP application [98]. Therefore, it is important to analyze molecular characteristics of fibroblasts and MSCs and their response to BMPs and growth factors.

1.7. Mass spectrometry (MS)-based biomarker discovery

Prognosis and diagnosis of pseudarthrosis on an early time point remains a major challenge in fracture treatment until today. Advances in new diagnostic methods will allow early and more accurate diagnosis of pseudarthrosis. Identification of patients with a high risk for pseudarthrosis development would lead to advanced treatment strategies and to a successful fracture healing [99]. Biomarkers can improve the early pseudarthrosis diagnosis and fracture healing prognosis. To identify new biomarkers, genes or proteins are screened which can serve as predictors of potentially unsuccessful fracture healing. In 2013, Pountos et al. postulated that an ideal biomarker for fracture healing should have the following qualities: early prediction of fracture healing response, prediction of non-union, high sensitivity, and easy obtainability [99].

Therefore, understanding discrepancies between proteomes of osteogenic stimulated MSCs and fibroblasts are analyzed for possible differences in protein expression. The

large-scale study of proteomes is called proteomics. Thus, the principle of proteomics is the identification and quantification of proteomes that are expressed by a specific cell, under defined conditions [100]. It is an important technology for the discovery and identification of clinically significant biomarkers [101].

1.7.1. Liquid Chromatography-nano-Electrospray Ionization-Mass Spectrometry (LC-nano-ESI-MS)

An essential analytical method in proteomics is mass spectrometry. This analytical technique is used for identification and quantification of proteins in biological samples and has three fundamental steps: ion production, analysis, and detection [102]. In general, the mass-to-charge ratio (*m/z*) of ionized molecules is measured in mass spectrometry [100]. The key units of a mass spectrometer are the ion source, the mass analyzer, and ion detector. The ion source is responsible for charging of the molecules, while the mass analyzers acquire the *m/z* information on the x-axis. In turn, peak intensities on the y-axis depend on the ion detector [103]. After the measurement of the mass-to-charge ratio of a peptide, bioinformatic tools are used to decode the complete amino acid sequence of the proteins [100].

Especially the LC-nano-ESI-MS (Liquid Chromatography – nano – Electrospray Ionization – Mass Spectrometry) based quantitative proteomic analysis is used for biomarker discovery in recent literature [99, 101]. Label-free bottom-up LC-nano-ESI-MS based proteomics provide qualitative and quantitative analysis of complex protein mixtures gathered from cell or tissue lysates. After proteolytic digestion of the lysates, for example with trypsin, the resulting peptide products are separated by liquid chromatography and then ionized/charged for subsequent mass spectrometry analysis [104]. In LC-nano-ESI-MS, the method for peptide charging is Electrospray Ionization (ESI), which is a soft ionization method. In the process of Electrospray Ionization, a high voltage is applied to a liquid containing the analytes of interest to create an aerosol. In a mass analyzer, the most central processing unit of a MS, the ions are separated according to their mass-to-charge ratio [100]. Sensitivity (ability to detect low-abundance peptides), resolution (ability to distinguish between ions of very similar *m/z* values), and mass accuracy (difference between measured *m/z* and exact *m/z* of an ion) of a mass spectrometer depends on the used mass analyzer [103]. Examples for mass analyzers are the quadrupole (Q), ion-trap, time-of-flight (ToF), Fourier transformation

ion cyclotron resonance (FTICR), and the orbitrap. In this study, a so-called "Q-Exactive" is used (**Figure 5**). This mass analyzer refers to couple a quadrupole mass filter (mass resolution around 2,000 and a mass accuracy of around 100 ppm for precursor selection) to an orbitrap analyzer (mass resolution more than 100,000). Overall mass resolution of a Q-Exactive is 140,000. Thus, it provides high analytical flexibility, power, and the ability to perform complex analysis, which is essential in proteomics [104, 105].

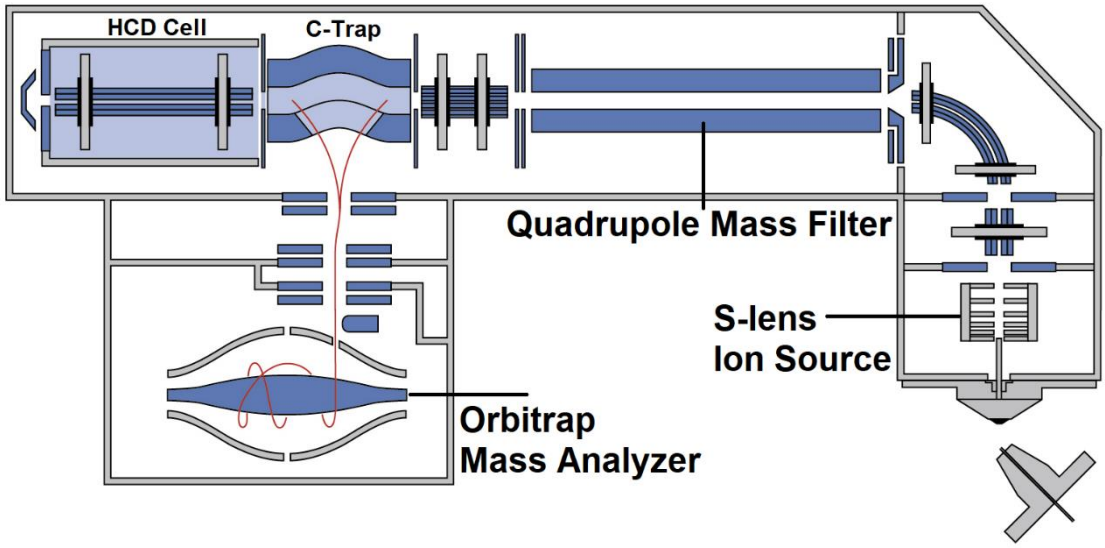

Figure 5: Schematic of a Q-Exactive. Q-exactive consists of six main components. These components are the ion source, an injection flatapole, quadrupole mass filter for precursor ion selection, a curved linear trap (c-trap) for short selection, a HCD (higher energy collisional dissociation) collision cell, and an orbitrap mass analyzer. (Modified after Michalski, A., et al 2011 [104])

The last element of a mass spectrometer is the ion detector. The signals produced in the detector will produce a mass spectrum, which is a record of ions as a function of the mass-to-charge ratio. Typically, electron multipliers (EM) are used for quadrupole or orbitrap mass analyzers. Such detectors have high detection efficiencies due to signal amplification [100].

1.7.2. Bioinformatics analysis of MS data

The next step in the proteomics approach is processing of the raw mass spectral data with different bioinformatic tools. The most important steps are protein identification and quantification, enrichment analysis, and network analysis (**Figure 6**).

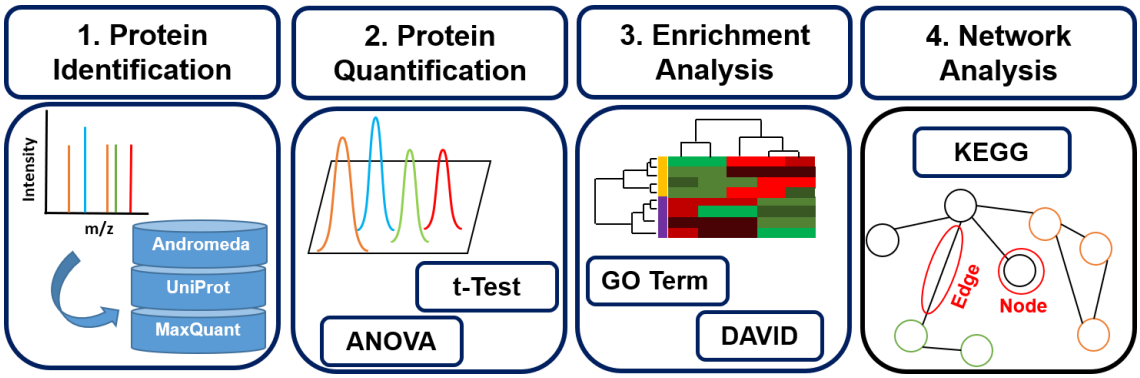

Figure 6: Bioinformatics tools for MS-based proteomics data analysis. Crucial steps in data analysis include protein identification with databases. Protein quantification and statistical analysis are applied to gain information of significant changes in protein levels between samples. For comprehensive analysis of proteomics data, enrichment and network analysis are utilized.

Peptide sequences are identified using search algorithms in databases such as MASCOT, MaxQuant or SEQUEST [106]. For each algorithm, the observed peptide spectra is compared to the theoretical ion spectra from the database to assign quality scores [107]. With increasing number of distinctive amino acid sequences, confidence in protein identification is getting higher [107]. The peptide sequences are taken from UniProt and NCBI databases [100].

Identification of proteins of a particular sample is only a first step in the whole approach [100]. Another crucial point in proteomics data analysis is protein abundance quantification. Spectra from separate LC-MS experiments for different samples are used in label-free quantification. For this approach, signal intensity of peptide ions of the fragmented proteins is used. Of course, normalization of the data is crucial for further analysis. MaxQuant is one of the most used software packages for this step in the analysis and it has implemented such normalization [106]. The next step is the statistical analysis of the now normalized data. With statistical tests, the data is examined for significant changes in protein levels between two different conditions [106]. T-Tests or ANOVA (analysis of variance) are used depending on the sample size [106, 108].

To identify correlations and topology between the proteins, pathway and enrichment analysis with bioinformatics tools such as DAVID (Database for Annotation, Visualization and Integrated Discovery), STRING, and Cytoscape are applied afterwards [109]. With enrichment analysis, proteins and their associated genes that are overrepresented in the samples of interest can be identified. The most used technique in this step is the gene ontology (GO) enrichment [106, 110]. The GO terms are a set of

predefined groups of different genes. The groups are assigned based on the functional properties of the genes. Each GO term has a unique identifier, and they are hierarchically clustered. The clusters describe the categories of the terms. The three main categories are: “biological process”, “molecular function” and “cellular component”. The GO enables the functional interpretation of the proteomics data [106, 110].

Finally, proteomics data can be analyzed to reconstruct protein networks such as protein-protein interaction or signaling networks. In such a network, the edges between nodes indicate the connection between the proteins/genes. An example for a network database used in proteomics is KEGG, the Kyoto Encyclopedia of Genes and Genomes [111]. With KEGG, comprehensive data analysis can be applied to access protein network information [111].

2. Objectives of this study

Understanding the underlying processes of bone regeneration after fracture is important in clinics and in research. Early diagnostic of pseudarthrosis development is essential for successful treatment approaches. Despite advanced surgical methods, 5-10 % of all fractures show pseudarthrosis development [5, 83]. There are several clinical and research approaches to treat pseudarthrosis, one of them is local treatment using growth factors (e.g. BMPs) [5]. Osteoblast differentiation of MSCs should be triggered by BMP application. However, using such factors for pseudarthrosis treatment is questionable. The abundant cell type in pseudarthrosis, the fibroblasts, respond to the same growth factors as MSCs. Thus, treatment of a bone fracture with BMPs can lead to enhanced fibrous tissue at the fracture site in form of osteoblast-like fibroblasts which prevents building of normal and healthy bone tissue. Moreover, mechanical stability is deteriorated because of impaired mineralization of the fibrous tissue [7, 13, 14].

This study aims at analyzing differences between osteoblasts and osteoblast-like fibroblasts as well as identification of potential biological biomarkers. The discovery of suitable biomarkers can enable development of new, advanced pseudarthrosis treatment strategies in the future. Such biomarkers can be useful in early pseudarthrosis diagnosis. Furthermore, biomarkers can help deciding the right treatment approach. In addition, patient-related and non-related risk factors for pseudarthrosis are complex and can influence fracture healing. Thus, a retrospective study is conducted in this thesis for

identifying possible risk factors for different pseudarthrosis types. Moreover, this work aims at explaining the importance of infection treatment in septic pseudarthrosis treatment. Therefore, a second retrospective study analyzes the impact of polymicrobial infections on pseudarthrosis.

Hypotheses:

1. Protein-level differences between osteoblast-like fibroblasts and osteoblasts result in pseudarthrosis. Analysis of MSCs and fibroblast response to growth factor stimulation can assist in understanding pseudarthrosis development.
2. Retrospective study of patients with aseptic pseudarthrosis identifies systemic risk factors, which are conceivably relevant for either hypertrophic or atrophic aseptic pseudarthrosis development.
3. Polymicrobial infections have a higher impact compared to monomicrobial infections on septic pseudarthrosis and lead to deteriorated postoperative outcome.

3. Material and Methods

3.1. Cell culture

Cells were obtained from human reaming debris of various patients, with the approval of the local ethics commission. The adult patients did not display any disease history related to bone metabolism. Mesenchymal stromal cells were taken from bone marrow; fibroblasts from bone tissue [112]. This method was published by Trinkaus et al. [113]. All samples were obtained from the Department of Trauma Surgery at the University Hospital of Giessen-Marburg/Campus Giessen. The experiments were approved by the local ethical committee of the Medical Faculty of the Justus Liebig University of Giessen (Reference number: AZ 106/06).

In this study, mesenchymal stromal cells (SCC) and fibroblasts (FC) served as control. Experimental cell types were osteogenic stimulated stromal cells (SCO) and osteogenic stimulated fibroblasts (FO). (**Figure 7**)

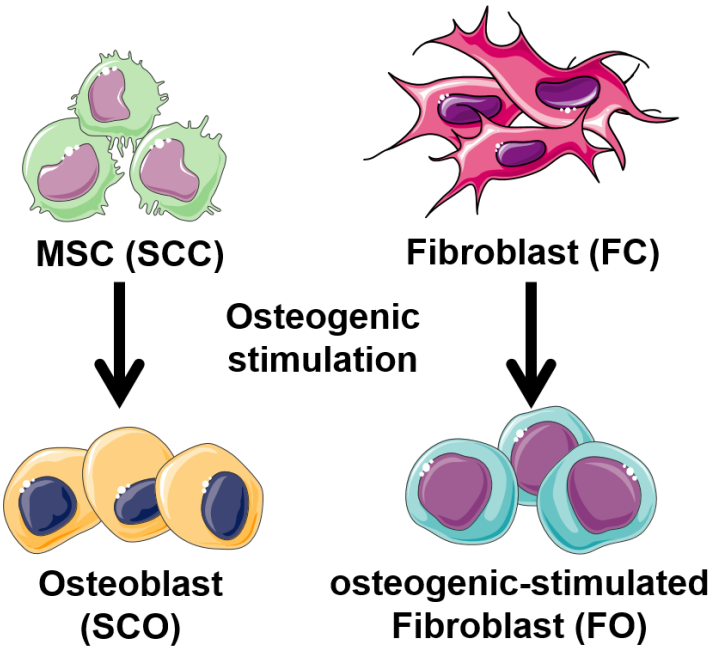

Figure 7: Schematic depicting for the analysis of human bone cells. The study hypothesized cellular differences between osteoblast-like fibroblasts (FO) and MSCs-derived osteoblasts (SCO) result in discrepant tissue properties during bone healing. Therefore, proteomes of fibroblasts and MSCs before and after osteogenic stimulation were characterized using several mass spectrometric methods to evaluate this hypothesis. (This figure was created using Servier Medical Art templates, which are licensed under a Creative Commons Attribution 3.0 Unported License; https://smart.servier.com. [30])

3.1.1. Materials and Devices

Table 3.1: List of chemicals used in cell culture experiments in this study.

Chemicals and Consumables	
Name	**Company, City, Country, [product number]**
Calcium chloride	Promocell, Heidelberg, Germany [C-34006]
Dexamethason	Sigma-Aldrich GmbH, Steinheim, Germany, [D8893]
1x Dulbeccos Modified Eagle Medium (DMEM)	Pan Biotec, Aidenbach, Germany [P04-548]
Eppendorf tubes (1.5 mL, 2 mL)	Sigma-Aldrich GmbH, Steinheim, Germany, [Z606316], [Z606324]
Fetal calf serum (FCS)	Biochrom, Berlin, Germany [S 0115, 0194X]
Glyceringelatine	Merck, Darmstadt, Germany [109242]
Glutamax 100x	Gibco by Thermo Fisher Scientific, Waltham, MA, [35050-061]

β-Glycerophosphate hydrate	Sigma-Aldrich GmbH, Steinheim, Germany, [G9422]
Greiner CELLSTAR® serological pipettes (5 mL, 10 mL, 25 mL)	Sigma-Aldrich GmbH, Steinheim, Germany, [P7615], [P7740], [P7865]
MesenPro RS™ Medium	Gibco by Thermo Fisher Scientific, Waltham, MA, [12746012]
Nuclear fast red-aluminum sulfate, 0.1 % solution	Merck, Darmstadt, Germany, [100121]
Paraformaldehyde (PFA)	Carl Roth GmbH, Karlsruhe, Germany, [0335.3]
10x Phosphate buffered saline (PBS), pH=7.4	Gibco by Thermo Fisher Scientific, Waltham, MA [70011044]
Penicillin / Streptomycin 10.000 U/mL	Gibco by Thermo Fisher Scientific, Waltham, MA, [15140122]
Petri dishes (6 cm diameter)	Sigma-Aldrich GmbH, Steinheim, Germany, [P5481]
Pipette tips (0.1-10 µL, 20-200 µL, 100-1000 µL)	Gilson, Inc., Middleton, WI, [F171201], [F171301], [F171301]
Silver nitrate	Carl Roth GmbH, Karlsruhe, Germany, [4500.1]
(+) Sodium-L-ascorbate	Sigma-Aldrich GmbH, Steinheim, Germany, [A7631]
Sodium carbonate	Sigma-Aldrich GmbH, Steinheim, Germany, [451614]
Sodium thiosulfate	Merck, Darmstadt, Germany, [106516]
Trypan Blue, 0.4 %	Sigma-Aldrich GmbH, Steinheim, Germany, [T8154]
Trypsin-EDTA, 0.05 %	Gibco by Thermo Fisher Scientific, Waltham, MA, [25300054]
Tissue culture flask (T75)	Sigma-Aldrich GmbH, Steinheim, Germany, [C7231]
Vitamin D3	Sigma-Aldrich GmbH, Steinheim, Germany, [D1530]

Table 3.2: List of devices used in cell culture experiments.

Devices	
Name	**Company, City, Country**
Centrifuge Hettich Rotina 380R	Andreas Hettich GmbH & Co. KG, Tuttlingen, Germany
Hemacytometer	Sigma-Aldrich GmbH, Steinheim, Germany
Incubator Kendro HERAcell	Kendro Laboratory Products GmbH, Langenselbold, Germany
Lamin Air HB2448 sterile bank	Heraeus Holding GmbH, Hanau, Germany
Leica microscope type 090-135.002	Leica Microsystems GmbH, Wetzlar, Germany
Water bath Grant PB1	Grant Instruments, Cambridge, UK

3.1.2. Procedure

Cell culture was realized under sterile conditions in a laminar flow hood. Incubation and culturing of cells were carried out at 37 °C in 95 % air-5 % CO_2 atmosphere. All used solutions were warmed to 37 °C before use in a water bath. Cells were passaged when they reached 70-80 % confluence. The composition of the applied culture media is represented in **Table 3.3** and **Table 3.4**.

Table 3.3: Cell culture medium for mesenchymal stromal control cells (SCC) used in this study.

Culture medium	
MesenPro RS™ Medium (1x)	+ 20 % FCS + 1 % (v/v) solution of antibiotics (Penicillin/Streptomycin) + 2 % GlutaMAX

Table 3.4: Cell culture medium for fibroblast control cells (FC).

Culture medium	
DMEM	+ 20 % FCS + 1 % (v/v) solution of antibiotics (Penicillin/Streptomycin) + 2 % GlutaMAX

3.1.3. Subculturing of monolayer cells

Adherent cell lines like fibroblasts and mesenchymal stromal cells grow as a monolayer attached to their culture flask and stop growing as soon as the available surface is covered completely by cells. Furthermore, toxic metabolite rises when cell lines are held longer in culture. To keep the cells alive and actively growing, it is inevitable to subculture them regularly. Medium is removed and cells are transferred from a previous culture into fresh growth medium with no toxic metabolites [114, 115].

Briefly, 1x PBS, dilution of 1:10 from 10x PBS stock solution, was used as washing solution. It was utilized to maintain a physiological pH and osmotic balance during washing of cells. For detachment of cells from the flask surface, a trypsin-EDTA-solution was used which contains 0.05 % trypsin and 0.02 % EDTA. All solutions were warmed up at 37 °C in a water bath before use. Subculturing of cells was performed at intervals of three to four days. Medium was removed with a disposable sterile pipette. Medium

residues were removed by washing cell monolayer with 20 mL 1x PBS. Washing solution was discarded and 3 mL of the 0.05 % trypsin-EDTA-solution were added to the T-flask and incubated at 37 °C for five minutes. After incubation, 3 mL new cell culture medium was added to stop trypsin reaction and to dissociate cells. In two T-flasks, 15 mL of culture medium was added, and, in each flask, 3 mL of cell suspension was casted. Afterwards, culture flasks were placed in the incubator.

3.1.4. Cell counting

Counting cells is an important and necessary step for monitoring cell viability and proliferation rate. It is also important for seeding cells for subsequent experiments. Total numbers of cells and percent viability were determined using a hemacytometer cell counter and the colorimetric dye Trypan Blue. Trypan Blue staining is a dye exclusion method. Dead cells allow the dye to permeate and therefore appear blue under light microscope. Living cells do not allow the dye to permeate the cell membrane and thus, the Trypan Blue is excluded [116, 117]. Before counting, glass hematocymeter and coverslip were cleaned with alcohol. Then, the coverslip was moistened with water and attached to the hemacytometer. Proper adhesion was indicated by the presence of Newton's refraction rings under the coverslip. Flask with cell suspension was gently swirled to ensure the evenly distribution of the cells. 0.5 mL of cell suspension were taken out by using a 5 mL sterile pipette and placed in an Eppendorf tube. From this, 100 µL of cells were taken into a new Eppendorf tube as well as 400 µL 0.4% Trypan Blue (final concentration 0.32 %). Solution was gently mixed and 100 µL of Trypan Blue-treated cell suspension was applied to the hemocytometer by filling both chambers underneath the coverslip. Cell suspension was allowed to be drawn out by capillary action. To focus on the grid lines of the hemocytometer, a Leica microscope was used with a 10x objective. Living cells were counted in all 4 sets of 16 squares [116, 118]. To calculate the number of viable cells/mL, an average cell count from each of the four sets of 16 corner squares was taken. This number was multiplied by 10^4 and by 5 to correct the 1:5 dilution from the Trypan Blue addition. The final value was the number of viable cells/mL in the original cell suspension.

3.1.5. Osteogenic stimulation

Osteogenic stimulation was performed in 6 cm diameter petri dishes in triplicates with osteogenic culture medium (**Table 3.5**). Cells were allowed to adhere for 48 hours on the Petri dishes. Osteogenic stimulation was carried out for four days until cell density of 30.000 cells per cm² was achieved. After four days, growth medium was removed, and cells were washed with cold 1x PBS and stored at -80 °C in sealed Petri dishes until use in proteomics study.

Table 3.5: Composition of culture medium for osteogenic stimulation.

Culture medium	
DMEM	+ 10 % FCS + Dexamethason (10^{-7} M) + 1 % (v/v) solution of antibiotics (Penicillin/Streptomycin) + (+) sodium-L-ascorbate ($5*10^{-5}$ M) + β-glycerophosphate hydrate (10^{-2} M) + vitamin D3 ($5x10^{-8}$ M) + calcium chloride (1,5mM)

3.1.6. Von Kossa staining

FO and SCO cells were stained with von Kossa to evaluate matrix mineralization. Briefly, medium was discarded, cells were washed with 1x PBS at 4 °C and fixed with 2 % PFA solution for 10 minutes. Samples were incubated for 60 minutes at room temperature (RT) in the dark in a 5 % silver nitrate staining solution. After staining, the sections were thoroughly washed in sterile distilled water and transferred to a 5 % sodium carbonate solution containing formalin. Then cells were washed and incubated for 10 minutes in a 5 % aqueous sodium thiosulfate solution. Cells were counterstained with a ready-to-use 0.1 % nuclear fast red-aluminum sulfate solution for 30 minutes at room temperature. The samples were then rinsed with sterile water, mounted and observed using light microscopy.

3.2. Proteomics

In this study bottom-up shotgun proteomics (**Figure 8**) was used. The proteins present in the different cell types and their abundance levels were quantified with this method.

Identifying differentially expressed proteins can result in exploring potential diagnostic marker. The general workflow for bottom-up proteomics contains homogenizing of the cells, protein isolation and purification. Complex mixtures of proteins are then subjected to enzymatic cleavage and the resulting peptides are separated based on their chemical or physical properties. Finally, peptides are analyzed using mass spectrometry [103, 119]. Proteomics studies were conducted at working group of Prof. Bernhard Spengler in the institute of inorganic and analytical chemistry of the JLU Gießen under supervision of Dr.rer.nat. Sabine Schulz.

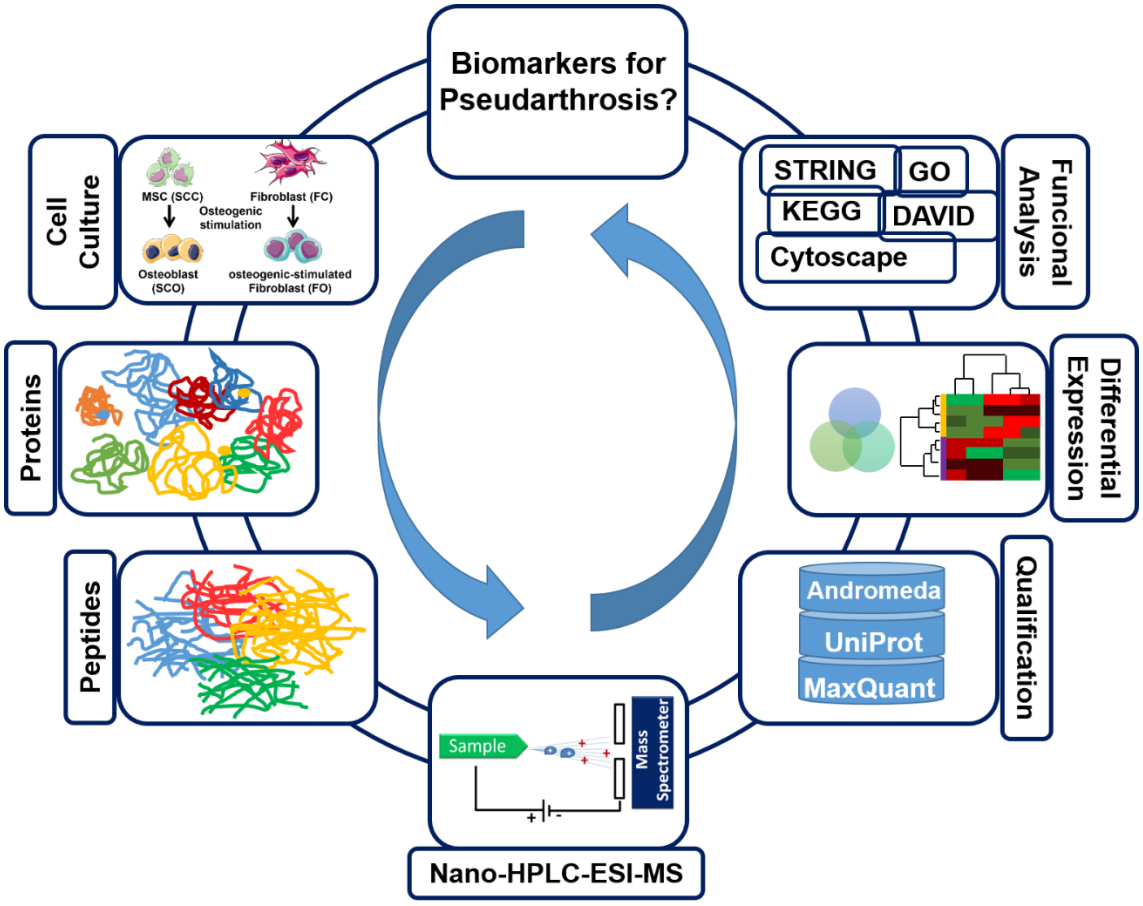

Figure 8: Bottom-up shotgun proteomics workflow. Proteomics was utilized to identify new biomarker for pseudarthrosis. In the widely used bottom-up proteomics approach, proteins were extracted from cells (SCC, SCO, FC, FO) and digested in solution with trypsin. Resulting peptides were analyzed by nano-HPLC-ESI-MS. Peptide information was transferred to protein level, and proteins were identified. Differential expression analysis was conducted to elucidate differences in protein expression of cells (SCC, SCO, FC and FO) and to explore potential biomarkers. The functional analysis of proteins revealed pathways and interactions. [modified after Schmidt, A, et al, 2014 [120]]

3.2.1. Materials and Devices

Table 3.6: List of chemicals and materials used in proteomics experiments.

Chemicals and Consumables	
Name	**Company, City, Country, [product number]**
Acetone	Merck, Darmstadt, Germany, [100014]
Acetonitrile (ACN), Rotisolv ®, HPLC ultra-gradient grade	Carl Roth GmbH, Karlsruhe, Germany, [T195.2]
Ammonium bicarbonate buffer	Fluka by Honeywell, Seelze, Germany, [09832]
Bovine serum albumin (BSA)	Carl Roth GmbH, Karlsruhe, Germany, [8076.2]
1,4-Dithio-DL-threitol (DTT) ≥99.5 %	Carl Roth GmbH, Karlsruhe, Germany, [6908.2]
Formic Acid (FA) 98 %	Sigma-Aldrich GmbH, Steinheim, Germany, [251364]
Iodoacetamide (IAA)	Sigma-Aldrich GmbH, Steinheim, Germany, [I6125]
LC/MS grade water	Sigma-Aldrich GmbH, Steinheim, Germany, [1.15333]
Phosphate buffered saline (PBS) 10x, pH 7.4	Gibco by Thermo Fisher Scientific, Waltham, MA, [70011044]
Pipette tips (0.1-10 µL, 20-200 µL, 100-1000 µL)	Gilson, Inc., Middleton, WI, [F171201], [F171301], [F171301]
Roti®-Nanoquant 5x	Carl Roth GmbH, Karlsruhe, Germany, [K880.1]
Trypsin, lyophilized powder, sequencing grade	Promega, Madison, WI, [V5111]
Trifluoroacetic acid (TFA)	Fluka by Honeywell, Seelze, Germany, [91701]
Tris-hydrochloride (HCl)	Sigma-Aldrich GmbH, Steinheim, Germany, [10812846001]
Zip Tip_{C18}	Merck, Darmstadt, Germany, [ZTC18M960]

Table 3.7: List of devices used in proteomics experiments.

Devices	
Name	**Company, City, Country**
Desiccator	Sigma-Aldrich GmbH, Steinheim, Germany, [SLW1590/02D]
Mini spin centrifuge	Eppendorf, Hamburg, Germany

Q-Exactive Mass Spectrometer	Thermo Fisher Scientific, Waltham, MA
LC Packings UltiMate™ Nano HPLC System	Dionex company by Thermo Fisher Scientific, Waltham, MA
Bandelin sonorex ultrasonicator	Bandelin, Berlin, Germany
Savant Speed Vac	Thermo Fisher Scientific, Waltham, MA
UV/Vis spectral photometer HP8453	Agilent, Santa Clara, CA
Vortex: IKA MS2 mini shaker	IKA®-Werke GmbH & Co. KG, Staufen im Breisgau, Germany
Water bath	Dinkelberg analytics, Galblingen, Germany
Weighing Balance	Mettler-Toledo GmbH, Gießen, Germany

Table 3.8: List of software used in proteomics experiments.

Software	
Name	**Company, City, Country**
Chromeleon Client Version 6.60 SP2 Build 1472	Dionex, Sunnyvale, CA
Cytoscape Version 2.8.3.	Donnelly Center, Toronto, Canada
DAVID Version 6.7	Laboratory of Human Retrovirology and Immunoinformatics, Frederick, MD
Enrichment Map Plug-in	Bader Laboratory at the Donnelly Center, Toronto, Canada
MaxQuant Version 1.5.3.17	Computational Systems Biochemistry, Max Planck Institute of Biochemistry, Martinsried, Germany
Office 2007	Microsoft, Redmond, WA
Perseus Version 1.5.2.6	Computational Systems Biochemistry, Max Planck Institute of Biochemistry, Martinsried, Germany
UniProt database	European Bioinformatics Institute, Swiss Institute of Bioinformatics, Protein Information Resource

3.2.2. Cell homogenization, protein isolation and purification

To isolate proteins from cells, samples were taken out of -80 °C storage and thawed for two hours in a desiccator at RT. After that, cells were washed two times with cold 1x PBS (PBS 10x concentration diluted 1:10 with LC/MS grade water). Cells were homogenized using a cell scraper and 100 µl of 50 mM Tris-HCl buffer and were transferred to 2 ml Eppendorf tubes. Samples were then vortexed and sonicated in an ultrasonicator two

times for 10 minutes for further homogenization and cell lysis. To separate cell cytosol from solid cell parts, samples were centrifuged at 10000 g for 5 minutes. Supernatant was discarded and the pellet, containing proteins, was suspended in 50 mM Tris-HCl.

3.2.3. Protein concentration determination

A colorimetric method for measurement of unknown protein concentrations is the Bradford assay. The Bradford assay protein determination is based on an absorbance shift of the dye Coomassie Brilliant Blue G-250 (CBB G-250) as a result of binding of the dye to proteins, preferably to alkaline amino acid residues. The color reaction is therefore dependent on the amount of basic and aromatic amino acids in the measured proteins [121, 122]. During this binding the absorption maximum of CBB G-250 changes from 465 nm (protonated, cationic form) to 595 nm (deprotonated, anionic form). The increase of absorbance at 595 nm can be monitored. It is proportional to the protein concentration. The Bradford assay is fast performable, with the CBB G-250 binding process almost complete in roughly two minutes, and with good color stability for at least one hour [121, 122]. In the present study, the premix Roti®-Nanoquant, 5x concentrate from Carl Roth, containing CBBG G-250, was used to determine protein concentration.

For determination of protein concentrations from unknown samples, a calibration curve of bovine serum albumin (BSA) was established and changes in the absorption wavelength of CBB G-250 were compared to this curve. For absorbance measurements, UV/Vis spectral photometer HP8453 from Agilent was used. As a stock solution of the standard test series, 0.4 mg/mL BSA in milli-Q-water was used. To each dilution of the standard and the sample test series, 800 µL of 1x Roti®-Nanoquant (Roti®-Nanoquant, 5x concentrate diluted 1:5 with Milli-Q-H2O) were added to a total volume of 1 mL. The final concentrations of the standard test series were 0, 1, 2, 4, 8, 12, 15, 20 and 25 µg/mL. The final dilutions of the sample test series were 1:2000, 1:1000, 1:2000/3, 1:400 and 1:800/3. Milli-Q-water and 1x Roti®-Nanoquant served as a negative control. Incubation time was 10 minutes. Measurement took place immediately after incubation. For measurement, samples were transferred into disposable poly(methyl methacrylate) (PMMA) cuvettes. Milli-Q-water was used as blank for the baseline.

To determine the protein concentration, the respective ratio $Q = \frac{A_{595\,nm}}{A_{465\,nm}}$ was plotted against the known BSA concentration. The concentrations of the unknown samples were

calculated according to the correlation line equation $y = m \cdot x + b$ for the standards (y = measured ratio Q, m = slope, b = y-axis intercept, x = protein concentration). To calculated protein concentrations, the final concentrations of the proteins both in standards and samples after adding the Roti®-Nanoquant solution must be considered [121, 122].

3.2.4. Enzymatic digestion of proteins

Mass spectrometry-based proteomic is less complex when performed on peptides gathered from whole proteome lysate instead of the proteins themselves. Enzymatic digestion with proteases is used to generate peptides. This experimental setup thereby relies on the used protease [123, 124]. The most commonly used protease today is trypsin because of its stringent cleavage specificity. Trypsin cleaves the carboxy-terminal (C-terminal) of the amino acids arginine and lysine in human proteins. Due to the relatively incidence of these amino acids, trypsin digestion leads to peptide fragments with an average length of 10 to 20 amino acids which is important for the identification of the proteins. Moreover, positive ionization of peptide fragments in mass spectrometry is enhanced by the presence of C-terminal basic residues [123-125]. Dithiothreitol (DDT), a reducing agent, and iodoacetamide (IAA) are used before enzymatic digestion of proteins. DTT breaks the disulfide bonds of cysteine residues. To avoid reformation of disulfide bonds, reactive thiol-groups of cysteines are alkylated with IAA. This improves cystein-containing protein digestion as well as detecting of cysteine-containing peptides [126, 127].

Briefly, 100 µL of 10 mM DTT were added to the samples. Samples were mixed and kept in water bath at 56°C for 45 minutes. After cooling down, 10 µL of 55 mM IAA were added to the samples. For tryptic digestion, 10 µL of trypsin (0.1 µg/µL in 10 mM NH_4HCO_3 buffer) were added and samples were kept at 37 °C overnight. In order to extract the tryptic peptides from the complex sample mixture and for desalting and enrichment of peptides, ZipTips packed with C18 reversed-phase material were used [128, 129]. Therefore, pH of samples was adjusted to a value below 4 (pH <4) using 2.5 % trifluoroacetic acid (TFA). ZipTip procedure is described as follows. ZipTips were washed and prepared using several steps and solutions: 5x10 µL 100 % Acetonitrile (ACN) followed by 5x10 µL 50 % ACN/0.1 % TFA and 5x10 µL 0.1 % TFA. Then peptides were bound to ZipTips by pipetting 10x up and down of the sample with the

setting of 10 µL on the pipette. To extract salts, ZipTips were washed 3x with 10 µL 0.5 % TFA. For the elution, 5 µL 50 % ACN/0.1 % TFA were taken into the ZipTip and pipette 3-4 times up and down. Then the solution was put into new sample tubes with known weight. Samples were dried in a speed-vac at 35 °C for 45 minutes in order to resuspend them in LC solvent A (0.1 % formic acid (FA) in 2% ACN) in a defined concentration of 1 µg/µL.

3.2.5. Nano-High Performance Liquid Chromatography (HPLC)

To separate peptides, an ultimate binary nano-high performance liquid chromatography (nano-HPLC) system from LC Packings (Dionex, Idstein, Germany) was used, which is a reversed-phase (RP) chromatography system. A RP-HPLC has a non-polar stationary phase and a polar liquid mobile phase. The mobile phase and the stationary phase are inverted. Hence the solved probe interacts with the non-polar stationary phase in the polar, aqueous solvent. A silica gel substituted with alkyls with a chain length of C2-C18 is often used as the non-polar stationary phase. The mobile phase is often composed of acetonitrile, water and TFA (0,1%). Acetonitrile is the most commonly used eluent because of its physical properties, like viscosity and UV permeability. TFA is given to the solvent as an ion-pair agent, which binds to a charged and non-charged molecule part to the ionic side chain of a peptide. Then hydrophobicity of the peptide changes as well as the chromatographic behaviour of the formed complex [130].

The Nano-HPLC in this study was operated in gradient mode (**Figure 9**); injected sample volume was 1.0 µg. By using a pre-focusing trap column (Acclaim PepMap C18 µ-pre-column with 5 µm particle size, 300 Å pore size, 300 µm in diameter and 5 mm length from LC Packings, a Dionex company, Thermo Fisher Scientific, Waltham, MA) and a fused-silica separation column (Acclaim PepMap100 C18 nano LC column with 3 µm particle size, 100 Å pore size, 75 µm in diameter and 15 cm length from Dionex, Thermo Fisher Scientific, Waltham, MA), reversed phase chromatographically separation was conducted.

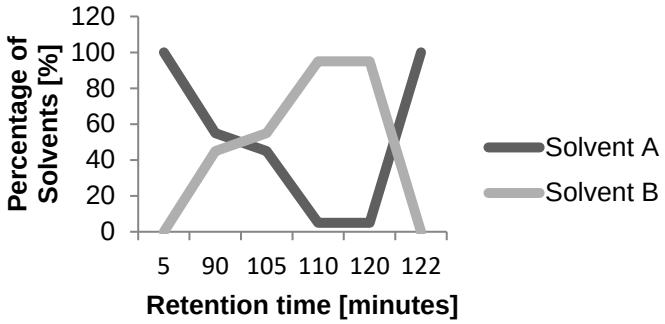

Figure 9: HPLC Gradient of Solvent A and B. Gradients of solvents provide better peptide peaks and the ability to elute analytes with a wide range of hydrophobicity values. In this RP-HPLC, the dynamic mixture of solvents A and B is used to achieve increase in the organic solvent B over the retention time, which leads to increase of the elution strength of the eluent [131, 132].

Two solvents were used for elution of peptides: A (0.1 % FA in 2 % ACN) and B (0.08 % FA in 80 % ACN) (**Figure 9**). Loading pump flow was set to 0.03 mL/min and HPLC pump flow rate was 0.3 µL/min.

3.2.6. Mass Spectrometric Analysis

A Q-exactive orbitrap (Exactive^{TM} Orbitrap, Thermo Fisher Scientific, Waltham, MA) was used in this study. The mass analyzer was directly coupled with the nano-HPLC using an electrospray ionization (nano-ESI) source with Chromeleon software (Chromeleon Client v.6.60 SP2 Build 1472, Dionex). The Q-Exactive mass spectrometer was operated in positive ion mode and data dependent mode. Survey scan range was set to 300 to 1800 m/z, with resolution of 70,000 at m/z=200 for 10 most abundant ions for Q- Exactive with charge of ≥2 was subjected. Mass accuracy was ±2 ppm. Q-Exactive uses higher energy collision dissociation (HCD) to induce the fragmentation of backbone of peptides.

MaxQuant software (version 1.5.3.17) was used for label free quantification (LFQ) [133]. Proteins were identified by correlating MS/MS spectra to the Andromeda search engine [134] against the Uniprot KB FASTA database (http://www.uniprot.org/) [135]. The taxonomy was restricted to Homo sapiens to avoid protein identification redundancy. As the enzyme parameter, trypsin was chosen. One missed cleavage was allowed. False discovery rate (FDR) cutoff of 1 % was applied at the peptide and protein levels. Initial precursor mass deviation of up to 4.5 ppm and fragment mass deviation up to 20 ppm were allowed. Threshold intensity was for peptide identification was set at 500.

3.2.7. Data Normalization in R

The raw data was analyzed using the R project for Statistical Computing (version 3.0.3). Different packages provided by Bioconductor (version 3.5) were used to process and normalize the mass spectrometric files. First, Pearson's correlation function of R was used to carry out the qualitative analysis of raw data. After that, data normalization in R was carried out, using Hmisc and MASS libraries. Fold change was calculated as the differences between each cell type using delta delta CT method considering housekeeping protein (peptidyl-prolyl cis-trans isomerase A) as controls. The differentially expressed proteins were obtained after applying the criteria of fold change (FC) $\geq |2|$ and $p \leq 0.01$.

3.2.8. Functional annotation

To obtain information of the protein involvement in bone healing, the generated protein list from the mass spectrometry experiments must be grouped in functional clusters. Those clusters are also called functional annotations. Therefore, differentially expressed proteins and their corresponding genes were annotated using the bioinformatics **D**atabase for **A**nnotation, **V**isualization and **I**ntegrated **D**iscovery (DAVID; version 6.7, https://david.ncifcrf.gov/) [136, 137]. This database provides information about enriched biological processes, protein-protein interactions, molecular functions and cellular components. Moreover, pathway information can be obtained through this online tool. To reach the best analytical results, the analysis was customized to a higher stringency thusly cutoff was increased. Here, biological processes, molecular functions and cellular components were used as annotation categories. For the data set in this study, functional gene categories were identified when they were significantly differentially expressed ($p<0.01$) and fold change was $> |2|$.

Protocol for functional annotation:

1. Open website under https://david.ncifcrf.gov/.
2. Submit protein/ gene list obtained from mass spectrometric experiments.
3. Select identifier (e.g. OFFICAL_GENE_NAME)
4. Choose list type as gene list.
5. Submit gene list.
6. Choose species (homo sapiens).
7. Click on functional annotation tool.

8. In annotation summary results click clear all in order to clear defaults.
9. Expand the option Gene Ontology and choose GOTERM with FAT options.
10. Expand pathway option and select Biocarta and KEGG.
11. Proceed to functional annotation clustering.
12. Expand options to reach the parameter panel.
13. There customize as preferred. Here, fold change and increased stringency were selected by lowering linkage threshold.
14. Download annotation file.
15. Genes in a cluster can be displayed by clicking on the red letter G.
16. Go back to main page and click functional annotation chart.
17. Download file and use it for enrichment map in Cytoscape.

3.2.9. Protein network analysis and enrichment map

GBA ("Guilt by Association") Network analysis was carried out to show relations between proteins detected by nano-HPLC-ESI-MS measurements *via* interaction partners with pseudarthrosis and neurofibromatosis (NF1) related genes. The NF1 gene was considered important in this work due to the fact, that recalcitrant bone healing and pseudarthrosis development is a common complication associated with NF1 [14]. To get an in-depth network, analysis was performed with two metasearch platforms, GeneMANIA (http://www.genemania.org/) and STRING (https://www.string-db.org/). They were used to predict the co-expressed and co-localized partners of the differentially expressed genes (CALM1, COL1A2 and GARS) and their interaction with NF1. Composite network analysis map was built by associates' plug-in of cytoscape 2.8.3. [138]. Cytoscape is a well-established platform for the visualization of molecular interaction networks and the integration of these networks with data [139].

At first network data was produced at GeneMANIA:

1. Go to http://genemania.org/.
2. Select Homo Sapiens.
3. Enter the gene list in the search dialogue (CALM1, COL1A2, GARS and NF1).
4. Select the network attributes (co-expression and co-localization).
5. Customize advanced options and choose "GO-based weighting" and click on "Biological Process based".

6. Maximal number of interactions was set to 20.
7. Click on search to obtain the interaction network.
8. Save the network as image.
9. Save the network data to input in cytoscape.

Second network was produced at STRING:

1. Go to https://www.string-db.org/.
2. Go to search and click on "Multiple Proteins by Names / Identifiers".
3. Enter the protein list in the dialogue (CALM1, COL1A2, GARS and NF1).
4. Select Homo Sapiens as organism and click on search.
10. Once the default network is generated, change settings. Select the network attributes (co-expression and co-occurrence).
11. Set maximal number of interactions to 20.
12. Set minimum required interaction score to "high confidence (0.700)".
13. Click "Update Parameter".
14. Export your current network as bitmap file.
15. Save the network data to input in cytoscape.

Both obtained network data was then put into cytoscape for network visualization.

1. Software installation: install cytoscape (http://www.cytoscape.org/).
2. Import both networks into the cytoscpae: File → Import → Network from Table (Text/MS Excel).
3. Specify interactions: "Source Interaction" and "Target Interaction" for each network.
4. Merge all networks using: Plug-ins → Advanced Network Merge.
5. Use VizMapper to change network settings (color, font, nod size, etc.)
6. Save the merged network.

For enrichment map visualization in cytoscape, DAVID enrichment file was used. The file must contain the following fields in the following sequence:

- Category (DAVID category)
- Term – gene set name
- Count – number of genes associated with this gene set
- Percentage – gene associated with this gene set/total number of query genes

- P-value – modified Fisher's exact p-value
- Genes – list of genes from query set that are annotated to this gene set
- List total – number of genes in query list mapped to any gene set in this ontology
- Pop hits – number of genes annotated to this gene set on the background list
- Pop total – number of genes on the background list mapped to any gene set in this ontology
- Fold enrichment
- Bonferroni
- Benjamini
- False discovery rate (FDR)

For generating enrichment map via cytoscape, the following protocol was used. The manual can be obtained at http://baderlab.org/Software/EnrichmentMap/Tutorial for further details.

1. Open cytoscape.
2. From top menu, select Plug-ins/Enrichment Map/Load Enrichment Results.
3. Select format of enrichment analysis results, analysis type: DAVID file.
4. Set p-value and FDR parameters. P-value cut-off and FDR Q-value cut-off can be used to control stringency of the analysis. Thusly, only gene-sets with enrichment statistics satisfying these thresholds will be displayed by enrichment map. Here, p-value cut-off was set to 0.001; FDR cut-off to 0.05. This gives more stringency than default cut-offs.
5. Select the similarity coefficient and its cut-off. If gene ontology (GO) derived sets are present, select overlap coefficient.
6. Generate enrichment map by clicking on the build button.
7. Save enrichment map as image.

3.3. Genomics

Molecular testing of gene expression complements the examination of observed differences in osteogenic stimulated fibroblasts in proteomics. At this, RNA molecule plays a critical role in transferring information which is encoded in the genome to the different forms of proteins. RNA is extracted from cells and thereafter cellular activity is

measured by techniques like real-time polymerase chain reaction (RT-PCR) or high throughput analysis [140].

3.3.1. Material and Devices

Table 3.9: List of chemicals used in genomics experiments in this study.

Chemicals and Consumables	
Name	**Company, City, Country, [product number]**
Chloroform	VWR International GmbH, Darmstadt, Germany [220114-321]
Ethanol 75 %	Sigma-Aldrich GmbH, Steinheim, Germany, [32205-M]
Eppendorf PCR tubes (0.5 mL, 1.5 mL, 2 mL)	Sigma-Aldrich GmbH, Steinheim, Germany, [Z606332], [Z606316], [Z606324]
dNTPs	Promega, Madison, WI, US, [U1511]
GoTaq qPCR Master Mix	Promega, Madison, WI, US, [A6001]
Isopropanol	Thermo Fisher Scientific, Waltham, MA, [9500-1]
Moloney Murine Leukemia Virus Reverse Transcriptase (M-MLV RT)	Promega, Madison, WI, US, [M1701]
Pipette tips (0.1-10 µL, 20-200 µL, 100-1000 µL)	Gilson, Inc., Middleton, WI, [F171201], [F171301], [F171301]
Random primers	Promega, Madison, WI, US, [C1181]
RNase-free water	Thermo Fisher Scientific, Waltham, MA, [10977035]
RNAsin Plus	Promega, Madison, WI, US, [N2511]
TRIZOL reagent	Thermo Fisher Scientific, Waltham, MA, [15596026]

Table 3.10: List of devices used in genomics experiments in this study.

Devices	
Name	**Company, City, Country**
AccuBlock D1100 digital dry bath	Labnet International Inc., Edison, NJ
Agilent 2100 Bioanalyzer	Agilent, Santa Clara, CA

Centrifuge Hettich Mikro 20	Andreas Hettich GmbH & Co. KG, Tuttlingen, Germany
Centrifuge Hettich Mikro 220R	Andreas Hettich GmbH & Co. KG, Tuttlingen, Germany
Nanodrop ND-1000	NanoDrop Technologies Inc., Wilmington, DE
7300 Real-Time PCR System	Applied Biosystem, Foster City, CA
Vortex Genie 2	Scientific Industries, Inc., Bohemia, NY

Table 3.11: List of software used in genomics experiments in this study.

Software	
Name	**Company, City, Country**
RefFinder (http://leonxie.esy.es/RefFinder/)	Dr. Zhang's Lab, Greenville, NC
DataAssist™	Applied Biosystems, Foster City, CA
Office 2007	Microsoft, Redmond, WA
SPSS statistics version 24	IBM, Armonk, NY

3.3.2. RNA isolation from cells

In this study, RNA isolation was performed with the final aim of performing RNA analysis to estimate differentially expressed genes. Cells were collected by scraping in PBS and centrifuged for five minutes. Total RNA was extracted from each sample using TRIZOL according to the manufacturer's protocol (Invitrogen Life Technologies, Germany). The invitrogen TRIZOL reagent is used to isolate high quality of RNA as well as DNA and proteins from a single sample. It is a monophasic solution of phenol, guanidine isothiocyanate, and other proprietary components. The TRIZOL reagent thereby facilitates the RNA isolation and maintains RNA integrity [141].

Briefly, samples are homogenized with TRIZOL reagent. Therefore, growth media was removed and 0.35 mL of TRIZOL reagent was added per $1x10^{-5}$ cells. Lysate was pipetted up and down several times to homogenize cells. Afterwards chloroform was added, and the homogenate was allowed to separate into three different phases by incubating for 5 minutes and centrifugation for 15 minutes at 12000 g at 4 °C. The clear upper aqueous layer contains the RNA, while an interphase and a red lower organic phase contains the DNA and proteins. Aqueous phase containing the RNA was then transferred into a new tube. 0.5 mL of isopropanol per 1 mL of TRIZOL Reagent was then added and samples were incubated for 10 minutes. After that, samples were centrifuged for 10 minutes at 12000 g at 4 °C. Total RNA precipitate formed a white gel-like pellet at the bottom of the

tube, while supernatant was discarded. For RNA washing, pellet was resuspended in 1 mL of 75 % ethanol per 1 mL of TRIZOL used for lysis. Samples were vortexed and centrifuged for 5 minutes at 7500 g at 4 °C. Supernatant was discarded and RNA pellets were air dried for 5-10 minutes. To solubilize RNA, pellet was resuspended in 20-50 µL of RNase-free water by pipetting up and down and incubating in a heat block set at 55 °C for 12.5 minutes. RNA yield was determined using the absorbance method. Absorbance at 260 nm provides total nucleic acid content, while absorbance at 280 nm determines sample purity. Ratio of absorbance at 260 nm and 280 nm is used to assess sample's RNA purity. A ratio of ~2.0 is accepted as pure for RNA. A lower ratio indicates the presence of contaminations like proteins or phenols or contaminants that absorb near 280 nm. In this study, a NanoDrop-spectrometer was used for RNA concentration analysis.

3.3.3. RNA quality analysis

RNA quality analysis and cDNA synthesis were performed in collaboration with the Department of Pediatrics of University Hospital Carl Gustav Carus of the TU Dresden as part of the TRR/SFB79. M.Sc. Felix Schulze performed those analyses.

Quality control was performed using an Agilent 2100 Bioanalyzer (Agilent, Böblingen, Germany) according to the manufacturers' instructions. By comparing the 28S to 18S RNA peak ratio (2:1 in non-degraded RNA-samples), RNA quality is controlled. The standard classified RNA quality depends on a 10-degree scale according to RNA degradation degree, a value of 1 means completely degraded RNA and 10 represents a fully intact RNA [140, 142]. RIN values above 6.5 were accepted and RNA was used for further analysis.

3.3.4. cDNA synthesis and real-time PCR

For cDNA synthesis Moloney Murine Leukemia Virus Reverse Transcriptase (M-MLV RT, Promega) was used. At first 1 µg RNA was mixed with 0.5 µL random hexamer (10 µM) and 0.5 µL oligo dT primer (10 µM) and filled up with H_2O to 25.4 µL reaction volume. Mixture was incubated at 70 °C for 10 minutes and afterwards cooled down (4 °C, 5 minutes). Reverse transcriptase mixture including buffer, dNTPs, RNAsin Plus (Promega) and MMLV-RT–H was added (complete reaction volume 30 µL). The reaction was performed at 42 °C for 60 minutes and inactivated at 95 °C for 5 minutes.

Obtained cDNA was stored at -20 °C until use. Following primers were used in semi-quantitative real-time PCR (**Table 3.12**).

Table 3.12: Primer List for real-time PCR.

	Gene name	**Primer Sequence**
GAPDH	Glyceraldehyde 3-phosphate dehydrogenase	F:5’ CCATGAGAAGTATGACAACAGCC 3’ R:5’ GGGTGCTAAGCAGTTGGTG 3’
ALAS1	Delta-aminolevulinate synthase 1	F:5’ AGATCTGACCCCTCAGTCCC 3’ R:5’ TCCACGAAGGTGATTGCTCC 3’
HPRT	Hypoxanthine-guanine phosphoribosyltransferase	F:5’ GACCAGTCAACAGGGGACAT 3’ R:5’AAGCTTGCGACCTTGACCAT 3’
EF-2	Elongation factor 2	F:5’ ATCATCGAGGAGTCGGGAGA 3’ R:5’ AGCACGTTCGACTCTTCACT 3’
ACTB	Beta-actin	F:5’ AGAGCTACGAGCTGCCTGAC 3’ R:5’ AGCACTGTGTTGGCGTACAG 3’
RPL41	Ribosomal protein L41	F:5’ AAGATGAGGCAGAGGTCCAA 3’ R:5’ TCCAGAATGTCACAGGTCCA 3’
RPL13a	Ribosomal protein L13a	F:5’ CGAGGTTGGCTGGAAGTACC 3’ R:5’ CTTCTCGGCCTGTTTCCGTAG 3’
B2M	Beta-2 microglobulin	F:5’ CACTGAATTCACCCCCACTGA 3’ R:5’ CTGCTTACATGTCTCGATCCCA 3’
PGK1	Phosphoglycerate kinase 1	F:5’ CCACTGTGGCTTCTGGCATA 3’ R:5’ ATGAGAGCTTTGGTTCCCCG 3’
RIPA2	Replication protein A2	F:5’ GGTTTTCCGCTATTCCCCCA 3’ R:5’ GGCTCGGGCTCTTGATTTCT 3’
PPIA	Peptidylprolyl isomerase A	F:5’ ACGTGGTATAAAAGGGGCGG 3’ R:5’ TGTCTGCAAACAGCTCAAAGG 3’
Col1a2	Collagen type I alpha 2 chain	F:5’ AGCCGGAGATAGAGGACCAC 3’ R:5’ CAGCAAAGTTCCCACCGAGA 3’
LH2	Procollagen-lysine,2-oxoglutarate 5-dioxygenase 2	F:5’ CTCGAGCATCCCCACAGATAA 3’ R:5’ TTTCTGGCCCCCTCCAATAC 3’
LOX	Lysyl oxidase	F:5’ CTGGCTACTTCCAGTACGGTC 3’ R:5’ GACATCTGCCCTGTATGCTGT 3’
CALM1	Calmodulin 1	F:5’ GCTCGCACCATGGCTGAT 3’ R:5’ TGGGTTCTGACCCAGTGACC 3’

GARS	Glycyl-tRNA synthetase	F:5’ GCCAGCAGGGAGATCTTGTG 3’ R:5’ ATCTTTGGGCTGTAACGCCA 3’

ALAS1, PPIA, PRT and EF-2 were selected controls and served as housekeeping genes. Candidate controls were LH2, LOX, GAPDH, HPRT, ACTB, RPL41, RPL13a, B2M, PGK-1 and RIPA-2. Targets were CALM-1, COL1A2 and GARS. For qPCR, GoTaq qPCR Master Mix (Promega) was used after manufacturer’s instructions. PCR was run at the Applied Biosystems 7300 Real-Time PCR System until the following thermoprofile: 95 °C 10 min, 40 cycles of 60 °C 1 minute and denaturation at 95 °C for 30 seconds. Afterwards melting curve was analyzed to determine specificity of reaction products.

3.3.5. Data analysis

qPCR data were analyzed for stable reference gene expression using the online tool RefFinder (http://leonxie.esy.es/RefFinder/). This tool contains GeNorm, NormFinder, Bestkeeper and delta delta Ct method algorithm which allows comparison and ranking of experimental candidates. Based on the rankings of each algorithm, the tool calculates geometric means to create a final overall ranking. The relative gene expression was calculated using DataAssist™ Software (Applied Biosystems).

3.4. Evaluation of potential pseudarthrosis marker

The potential pseudarthrosis marker found in proteomic and genomic experiments were glycyl-tRNA synthetase (GARS) and Calmodulin (CALM1). To analyze those two markers, pseudarthrosis tissue samples from human patients were used for histological and immunohistochemical (IHC) staining. Since it is difficult to obtain human tissue control samples, samples from animal models were used as well. Pseudarthrosis biomarker in a fracture of a pseudarthrosis mouse model was analyzed and compared to the fracture of a wild type mouse model. For visualization and quantification of various cell types, proteins and matrix mineralization during fracture healing, histological staining was conducted on these tissues.

3.4.1. Materials and Devices

Table 3.13: List of materials used in pseudarthrosis sample analysis.

Chemicals and Consumables	
Name	**Company, City, Country, [product name]**
ABC-AP Kit	Vector Laboratories, CA, [AK-5200]
Acetone	Carl Roth GmbH, Karlsruhe, Germany, [T906.1]
Acid fuchsin	Waldeck, Münster, Germany, [1A-504]
Alcian blue	Waldeck, Münster, Germany, [2c-005]
Ammoniac 32%	Carl Roth GmbH, Karlsruhe, Germany, [A990.1]
Anti-GARS (EPR7157)	Abcam, Cambridge, United Kingdom, [ab125008]
Anti-Calmodulin (EP7994)	Abcam, Cambridge, United Kingdom, [ab45689]
Bloxall blocking solution	Vector Laboratories, CA, [SP-6000]
Brilliant Crocein R	Waldeck, Münster, Germany, [1B-109]
Buprenorphin (Temgesic®)	Reckitt Benckiser Healthcare Ltd., Slough, UK
Citric acid	Sigma-Aldrich GmbH, Steinheim, Germany, [251275]
Cover slips Automat Star 24 x 50 mm	Engelbrecht GmbH, Edermünde, Germany, [K12450a1,5]
Cryofilm	Section lab Co. Ltd., Hiroshima, Japan, [C-MK001-B2]
Dako dilution buffer	Agilent, Santa Clara, CA, [S2005]
Ethylenediaminetetraacetic acid (EDTA)	Merck, Darmstadt, Germany, [108418]
Eosin G	Carl Roth GmbH, Karlsruhe, Germany, [7089.1]
Ethanol	Carl Roth GmbH, Karlsruhe, Germany, [5054.1]
Eppendorf tubes (1.5 mL, 2 mL)	Sigma-Aldrich GmbH, Steinheim, Germany, [Z606316], [Z606324]
Filter paper	Carl Roth GmbH, Karlsruhe, Germany, [HK83.1]
Formic acid	Merck, Darmstadt, Germany, [100264]
Gelatine	Merck, Darmstadt, Germany, [104070]
Glacial acetic acid	Merck, Darmstadt, Germany, [137000]
Hematoxylin after Shandon	Thermo Fisher Scientific, Waltham, MA, [6765015]
n-Hexane	Carl Roth GmbH, Karlsruhe, Germany, [T908.1]
Hydrochloric acid (HCl) 25 %	Carl Roth GmbH, Karlsruhe, Germany, [6331.1]

Isoflurane	Isotec 4, Groppler medical, Deggendorf, Germany
Methylgreen	Vector Laboratories, CA, USA, [H-3402]
Microlance 3, 0.55 × 25 mm	Becton Dickinson & Company Limited, Drogheda, Co. Louth, Irland, [BEC 300400]
MX35 premier+ microtome blade	Thermo Fisher Scientific, Waltham, MA, [3052835]
Paraformaldehyde (PFA)	Carl Roth GmbH, Karlsruhe, Germany [0335.2]
Phosphotungstic acid	Merck, Darmstadt, Germany, [1005830250]
Pipette tips (0.1-10 µL, 20-200 µL, 100-1000 µL)	Gilson, Inc., Middleton, WI, [F171201], [F171301], [F171301]
Saffron du gatinais	Waldeck, Münster, Germany, [5A394]
SCEM-L embedding medium	Section lab Co. Ltd., Hiroshima, Japan, [C-EM002]
Silver nitrate	Sigma-Aldrich GmbH, Steinheim, Germany, [31630]
Slides SuperFrost Plus	R. Langenbrinck GmbH, Emmendingen, Germany [03-0060]
Sodium chloride (NaCl)	Sigma-Aldrich GmbH, Steinheim, Germany, [31434]
Sodium thiosulfate	Merck, Darmstadt, Germany, [1065090100]
Succrose	Carl Roth GmbH, Germany, [9097.1]
Terumo spinal needle 17, 0.5 × 0.9 mm	Thermo Europe N. V., Leuven, Belgium, [SN*1870]
Tris-(hydroxymethyl)-aminomethan (Tris) base	Carl Roth GmbH, Karlsruhe, Germany, [2449.1]
Tri-sodium citrate dihydrate	Sigma-Aldrich GmbH, Steinheim, Germany, [1.06432]
Triton-X-100	Merck, Darmstadt, Germany, [1086031000]
VectaMount	Vector Laboratories, CA, [H-5000]
Vector Blue – AP substrate	Vector Laboratories, CA, [SK-5300]
Vector Magenta– AP substrate	Vector Laboratories, CA, [SK-510]
VitroClud	R. Langenbrinck GmbH, Emmendingen, Germany [04-0001]
Weigert's iron hematoxylin (Solution A & B)	Carl Roth GmbH, Karlsruhe,Germany, [9192.1]
Xylol	Carl Roth GmbH, Karlsruhe, Germany, [9713.1]

Table 3.14: List of devices used in pseudarthrosis sample analysis.

Devices	
Name	**Company, City, Country**
Camera DFC7000	Leica Microsystem Ldt., Wetzlar, Germany
Contact thermometer IKA ETS-D4 fuzzy	IKA®-Werke Gmbh & Co. KG, Staufen im Breisgau, Germany
Cryostat Leica CM3050S	Leica Biosystems Nussloch GmbH, Nussloch, Germany
Fluorescence X-Cite 200DC	Lumen Dynamics Group Inc., Mississauga, Ontario, Canada
Incubator	Memmert GmbH & Co KG, Schwabach, Germany
Leica microscope DM5500	Leica Microsystem Ldt., Wetzlar, Wetzlar, Germany
Leica microscope 090-135.002	Leica Microsystem Ldt., Wetzlar, Germany
Magnetic stirrer	IKA®-Werke Gmbh & Co. KG, Staufen im Breisgau, Germany
Nikon DsFi 1 digital	Nikon, Tokio, Japan
Rotary microtome RM 2155	Leica Biosystems Nussloch GmbH, Nussloch, Germany
Vortex Genie 2	Scientific Industries, Inc., Bohemia, NY

Table 3.15: List of software used in pseudarthrosis sample analysis.

Software	
Name	**Company, City, Country**
LASX version 3.0	Leica Microsystem Ldt. Wetzlar, Germany
Office 2007	Microsoft, Redmond, WA
SPSS statistics version 24	IBM, Armonk, NY

3.4.2. Human pseudarthrosis samples

Tissues came from patients who underwent a pseudarthrosis operation. Included were patients who have completed the 18th year of life and had a fracture healing delay of >6 months. Excluded were patients with a delay in fracture healing of <6-month, pregnant patients and patients with an infectious pseudarthrosis.

The experiments were approved by the local ethical committee of the Medical Faculty of the Justus Liebig University of Giessen (Reference number: AZ 79/17). Pseudarthrosis

samples as well as characteristics of the pseudarthrosis type are presented in **Table 3.16**. Weber and Cech classified non-union regarding their biological aspects. In this classification, pseudarthrosis are differentiated in hypertrophic ("vital") and atrophic ("avital") pseudarthrosis. This classic classification is still used for the basic evaluation of non-unions [143].

Table 3.16: Pseudarthrosis samples and localization of pseudarthrosis in patients.

Sex	Age	Localization	Notes
M	77	Femur	Aseptic hypertrophic pseudarthrosis
M	57	Metatarsal	Aseptic hypertrophic pseudarthrosis
F	61	Femur	Aseptic atrophic pseudarthrosis
F	73	Humerus	Aseptic atrophic pseudarthrosis

Pseudarthrotic tissue was collected from the fracture cap during revision surgical treatment and fixed in 4 % PFA for 24h. Samples were used for cryo embedding.

3.4.3. Cryo Embedding

For cryo embedding, human pseudarthrosis samples were fixed in 4 % PFA for 24 hours. Afterwards, samples were put in sucrose solutions (10 %, 20 %, 30 %) for 24 hours each in order to dehydrate the tissue. Samples were then placed in stainless steel molds and mounted with embedding medium. The molds filled with medium were dipped into a n-hexane beaker, which was already placed in a Dewar vessel filled with dry ice/acetone mixture. After hardening of the block, molds were removed, and blocks were wrapped in cellophane and immediately stored at -80 °C. A cryostat microtome was used to cut 4-µm-thick-sections. Samples were cut with the Kawamoto method using Kawamoto's films [144]. Therefore, films were placed on the surface of the block; the block was lowered slowly over the edge of the blade and grabbed with pliers during cutting. Film with the cut section was placed on a glass slide adhered to double sided tapes.

3.4.4. Hematoxylin and Eosin (H&E)

The hematoxylin-eosin (H&E) stain is one of the standard stains for histological examination of human tissue and allows a general overview of the sections. Basophilic/hematoxophilic structures, like nuclei or rough endoplasmic reticulum, are

stained in blue, while acidophilic/eosinophilic structures, like cell membrane, proteins, mitochondria, will be stained in red/pink [145, 146].

H&E staining was done for the human pseudarthrosis tissue samples. Eosin solution was prepared by dissolving 10 g of eosin in 1000 mL aqua dest, adding 10 drops of glacial acetic acid and stirring for 30 min at RT. Cryostat sections were left at room temperature (RT) for 30 minutes and then rehydrated in distilled water for 5 minutes. After that, sections were stained with hematoxylin solution for 30 seconds and washed with distilled water. For blueing, sections were put into running tap water for 10 minutes and washed with distilled water. For staining of connective tissue, slides were put into 1% fresh-filtered eosin solution for 1 minute and then washed with distilled water. After that sections were rehydrated using an ascending percentage of ethanol 70 %, 80 %, 96 %, 100 % for 5 minutes each, cleared in xylol, two changes for 5 minutes each and cover slipped after mounting with vitroclud.

3.4.5. Movat's Pentachrome

The Movat's pentachrome staining differentiates bone healing processes like cartilage formation, hypertrophy, and matrix mineralization in detail [146, 147]. The staining can be used for descriptive histology as well as for histomorphometry. Thus, this stain is useful in the study of bone healing. In this colouring method, mineralized tissue is shown in yellow. Cartilage is shown in green, while new formed osteoids are red and nuclei in brown. In this study, human pseudarthrosis samples were stained with Movat's pentachrome. Following solutions had to be prepared (**Table 3.17**).

Table 3.17: Movat's pentachrome solutions.

Solution	Preparation
25 % Ammonia	78 mL of ammonia (32 %) + 22 ml aqua dest
Alkaline ethanol	20 mL of ammonia (25 %) + 180 mL ethanol 96 %
Weigert's hematoxylin	Solution A: Solution B mix in 1:1 ratio (directly before use)
Brilliant grocein-fuchsine	Solution A: 0.1 g Brilliant grocein R in 99.5 mL aqua dest. and 0.5 mL glacial acetic acid Solution B: 0.1 g fuchsine acid in 99.5 mL aqua dest and 0.5 mL glacial acetic acid

	Working solution: Mix A and B in 5:1 ratio
Phosphotungstic acid	Dissolve 5 g phosphotungstic acid in 100 mL aqua dest
Saffron du Gatinais	Dissolve 6 g Saffron du Gatinais in 100 mL 100 % ethanol and incubate for 48 hours at 50 °C, filtrate before use

Cryostat sections were left at room temperature (RT) for 30 minutes and then rehydrated in distilled water for 2 minutes. The following steps were conducted:

1. Stain in alcian blue for 10 minutes.
2. Wash in running tap water for 5 minutes.
3. Stain in alkaline ethanol for 1 hour.
4. Wash in running tap water for 10 minutes.
5. Rinse in distilled water.
6. Place in Weigert's iron hematoxylin stain for 10 minutes.
7. Rinse in distilled water.
8. Wash in running tap water for 15 minutes.
9. Place in brilliant crocein R-fuchsine solution for 12 minutes and 30 seconds.
10. Place in 0.5 % aqueous acetic acid for 30 seconds.
11. Place in 5 % phosphotungstic acid for 20 minutes.
12. Place in 0.5 % aqueous acetic acid for 2 minutes with continuous shaking.
13. Place in three changes of absolute ethanol for 5 minutes each.
14. Place in the saffron du gâtinais dye for 1 hour.
15. Dehydrate quickly in absolute ethanol, 3 changes. Then place it in absolute ethanol for 2 minutes.
16. Clear in xylol, two changes for 5 minutes each.
17. For cryostat sections, do not forget to cut the golden edges of the film before mounting, drain-dry then mount.
18. Cover slip slides after mounting, use a resinous mounting medium (VitroClud).

3.4.6. Immunohistochemical staining

Immunohistochemical staining (IHC) identifies antigens on tissue sections by exploiting the principle of antibodies binding specifically to antigens. Thus, IHC is used to evaluate the possible pseudarthrosis biomarker found in proteomic experiments in human

pseudarthrosis tissue sections. Generally, this technique contains several steps. Staining of the potential biomarkers is the analytical part of the IHC process and encompasses antigen retrieval, application of the primary antibody and visualization system as well as counterstaining. During tissue fixation, antigens may have been altered, so the antigen retrieval step is necessary for recovery of the antigens epitopes. This is done either by heat (heat-induced epitope retrieval; HIER) or by enzymatic degradation [148, 149]. After retrieval of antigens, endogenous enzymes are blocked, and primary antibody is applied that specifically binds to the antigen of interest. The secondary antibody carries an enzymatic label. Upon application it binds to the primary antibody. The antigen/antibody complex signal is amplified and visualized by use of a detection system like the avidin-biotin complex (ABC). In the ABC method, the secondary antibody is biotinylated, while the detection system is encompassed of avidin mixed with biotin which is linked to an appropriate label (enzyme, e.g. alkaline phosphatase AP). The avidin and biotinylated alkaline phosphatase are incubated for about 30 minutes before application. Thereby a large complex with numerous molecules of labels is developed. Afterwards, an alkaline phosphatase (AP) substrate solution is used. AP catalyses the hydrolysis of phosphate groups from the substrate, resulting in a coloured insoluble precipitant depicting the antigen. To visualize nuclei and overall tissue architecture, counterstaining is performed as last step before sections are dehydrated, mounted and cover-slipped [148-150]. For the IHC staining, following solutions were prepared (**Table 3.18**).

Table 3.18: Immunohistochemistry solutions.

Solution	Preparation
10x Tris-NaCl-Buffer (TBS)	Dissolve 60.57 g Tris Base and 87.66 g NaCl in 800 mL distilled water, adjust pH with 25 % hydrochloric acid (HCl) to 7.4, fill up to 1000 mL with distilled water.
1x TBS	Dilute the above in the ratio of 1:10 with distilled water
Tris-Washing buffer	TBS 1x, 0.025 % Triton-X-100 To 100 ml TBS 10x add 0.25 g of Triton X-100 and make the volume up to 1000 mL with distilled water.
Tris-HCl-Buffer	For 10x Tris-HCl-Buffer: Dissolve 121.1 g Tris Base in 900 mL distilled water, adjust pH with 25 % HCl to 8.3, fill up to 1000 mL with distilled water

1x Tris-HCl-Buffer	Dilute the above in the ratio of 1:10 with distilled water
Tris-EDTA-Buffer	Dissolve 1.21 g Tris Base and 0.37 g EDTA in 1000 mL distilled water. Adjust pH to 9.0 with 10 N NaOH.
Citrat-Buffer pH 6,0	Solution A: 0.1 M citric acid Dissolve 2.1 g in 100 mL distilled water. Solution B: 01 M Tri-Sodium citrate dehydrate 29.4 g in 1000 mL distilled water. Mix 41 mL of solution B with 400 mL distilled water. Adjust pH to 6.0 with solution A and fill up to 500 mL with distilled water.
ABC-AP complex	Mix ABC-AP complex (Vector Laboratories) 30 minutes before use. 5 µL reagent A and 5 µL reagent B in 500 µL 1xTBS.
AP-Substrate	Vector® Red (Magenta) or Vector®Blue: Add 2 drops of reagent 1, 2 drops of reagent 2 and 2 drops of reagent 3 to 5 mL of Tris HCl buffer
Acetone/glacial acetic acid	100 mL acetone + 50 µL glacial acetic acid
Silver staining	Solution A: 1 % formic acid + 2 % gelatine Dissolve 0.5 g gelatine from bovine skin in 24.7 mL bidistilled water and add 250 µL formic acid. Solution B: 50 % silver nitrate Dissolve 5 g silver nitrate in 10 mL distilled water. Mix solutions A and B in a 1:2 ratio.

Cryo sections: leave for 30 minutes at RT in 1xPBS, proceed with step 1.

1. Place in technical acetone for 10 minutes.
2. Place in mixture of technical acetone and washing buffer (1:1) for 10 minutes.
3. Wash slides in washing buffer for 2x10 minutes.
4. HIER-antigen-retrieval for 1 hour at 60 °C, then cool for 10 minutes in ice.
5. Wash slides in washing buffer for 2x5 minutes.
6. Block endogenous enzymes with bloxall blocking solution for 10 minutes.
7. Wash slides in washing buffer for 2x5 minutes.
8. Block with universalserum from ABC-AP kit (Vector Laboratories); 1 drop of universalserum in 5 mL of 1xTBS.
9. Remove the blocking.

10. Incubate with primary antibody at 4 °C overnight.
11. Remove the antibody.
12. Wash slides in washing buffer for 2x5 minutes.
13. Add secondary antibody and incubate for 30 minutes.
14. Wash slides in washing buffer for 2x5 minutes.
15. Add ABC-AP complex for 30 minutes at RT.
16. Wash slides in washing buffer for 2x5 minutes.
17. Wash slides in distilled water for 5 minutes.
18. Add AP substrate until a clear colour is detected.
19. Wash slides in distilled water for 2x5 minutes.
20. Counter stain with methylgreen or silver and mount.

Procedure for counterstaining with methylgreen is as following:

1. Add methylgreen to slides and incubate for 5 minutes at 60 °C.
2. Wash with distilled water until no colour is washed out anymore.
3. Incubate slides in distilled water for 1 minutes.
4. Dip slides 5-10x in a mixture of acetone/glacial acetic acid
5. Dehydrate in 95 % and then in 100 % ethanol for 1 minute each.
6. Dry slides for 30 minutes at 60 °C in incubator.
7. For cryostat sections, do not forget to cut the golden edges of the film before mounting, drain-dry then mount.
8. Cover-slip slides after mounting; use a resinous mounting medium (Vitroclud).

For the CALM1 primary antibody (rabbit monoclonal, EP799Y, ab45689), a concentration of 1:2000 in Dako antibody dilution buffer with background reducing components was used on paraffin slides and cryo sections. Antigen retrieval was done with Tris-EDTA-Buffer for one hour at 60 °C. For AP-substrate Vector Blue (Vector laboratories) was used. For human pseudarthrosis samples methylgreen was used as counter stain.

For the GARS primary antibody (rabbit monoclonal, EPR7157, ab125008), a concentration of 1:100 in Dako antibody dilution buffer was used on paraffin and cryo sections. Antigen retrieval was done with citrate buffer for one hour at 60 °C. For AP-substrate Vector Red (Vector laboratories) was used. Methylgreen was used as counter stain for human pseudarthrosis samples.

3.4.7. Microscopy

A Leica microscopy system (Leica DM5500 photomicroscope equipped with a DFC7000 camera and operated by LASX software version 3.0; Leica Microsystem Ltd., Wetzlar, Germany) was used for images. From Movat's pentachrome and H&E stained sections, 10x magnification overviews were conducted. GARS and CALM stained sections were photographed with 10x magnification for overviews and 20x and 40x magnification for detailed images. Fluorescent visualization of anti-GARS was measured using Texas-Red filter (Leica Microsystem Ltd., Wetzlar, Germany) at an emission of >560 nm. The excitation wavelength range was set from 365 nm to 560 nm for fluorescent substrate (Vector Red: Excitation: broad excitation spectrum, approx. 365 nm to 560 nm; Emission: above 560 nm).

Fluorescent visualization of anti-CALM1 was measured using Texas-Red filter (Leica Microsystem Ltd., Wetzlar, Germany) at an emission of >560 nm. The excitation wavelength range was set from 365 nm to 560 nm for fluorescent substrate (Vector Blue: Excitation: broad, peak at ~500 nm; Emission: broad, peak at ~680 nm).

Additionally, von Kossa staining of cells was studied by inverted light microscopy using a Leica microscope type 090-135.002 (Leica Microsystems GmbH, Wetzlar, Germany) equipped with a Nikon Ds-Fi1 digital camera (Nikon, Tokio, Japan). Magnification was 40x.

3.5. Comparison of atrophic and hypertrophic pseudarthrosis

The etiology of several diseases, including cancer, autoimmune disorders, and metabolic conditions, is connected to specific amino-acyl tRNA synthetases like GARS [151-153]. CALM1, acts as a calcium sensor and binds to calcium. In turn, the formed protein-calcium complex is involved in the regulation of several cellular processes, including smooth muscle contraction, inflammation, apoptosis, and immune response [154-156]. In our study we hypothesized that patient's risk factors increase the risk of pseudarthrosis. Special attention was thereby paid to factors like allergies, overweight, medical drug usage, morbidities like diabetes mellitus as well as age and gender of patients. Those risk factors have an impact on inflammation, immune response, and metabolic conditions. Moreover, this study compared characteristics of atrophic and hypertrophic

pseudarthrosis patients to determine whether systemic factors influence type of pseudarthrosis.

Patient's data was collected by PD Dr.med. Markus Rupp and PD Dr.med. Adrian Skwara. Data collection was a retrospective analysis of patient's data from 2005 to 2010 in the University of Münster. It was approved by the local ethical committee of medical association of Westfalen-Lippe and the medical faculty of the University of Münster. According to the Weber-Cech classification pseudarthrosis were classified as hypertrophic and atrophic by radiological assessment. Thusly, pseudarthrosis were classified as atrophic when no callus formation and no signs of bony bridging of the fracture gap was seen on X-rays before surgical revision. Callus formation without joined fracture ends were rated as hypertrophic pseudarthrosis.

3.5.1. Including and excluding criteria

Study included patients with a fracture non-union (fracture healing delay > six months). Patients with an age of above 18 years were included in the study. This age was chosen because skeletal maturity is achieved by approximately 18 years of age. Excluded were patients with a delay in fracture healing less than six months, pregnant and nursing patients, and patients with a septic pseudarthrosis.

3.5.2. Potential risk factors for aseptic pseudarthrosis

By evaluating of risk factors for non-unions, we hypothesized that the probability of fracture pseudarthrosis can be determined. The following data were assessed for all participants.

- Age and Gender

  Age and gender of pseudarthrotic patients were evaluated in this study. Time between osteosynthesis of the fracture and pseudarthrosis revision surgery was also determined.

- Body mass index (BMI, calculated as weight in kilograms (kg) divided by height in meters squared (m^2))

  People were considered obese with a BMI over 30 kg/m^2. The range of 25-30 kg/m^2 was defined as overweight, 18.5-25 kg/m^2 as normal weight and <18.5 kg/m^2 as underweight [157, 158].

- Osteosynthesis (medullary nail, cerclage, screw fixation, plate)

Main fracture fixation was evaluated, such as intramedullary nailing, plating, screw fixation and wire cerclage fixation. In case of an osteosynthesis combination, main osteosynthesis procedure was chosen.

- Fracture type (closed/open)

  Fractures were distinguished between open and closed fractures.

- Loosening of implant (yes/no)

  As possible reason for pseudarthrosis development implant loosening was assessed by X-rays taken before revision surgery. Signs of implant movement were plate-, screw- and wire-breakage as well as lysis zones around the implants.

- Allergy (yes/no; number of allergies)

  Type and number of allergies were assessed from the medical records of pseudarthrosis patients.

- Morbidities (diabetes mellitus (DM), nicotine, cardiovascular disease (CD))

  Common risk factors for pseudarthrosis development such as nicotine abuse, diabetes mellitus and cardiovascular diseases as well as combinations of those morbidities were assessed for all patients.

- Types of pseudarthrosis (atrophic, hypertrophic)

  According to the Weber-Cech classification, pseudarthrosis samples were classified as either atrophic or hypertrophic [143, 159, 160]. Atrophic pseudarthrosis was diagnosed when no callus and no signs of bony consolidation in the fracture gap was seen. Pseudarthrosis were considered as hypertrophic when callus formation around the fracture gap and calcification without enough consolidation within the fracture zone was seen.

- Non-steroidal anti-inflammatory drug (NSAID) (known to influence bone healing)

- Leucocytes [Tsd/µL]

  Laboratory tests before non-union revision surgery provided information of leucocytes (Tsd/µL).

- Osteosynthetic concomitant injuries (yes/no)

  Concomitant injuries were assessed as well in this study.

3.6. Microbial infections in septic non-unions

In orthopaedic surgery, infections seem to complicate successful fracture healing. That is the reason why it is important to diagnose infections and to treat them. In this study

incidence and rates of microbial infections in septic pseudarthrosis were evaluated. Furthermore, potential risk factors and post-operative outcome factors of monomicrobial and polymicrobial infections as well as germ-changes within course of pseudarthrosis treatment were analyzed. In focus of the study was also the number of surgical revisions in patients with septic pseudarthrosis.

Patient's data was collected by medical doctoral students Tamina Denise Menges and Tobias Wagner under my supervision. Data came from the department of trauma, hand and reconstructive surgery of the university hospital Giessen and Marburg, campus Giessen. The ethics committee of the Justus-Liebig-University Giessen, Germany, approved the study, AZ 68/18. Data was obtained from the clinical electronically data processing system. Medical records of all surgically treated patients suffering from septic pseudarthrosis between January 2010 and December 2017 was retrospectively reviewed in this study.

3.6.1. Including and excluding criteria

Study included patients with a septic fracture pseudarthrosis (fracture healing delay > six months). Patients with an age of 18 years or older at time of revision surgery were included in the study. This age was chosen because skeletal maturity is achieved by approximately 18 years of age. Excluded were patients with a delay in fracture healing less than six months, pregnant and nursing patients. Only pseudarthrosis in the long bones of the arms and legs (femur, tibia, fibula, humerus, radius and ulna) were included in this study.

Septic pseudarthrosis was diagnosed if at least one of the following criteria were present:

- presence of a sinus tract
- purulent discharge
- exposed osteosynthesis material
- positive microbiological culture result
- histologically confirmed infection (>5 granulocytes per field of view at a magnification of 400x)
- >2000 leucocytes/µL in synovial fluid
- >70% of cells were identified as granulocytes in synovial fluid of concomitant septic arthritis

Patient's medical history and clinical symptoms like erythema, swelling, rest pain and pain on weight bearing were considered as suggestive parameter for septic pseudarthrosis. Elevated infection parameters in laboratory tests and radiological signs of infection (osteolysis, implant loosening, sequester formation) were also considered as septic parameters.

3.6.2. Microbial diagnosis

After each revision surgery, microbiological cultures of intraoperatively collected tissue were generated. Tissue samples, sonication fluid of osteosynthesis implants or synovial fluid in case of joint involvement were used for these microbiological cultures. Samples were cultured on blood agar plates incubated at 37 °C seven days (aerobic microorganisms) and for 14 days (anaerobic microorganisms), respectively. Microorganisms were identified and antimicrobial susceptibility testing using standard microbiological techniques were performed afterwards. Only initial proof of polymicrobial infections was regarded as polymicrobial infections. Consecutively determined different pathogens during surgical treatment were regarded as germ-changes

3.6.3. Potential risk factors for septic pseudarthrosis

Potential risk factors for septic pseudarthrosis were evaluated in this study to test the hypothesis that the probability of septic fracture pseudarthrosis can be determined. The following characteristics were assessed for all participants in this study:

- Age and Gender
- Body mass index (BMI, kg/m^2)
- Osteosynthesis (medullary nail, cerclage, screw fixation, plate)
- Fracture type (closed/open)
- Loosening of implant (yes/no)
- Allergy (yes/no; number of allergies)
- Types of pseudarthrosis (atrophic, hypertrophic)
- Fracture localization after AO/OTA

  Fracture localizations were classified with an alphanumeric coding scheme after the AO/OTA foundation. Advantage of the standardized fracture classification is the use of the obtained data in retrospective studies [161].

- ASA (American Society of Anaesthesiologists) classification

  Physical status of patients was classified utilizing the ASA classification system. Class I were patients with normal health, non-smoking, no medical abuse. Patients with severe systemic disease, current smoker, obesity (30<BMI<40), mild lung disease, controlled DM were classified as class II. Class III patients had severe systemic diseases and substantive functional limitations, i.e. poorly controlled DM, lung disease, morbid obesity (BMI>40). Class IV were patients with severe systemic disease that is a constant threat to life. Class V patients were patients without expectation to survive without operation [162, 163].
- Morbidities (diabetes mellitus (DM), nicotine, cardiovascular disease (CD), thyroid disease, autoimmune diseases)
- Osteosynthetic concomitant injuries (yes/no)
- Laboratory values: Leucocytes [Tsd/µL]
  CRP (c-reactive protein) [mg/L]

3.7. Statistical analysis

Data were analyzed using SPSS statistics version 24.0 (IBM, SPSS Inc., Armonk, NY). Collected data sets from proteomics, RT-PCR and clinical data were explored for normality with descriptive statistics. In case of normality, Student's T test was used to determine if the means of two sets of data are significantly different from each other. Significance analysis for non-parametric distribution was performed using Mann-Whitney U-test or Wilcoxon's signed rank sum test.

Frequencies for all pseudarthrosis risk factors were calculated. For analyses of differences between patients, the chi-squared (χ^2)-test or Fischer's exact test was applied for categorical variables. Wilcoxon's signed rank sum test and the Mann-Whitney U-test were applied for between-group comparisons from clinical data. The critical value for significance was set at $p<0.05$. Data were exhibited in graphs as means ±SEM.

4. Results

4.1. Cell culture

4.1.1. Von Kossa showed lower matrix mineralization in osteogenic stimulated fibroblasts

Mesenchymal stromal cells and fibroblasts share many characteristics such as the potential to differentiate to osteoblasts, adipocytes, and chondrocytes. The differentiation capacity of fibroblasts (FC) and MSCs (SCC) derived from human patients was evaluated for osteoblast differentiation. Therefore, cells were cultured in medium supplemented with osteogenic induction components. Von Kossa staining showed mineralized patches of MSCs and fibroblasts treated with osteogenic medium (**Figure 10**). Descriptively, MSCs-derived osteoblasts (SCO) showed higher matrix mineralization compared with osteoblast-like fibroblasts (FO).

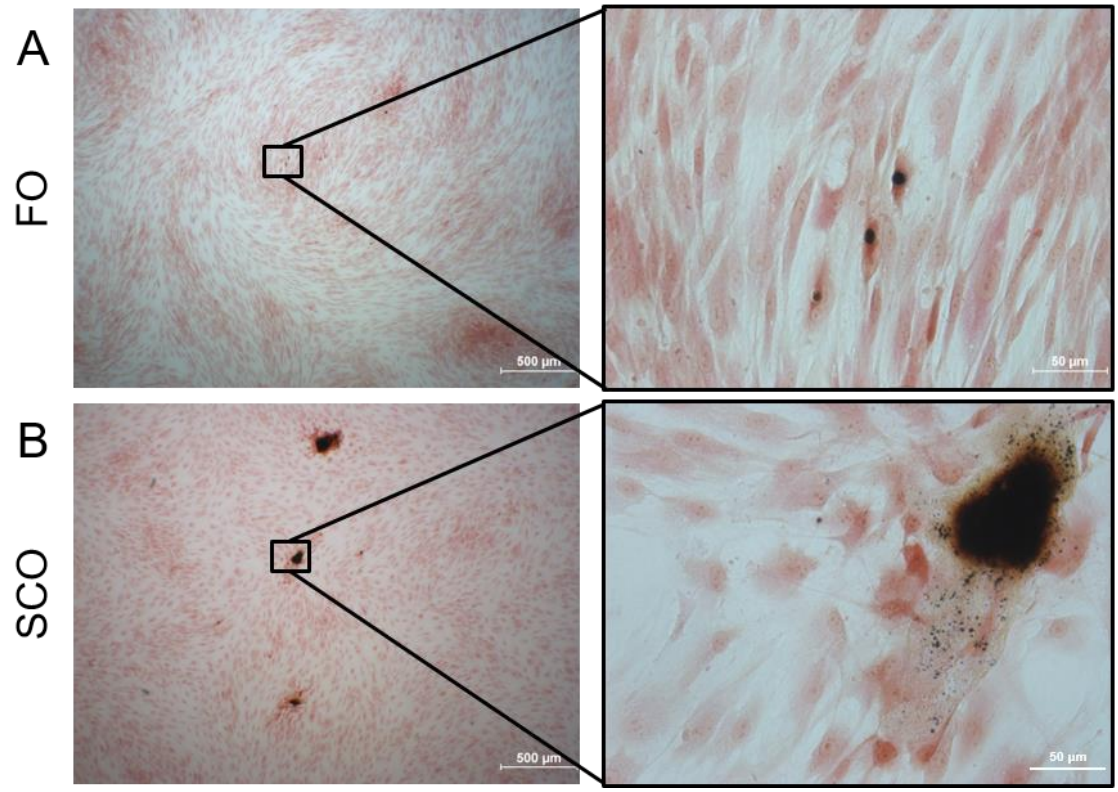

Figure 10: Von Kossa staining indicated differentiation capacity and matrix mineralization in osteogenic simulated cell indicated by black patches. A) Fibroblasts were induced to differentiate into osteoblast-like cells (FO). Matrix mineralization was seen as black patches in von Kossa staining. B) MSCs were differentiated into osteoblasts (SCO). Descriptively, matrix mineralization of MSC-derived osteoblasts was higher when compared with osteoblast-like fibroblasts Magnification: left panels 10x, right panels 40x.

Successful differentiation of fibroblasts into osteoblast-like fibroblasts encouraged proteome analysis of the four different cell types. Therefore, bottom-up proteomics was conducted with nano-HPLC-ESI mass spectrometry to analyze up- and down-regulation of proteins and genes in differentiated fibroblasts and MSCs.

4.2. Proteomics

4.2.1. Mass spectrometry identified biomarker to distinguish cell types

Mass spectrometry was successfully used to address the characterization of mesenchymal stromal cells and fibroblasts before and after osteogenesis. Out of the 2470 total protein, 193 proteins were common in all biological (SCC, SCO, FC, FO) and technical replicates, so they were considered as high abundant.

Corresponding to the 193 proteins, their gene symbols were imported into DAVID online tool for functional annotation and gene enrichment analysis and a total of 174 terms were generated. Significant terms (p<0.01) in which CALM1 and/or GARS were involved were highlighted (**Figure 11**).

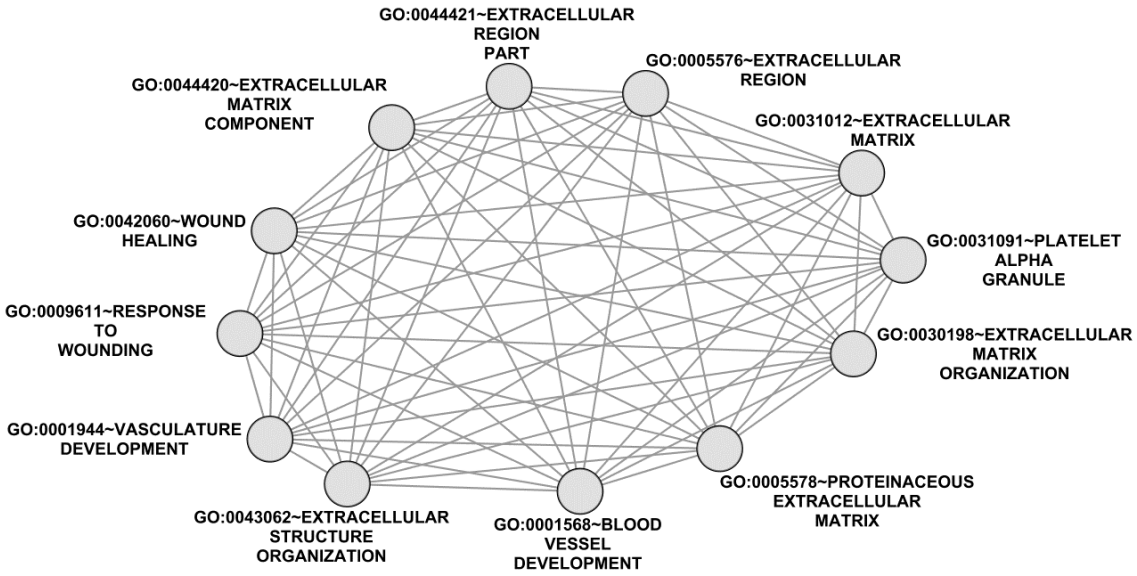

Figure 11: Enrichment map network analysis of genes corresponding to proteins found in mass spectrometry analysis. Under the up-regulated gene ontologies, extracellular matrix (ECM) components, like structure organization, region part, organization, and proteinaceous ECM were connected to blood vessel, platelet granule and vasculature development. Moreover, up-regulated genes were connected to wound healing and response to wounding. Up-regulation of those genes could explain the inferior mineralization.

From mass spectrometry analysis, the intensity values with the list of proteins were obtained. The quality of the data was tested by computing correlation between different cells types. No replicates were removed. The data was normalized using delta delta ct method. The differentially expressed proteins were obtained after applying the criteria of fold change (FC) ≥ |2| and p-value ≤ 0.01. Three proteins (**Table 4.1**) were differentially expressed under osteogenic differentiation of fibroblasts.

Table 4.1: Differentially expressed proteins in fibroblasts after osteogenic stimulation. Protein functions were identified using UniProt and GeneCards databases. [135]

No	Protein Name	Function	Gene Name	FC	p-value
1	calmodulin 1	Calcium-binding protein which mediates the control of enzymes, ion channels and other proteins.	CALM1	2.07	0.000931
2	collagen type I alpha 2	Member of group I collagens. A fibrillar forming collagen.	COL1A2	2.09	0.00309
3	glycine-tRNA synthetase	Aminoacyl-tRNA synthetase that charge tRNAs with their cognate amino acids.	GARS	2.09	0.00677

GBA (guilt by association) network analysis was used to predict the interactions of the possible candidate biomarkers with NF1. Therefore, CALM1, COL1A2, GARS and NF1 were put in the query of two different meta-search platforms and analysis was conducted. NF1 was included into the network analysis because mutations in NF1 causes neurofibromatosis 1, an autosomal dominant disease. Tibial pseudarthrosis and persistent fracture pseudarthrosis are among the manifestations associated with neurofibromatosis 1 [164]. Results from the meta-search platforms GeneMANIA (**Figure 12 A**) and STRING (**Figure 12 B**) showed the same genes in both meta-searches. Among these genes are several collagens, COL1A1, COL3A1 COL5A1 and COL6A3, which were co-expressed with COL1A2. COL1A2 showed also co-expression with SPARC (Secreted protein acidic and rich in cysteine) and LUM (Lumican Proteoglycan) in both platforms. However, network comparison also illustrated differences in data obtained from both platforms. Interestingly, STRING meta-search did not obtain information about interaction of NF1 and CALM1 under the given parameter (co-localization, co-expression, high confidence interaction score 0.700) with any other gene.

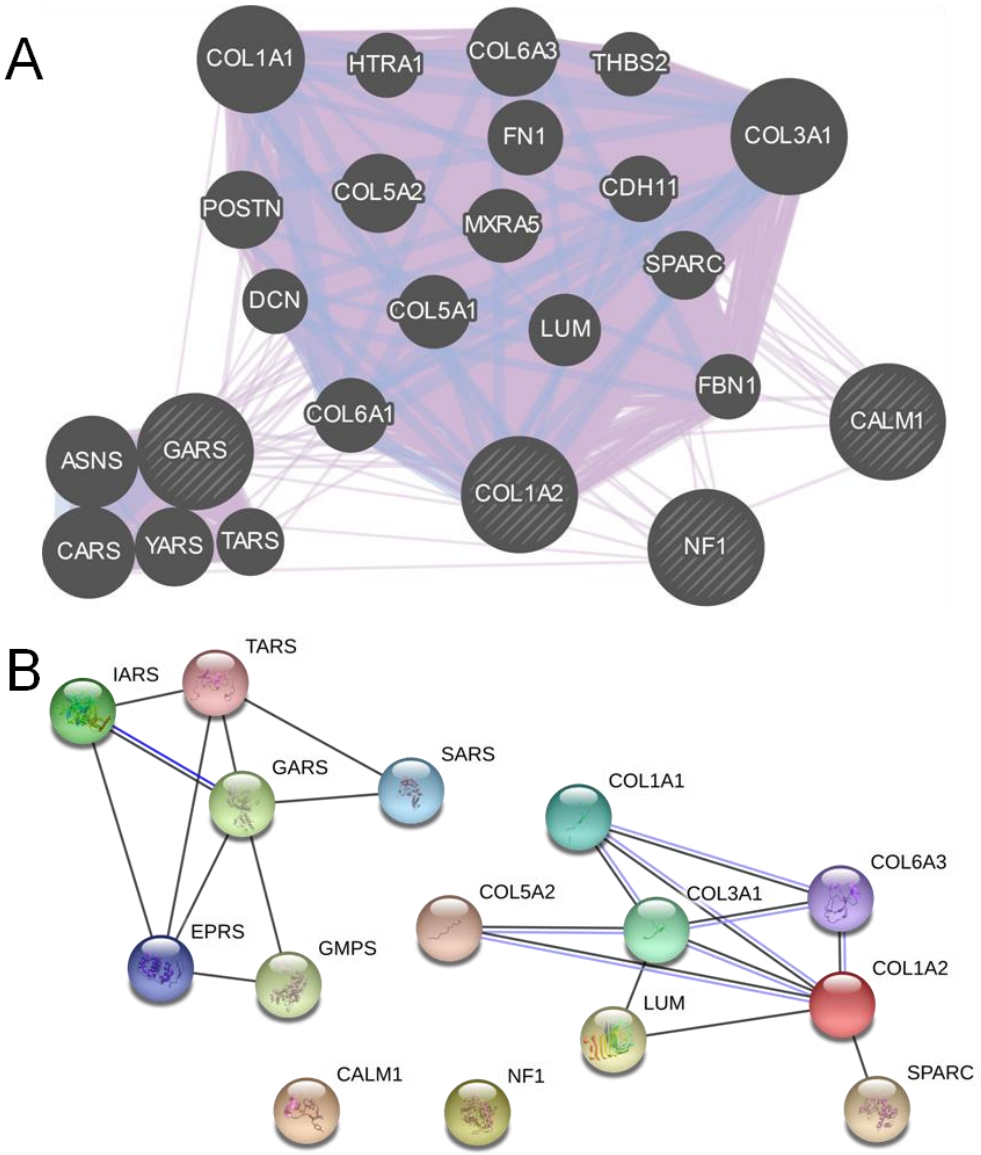

Figure 12: GeneMANIA and STRING results for network analysis revealed differences in the meta-search platforms. The network view summarizes the network of predicted interactions. The network nodes are proteins. The edges represent the predicted functional associations. A) GeneMANIA network showed co-expression and co-localization of 20 genes with CALM1, COL1A2, GARS, and NF1 indicated by edges. B) STRING analysis resulted in two clusters, one cluster with GARS in the center and the other with COL1A2. Blue edges indicate co-occurrence and black edges show co-expression. In STRING meta-search, CALM1, and NF1 showed no co-expression or co-occurrence in the network with other genes.

To get an in-depth network analysis, results from both platforms were merged with cytoscape (**Figure 13 A**).

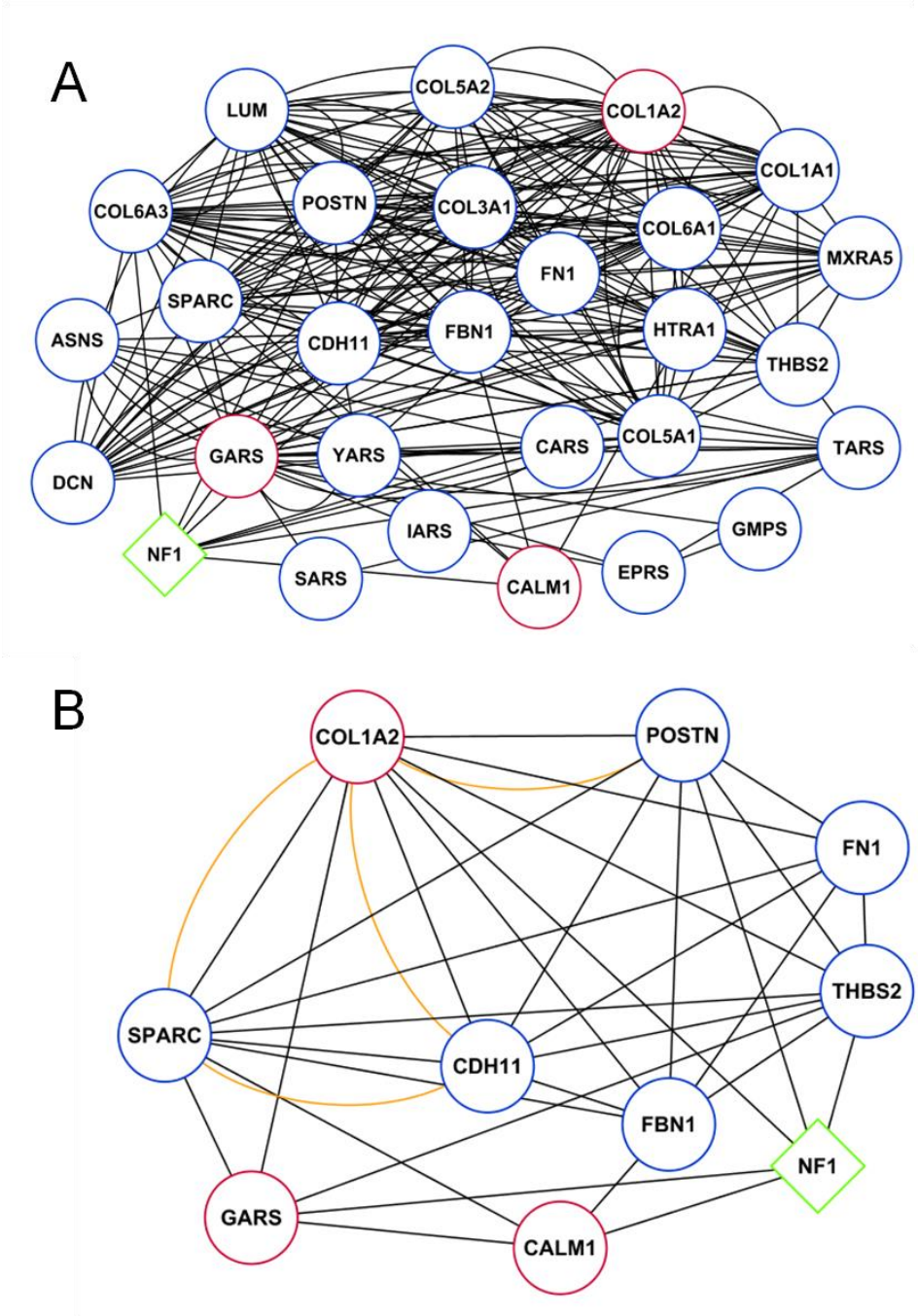

Figure 13: Merged network map showed interaction of candidate biomarkers (GARS, CALM1 and COL1A2) with NF1. The network nodes are proteins. The edges represent the predicted functional associations. A) Datasets from GeneMANIA and STRING were merged in cytoscape to add more evidence to the results from the quantitative proteomic study. Network illustrates the degree of connectivity and interactions of genes. B) After selection of genes relevant to bone, pseudarthrosis, and NF1, network showed interactions of those genes with the predicted biomarkers CALM1, COL1A2, and GARS. Black edges indicate co-expression while orange edges indicate co-localization.

To narrow down the list and enhance reliability of the results, genes related to bone diseases ECM and immune system were selected in the merged network to predict the interactions of candidate biomarkers with these genes (**Figure 13 B**).

Network analysis revealed interaction of possible pseudarthrosis biomarkers with genes related to bone, bone diseases, ECM, NF1, and immune system. Protein functions of those genes were identified using UniProt and GeneCards databases. [135]

CALM1 showed direct interaction with GARS, FN1, NF1, and SPARC. COL1A2 showed co-expression and co-localization with CDH11, FBN1, FN1, GARS, NF1, POSTN, SPARC, and THBS2. GARS showed apart from co-expression with CALM1, COL1A2, and NF1, direct interaction with SPARC and THBS2.

CDH11 (cadherin-11) is a calcium-dependent cell adhesion protein which is involved in the canonical Wnt pathway and plays a role in bone formation. In this network analysis, CDH11 was directly connected to the potential biomarker COL1A2.

Another gene which is directly involved in bone formation is FN1 (fibronectin 1). Functions of FN1 are binding of cell surfaces and compounds such as collagen and fibrin. Moreover, FN1 is involved in cell adhesion, wound healing and is essential for osteoblast mineralization. FN1 showed direct interaction with the possible biomarkers CALM1 and COL1A2.

SPARC (secreted protein acidic and rich in cysteine, also osteonectin) is also required for bone matrix mineralization. Here, SPARC showed direct interaction with CALM1, Col1A2 and GARS.

Directly connected with COL1A2 was also POSTN (periostin) which was also directly connected to NF1. POSTN not only induces cell attachment and is involved in cell adhesion, but it also enhances incorporation of BMP1 (bone morphogenetic protein 1) in the fibronectin matrix of connective tissue.

THBS2 (thrombospondin-2) is an adhesive glycoprotein that mediates cell-to-cell and cell-to-matrix interactions. It may also be involved in the modulation of cell surface properties of mesenchymal stem cells. In this analysis, THBS2 showed direct interaction with GARS, COL1A2, and NF1.

FBN1 (fibrillin-1) is an extracellular matrix glycoprotein which serves as a structural component of calcium-binding microfibrils and was also directly connected to CALM1 and COL1A2.

Protein expressions in osteoblasts derived from MSCs and osteoblast-like fibroblasts were different after the osteogenesis, pointing out that their behavior in bone repair might be different. Thus, this study aimed to evaluate CALM1 and GARS and their potential role as biomarkers for pseudarthrosis.

To validate results found in proteomics, genome experiments of the four different cell types were conducted as well. Therefore, RT-PCR was utilized.

4.3. Genomics

4.3.1. RT-PCR confirmed results found in proteomic studies

Expression of several genes was determined by RT-PCR. Molecular testing of gene expression verified the identification of the potential pseudarthrotic biomarker found in proteomics. CALM1, COL1A2, and GARS were down-regulated after osteoblastic differentiation of MSCs and fibroblasts, although not significantly (**Figure 14**).

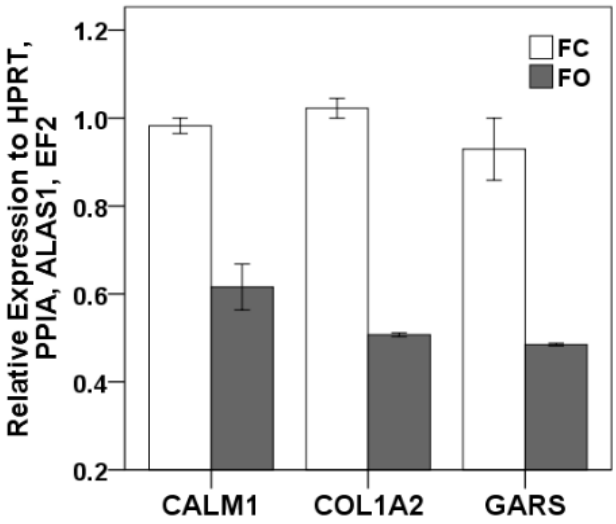

Figure 14: Relative expression displayed discrepancies in gene expression between osteogenic differentiated fibroblasts and control cells. Under osteogenic differentiation, fibroblasts (FO) showed lower expression of CALM1, COL1A2, and GARS when compared to control fibroblasts (FC).

To further evaluate potential biological pseudarthrosis marker, GARS and CALM1 were tested *via* immunohistochemical (IHC) staining on human pseudarthrosis samples.

Descriptive histology with two different staining was performed to identify the different tissues in human pseudarthrosis samples.

4.4. Validation of potential biomarker in human

4.4.1. Descriptive histology revealed impaired bone healing

To evaluate quality of human pseudarthrosis samples, cryo sections were stained with hematoxylin and eosin (H&E). Histological examination showed that pseudarthrosis samples from human patients had large portions of fibrous tissue. However, staining also revealed differences between atrophic and hypertrophic samples. Compared with hypertrophic pseudarthrotic samples, atrophic pseudarthrosis showed less calcified patches (**Figure 15**). Moreover, cellular density of atrophic pseudarthrosis was lower compared to other samples. Atrophic pseudarthrosis showed also more granulation tissue and erythrocytes compared to hypertrophic samples. In hypertrophic pseudarthrosis, bone structures could be seen as well as cartilage.

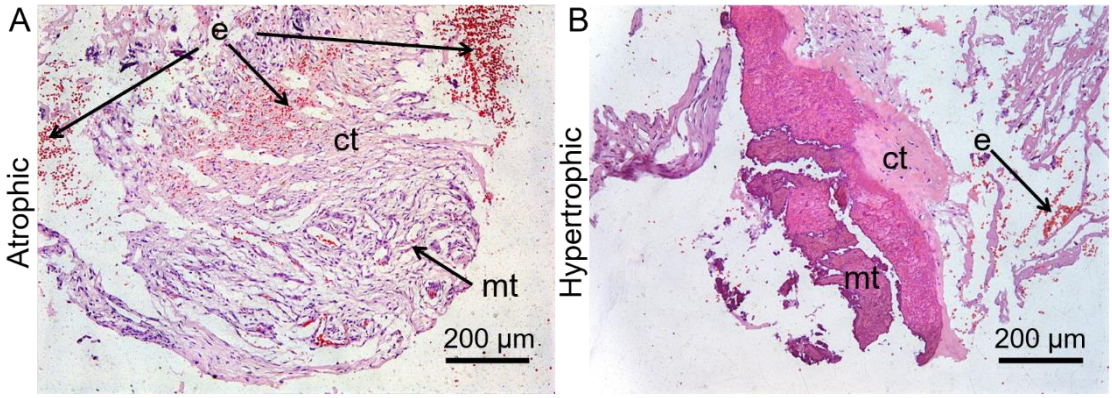

Figure 15: Histological analysis showed lower calcified patches in atrophic pseudarthrosis. Calcified tissue is presented as a compact structure in dark pink, connective tissue in light pink. Blue dots represent nucleated cells. Erythrocytes are colored bright red. A) Atrophic pseudarthrosis showed fibroblasts and cartilage. Granulation tissue and erythrocytes were more present in atrophic pseudarthrosis when compared with hypertrophic pseudarthrosis. B) Compared with atrophic pseudarthrosis, hypertrophic pseudarthrosis showed more compact calcified patches. (Magnification: 10x, ct=connective tissue, e=erythrocytes; mt=mineralized tissue)

For descriptive histology of the samples, Movat's pentachrome staining was used. The main types of tissues in both, atrophic and hypertrophic pseudarthrosis samples, included fibrous, cartilaginous, and connective tissues in varying degree.

In general, the two atrophic human pseudarthrosis samples showed more granulation tissue than the hypertrophic pseudarthrosis samples. In bone fracture, granulation tissue matures and develops into a soft callus with fibrous tissue. However, atrophic pseudarthrosis samples showed lower cellular density and tissue area compared with

hypertrophic pseudarthrosis (**Figure 16 A**). In contrast to the atrophic pseudarthrosis samples, the hypertrophic non-unions showed larger areas of mineralized tissue. Fibrous tissue and fibrocartilage were also seen in hypertrophic pseudarthrosis (**Figure 16 B**).

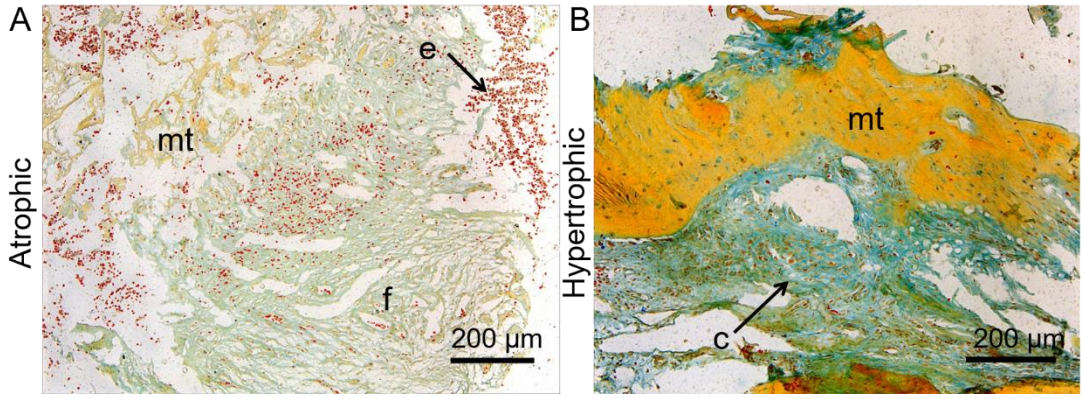

Figure 16: Movat's pentachrome stain revealed impaired bone healing in atrophic and hypertrophic pseudarthrosis. The different tissue types were colored as followed: non-mineralized cartilage (c)=blue-green, mineralized tissue (mt)=yellow, and monocytes (e.g. erythrocytes) e=red. A) Atrophic pseudarthrosis showed large area of granulation tissue as well as fibrous tissue. However, only small areas of mineralization were detected. B) Hypertrophic pseudarthrosis showed high area of fibrocartilagous tissue. Also, large compact portions of mineralization could be observed in hypertrophic pseudarthrosis samples as well as parts of woven bone. (Magnification: 10x c=cartilage, e=erythrocytes; mt=mineralized tissue; f=fibrous tissue)

In detail, atrophic pseudarthrosis showed mostly fibrous tissue, fibrocartilaginous tissue as well as granulation tissue (**Figure 17**). Moreover, both atrophic pseudarthrosis samples displayed affected bone matrix mineralization. Mineralization tissue was not compact in the two atrophic pseudarthrosis samples and multiple non-mineralized areas were seen. Presented cells were generally oligocellular, with fibroblast-like cells as majority of cells. Only few osteoclasts and osteoblasts were detectable in the atrophic pseudarthrosis samples. Also, no hypertrophic chondrocytes and cartilaginous tissue were seen in atrophic samples.

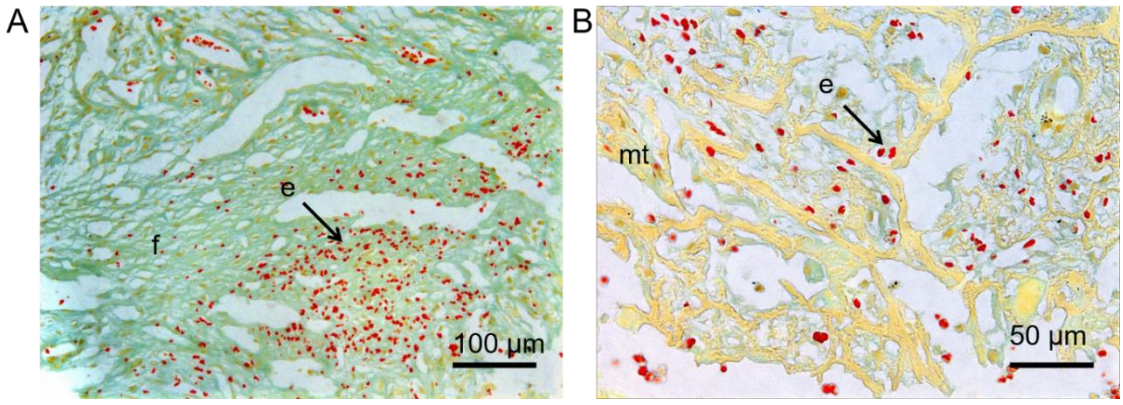

Figure 17: Atrophic pseudarthrosis stained with Movat's pentachrome showed less mineralization (yellow) and large areas of fibrous tissue (green). A) Mostly fibrocartilaginous tissue (f, green) could be observed. Granulation tissue with a large number of monocytes was seen as well (e, red). B) Occasional mineralized structures were seen in yellow (mt). (Magnification: A=20x, B=40x; f=fibrous tissue, e=erythrocytes; mt=mineralized tissue)

Movat's pentachrome stainings of hypertrophic pseudarthrosis showed different cellular background compared to atrophic pseudarthrosis. Disarranged spherical osteocytes were present in hypertrophic pseudarthrosis, revealing impaired bone healing. Bone remodeling of cortical bone could be seen by observing cutting cones within the woven bone area. In those tunnels, osteoclasts remove damaged bone. In normal healing, osteoblasts follow the cutting-cones, refilling the generated cap by generating osteoid, which later mineralizes to bone. However, in hypertrophic pseudarthrosis sample, neither osteoblasts nor osteoid was seen around the cutting-cone tunnel, even in 40x (**Figure 18 A**). Fibrous tissue was developing into fibrocartilage in hypertrophic pseudarthrosis samples. Nevertheless, collagen fibers within the fibrocartilage were not well arranged. The altered collagen fibers arrangement indicated alterations in bone matrix. Mineralization and demineralization processes are correlated with vascularization [165]. In hypertrophic pseudarthrosis samples, irregular shaped blood vessels were seen. Moreover, those blood vessels (**Figure 18 B**) were seen in cartilage tissue, indicating inferior mineralization.

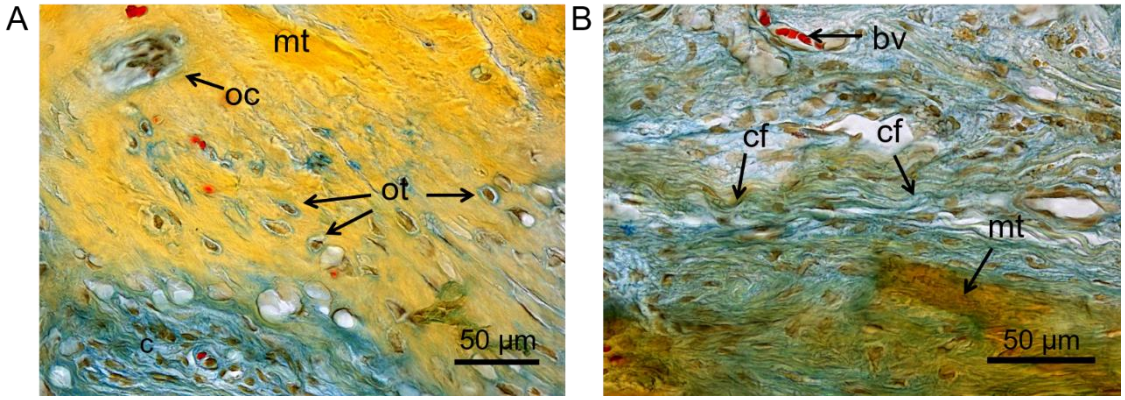

Figure 18: Hypertrophic pseudarthrosis featured deteriorated arrangement of osteocytes and collagen fibers in Movat's pentachrome stainings. A) Disarranged spherical osteocytes were observed in mineralized tissue. Osteoclasts in cutting-cone shows bone remodeling. However, no osteoblasts were seen and no new formed osteoid to fill the cutting-cone, thusly revealing impaired bone remodeling. B) Mineralized tissue patches appeared yellow-brown in areas of hypertrophic cartilage. Also, collagen fibers were exhibited in cartilage tissue. Nevertheless, collagen fibers were disarranged in hypertrophic pseudarthrosis. Moreover, irregular shaped blood vessels were seen. (Magnification: 40x; bv=blood vessel, c=cartilage, cf=collagen fiber, mt=mineralized tissue, oc=osteoclast, ot=osteocytes)

After descriptive examination of pseudarthrotic tissue from human patients, the two potential biomarkers calmodulin 1 (CALM1) and glycine tRNA synthetase (GARS) were assessed by IHC. Movat's pentachrome stain was thereby helpful in understanding in which specific tissue, CALM1 and GARS were expressed in atrophic and hypertrophic pseudarthrosis.

4.4.2. Immunohistochemical staining of human pseudarthrosis

To validate the potential biomarkers found in genomics and proteomics, human pseudarthrotic tissue sections were immunohistochemical (IHC) stained for GARS and CALM1.

In general, both staining reactions could clearly be differentiated from the lack of signal in the negative control (secondary antibody only, data not shown). GARS and CALM1 positive signals were seen in both, atrophic and hypertrophic pseudarthrosis samples. However, IHC of CALM1 and GARS revealed different expression localization of both biomarkers within pseudarthrosis tissue.

CALM1 and GARS signals in atrophic pseudarthrosis

Fibrous and cartilage tissue was immune-stained positive for CALM1 in atrophic pseudarthrosis (**Figure 19 A+B**), while GARS-positive signals could be observed in mineralized tissue.

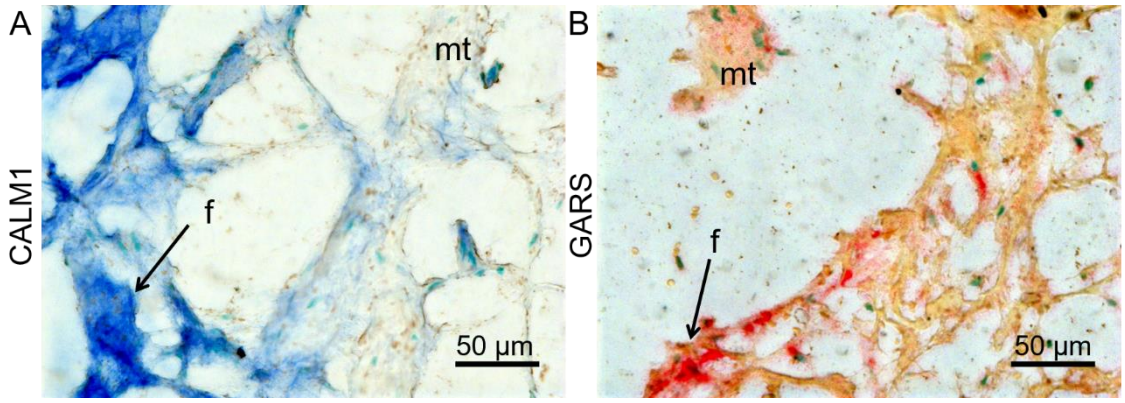

Figure 19: Expression of potential biomarker in atrophic pseudarthrosis. A) CALM1 (blue) signals were seen in fibrous tissue. B) GARS (red) signals were also visible in fibrous tissue. Moreover, GARS signals could be observed in mineralized tissue. (Magnification: 40x, f=fibrous tissue, mt=mineralized tissue)

CALM1 and GARS signals in hypertrophic pseudarthrosis

In contrast to the atrophic pseudarthrosis samples, the two hypertrophic pseudarthrosis samples showed signals of CALM1 in chondrocytes and fibrous tissue (**Figure 20 A**). In contrast to CALM1, GARS was not seen in chondrocytes but in fibrous tissue and mineralized tissue (**Figure 20 B**).

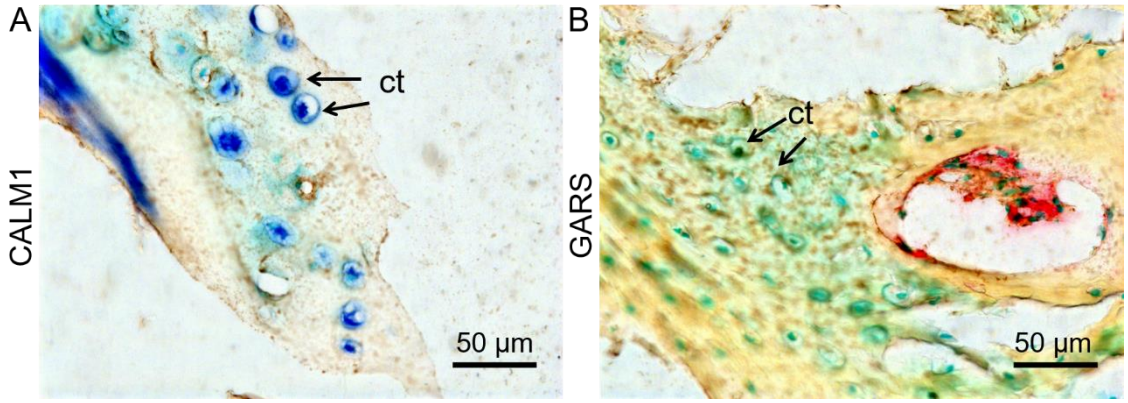

Figure 20: Chondrocytes exhibited CALM1 but not GARS in hypertrophic pseudarthrosis. A) CALM1 signals in chondrocytes. B) Chondrocytes do not express GARS. GARS signal was seen in fibrous tissue. (Magnification: 40x, ct=chondrocytes)

Fluorescence overlay image of hypertrophic pseudarthrosis stained with GARS and CALM1 showed also different localization of GARS and CALM1 in the tissue (**Figure 21**). While GARS was more present within the mineralized tissue, CALM1 was seen in cartilage tissue as well as in fibrous tissue.

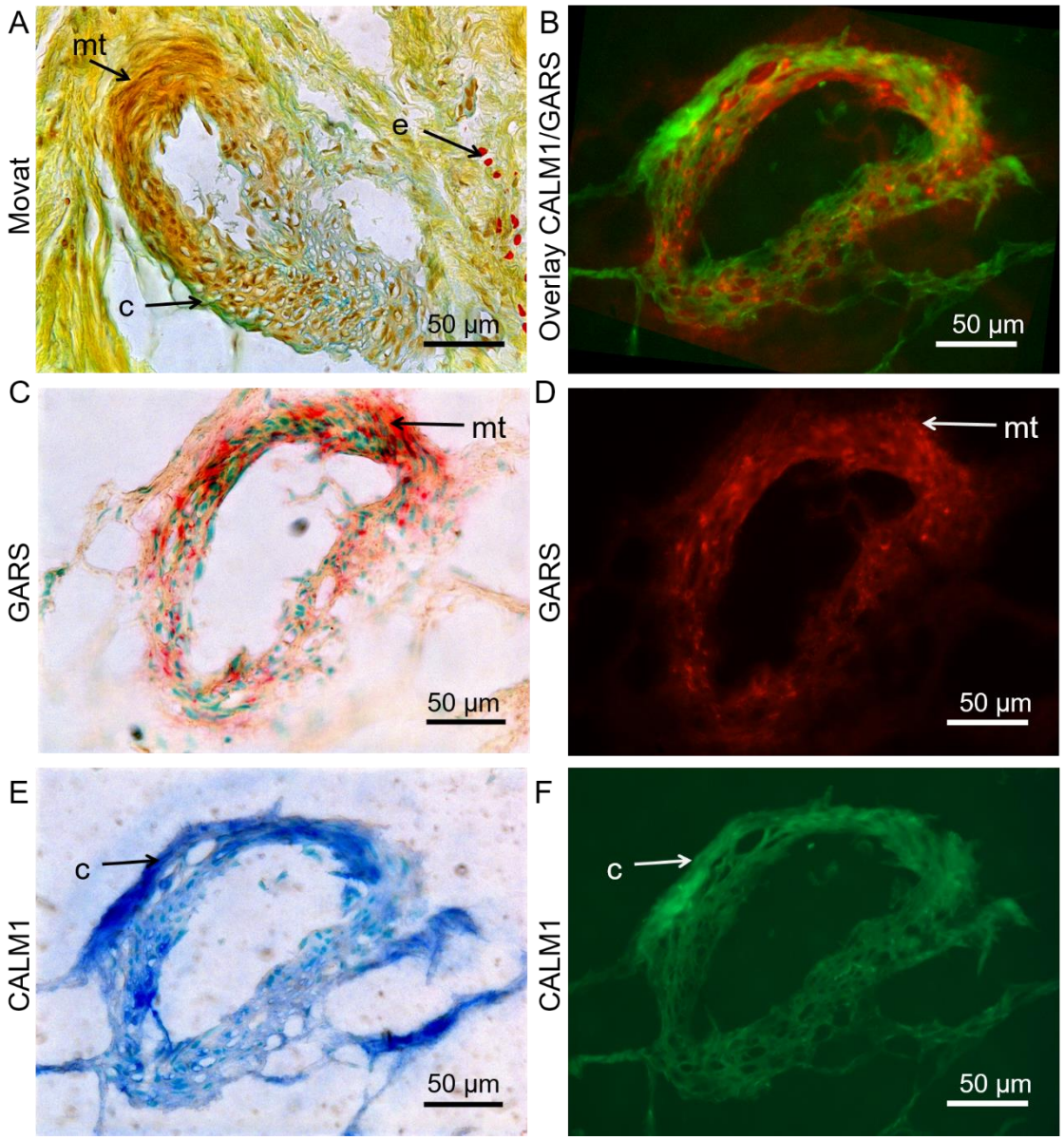

Figure 21: Localization of GARS and CALM1 in hypertrophic pseudarthrosis. A) Movat's pentachrome staining of hypertrophic non-union showed areas of mineralized tissue in yellow. Cartilage was seen in blue-green. B) Fluorescence overlay showed different localization of GARS (red) and CALM1 (green). C) GARS (red) was more present within the mineralized tissue. D) Fluorescence Image of GARS. E) CALM1 (blue) was seen in cartilage tissue as well as in fibrous tissue. F) Fluorescence image of CALM1. (Magnification: 40x; e=erythrocytes, c=cartilage, mt=mineralized tissue)

To assess if pseudarthrosis formation is linked to diseases and risk factors which are also connected to the two possible biomarkers, a clinical study was performed. The study's focus lied particularly in the analysis of the possible connection to allergies, morbidities like metabolic disorders and other risk factors.

4.5. Comparison of aseptic atrophic and hypertrophic pseudarthrosis

4.5.1. Demographic data of clinical study

In a peer-reviewed publication (equal contribution with first author M. Rupp), parts of this study were published in 2019 [17]. In total, 206 patients with diagnosed pseudarthrosis took part in the retrospective clinical study. From these 206 participants, 36 had to be excluded after diagnosis of infectious pseudarthrosis. Furthermore, 8 participants were excluded because they were under the age of 18 at the time of fracture. Thus, 162 participants with atrophic and hypertrophic pseudarthrosis remained in the study.

Overall, 92 (56.8 %) patients were men, and 70 (43.2 %) patients were woman. The average age was 51.30 ± 16.34 years (ranging from 19 to 88 years).

Of 162 participants in the study, 99 (61.1 %) suffered from a hypertrophic pseudarthrosis, while 63 patients (38.9 %) had an atrophic pseudarthrosis. Interestingly, hypertrophic pseudarthrosis was more frequent in male patients, 62 (62.2 %). Thirty-seven (37.8 %) patients with hypertrophic pseudarthrosis were female. In atrophic pseudarthrosis, there were almost even numbers of male and female patients with 33 (51.6 %) female and 31 (48.4 %) male patients.

4.5.2. Impact of allergies on fracture healing

As GARS and CALM1 are involved in auto-immune diseases and immune response, impact of allergies to the building of pseudarthrosis was evaluated in this clinical study. Frequency analysis (**Figure 22**) showed that majority of the 162 patients were allergy-free (122, 75.3 %), while 40 patients (24.7 %) had at least one allergy.

Patients with allergies mostly had one allergy (25, 62.5 %) followed by two allergies (11, 27.5%) and three diagnosed allergies (4, 10.0%). The following allergies were assessed in the study: 25 patients were allergic against medical drugs (43.9 %), 14 patients had contact allergies (24.6 %), 9 patients were allergic against pollen (15.2 %). There were 4

allergies against metals (7.0 %), 3 insecticide allergies (5.3 %), 1 food allergy (1.8 % of all allergies) and 1 allergy against contrast agents (1.8 %).

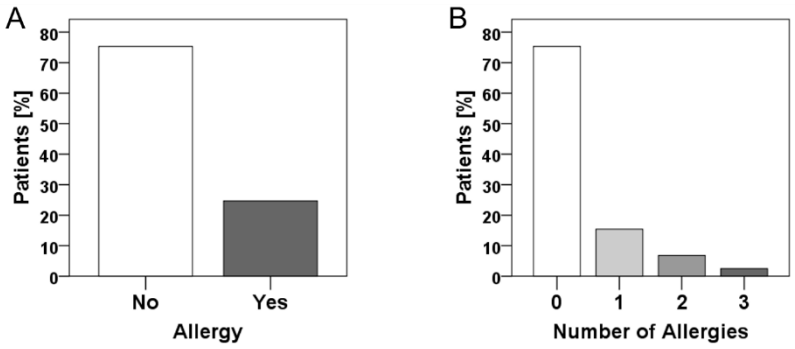

Figure 22: Study revealed that patients with pseudarthrosis had mostly one allergy or none at all. A) More patients had no allergy compared to the patients with allergies. B) Percentage of patients with allergies was lower the more allergies patients had. 122 (75.3 %) patients had no allergy, while 25 (15.4 %) patients had one allergy. There were 11 (6.8 %) patients with two allergies and 4 (2.5 %) patients with three allergies. (frequency analysis)

Patients who needed revision surgery for hypertrophic pseudarthrosis had an allergy in more than 30.3 % (30 patients), atrophic pseudarthrosis patients in less than 17.2 % (11 patients). However, difference was not significant (p=0.069).

Interestingly, there was a significant difference between the ages of allergy-free patients in the type of pseudarthrosis (**Figure 23**). Patients with an atrophic pseudarthrosis were older compared to patients with hypertrophic non-union (p=0.020).

Moreover, patients with allergies were younger in the group with atrophic pseudarthrosis. By looking into more details, the study also revealed, that there are significant differences in the age of patients with atrophic pseudarthrosis and the number of allergies. Patients with two allergies were significantly younger than patients with none (p=0.049) or one allergy (p=0.015).

In hypertrophic pseudarthrosis patients, age was higher in patients with three allergies when compared with other groups, although not significant. Nevertheless, a trend was seen in those patients. The more allergies they had, the older they were.

Descriptively, numbers of allergies also had an impact on leucocytes, BMI, and time between first operation and revision (**Figure 24**). In atrophic pseudarthrotic patients, leucocytes were higher when patients had one allergy compared to none allergy and two allergies (p=0.025). Hypertrophic non-union patients showed a more homogenous count of leucocytes.

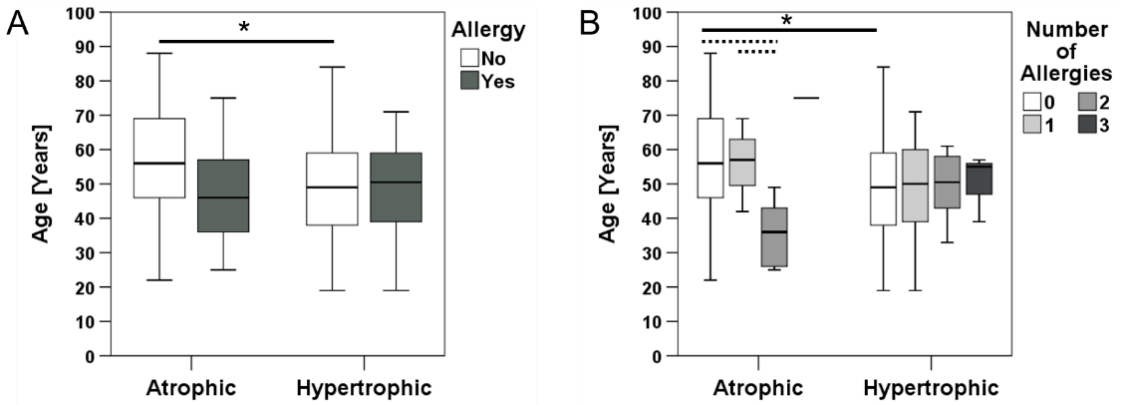

Figure 23: Age of patients differed with numbers of allergies. A) Allergy-free patients with an atrophic non-union were significantly older than patients with a hypertrophic non-union (p=0.020). B) Number of allergies was correlated to age of patients with atrophic pseudarthrosis. Patients with two allergies were significantly younger compared to patients with one (p=0.015) or non-allergy (p=0.049). In hypertrophic pseudarthrosis, patients' age was higher in patients with two allergies, although not significant. Moreover, age of patients is more homogenous compared with atrophic pseudarthrosis patients. (Mann Whitney U test, *=p≤0.05)

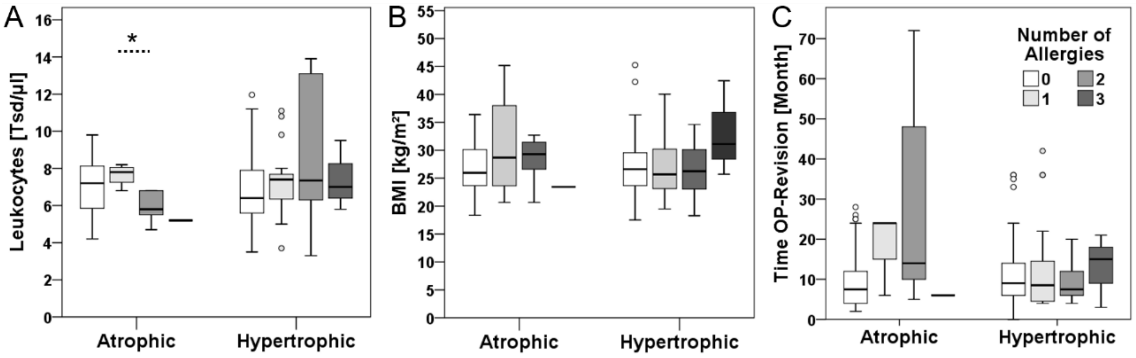

Figure 24: Inhomogeneity in patients with atrophic pseudarthrosis and increasing number of allergies. A) Leucocytes count was significantly higher in atrophic pseudarthrosis patients with one allergy compared to non-allergy or two allergies. Hypertrophic pseudarthrosis patients showed more homogeneity. B) BMI of patients is higher the more allergies patients had in both groups, hypertrophic and atrophic pseudarthrosis patients. C) Time between operation and revision is inhomogeneous in patients with atrophic pseudarthrosis. In hypertrophic pseudarthrosis patients, time between first surgery and revision is highest in patients with three allergies compared to other groups, although not significant. (Mann Whitney U test, *=p≤0.05)

BMI of patients with either atrophic or hypertrophic non-union was by trend increasing with increased number of allergies, although not significantly (**Figure 24 B**). Duration time between first surgery and revision was highest in patients with three allergies in

hypertrophic pseudarthrosis patients. There was an inhomogeneity in patients with atrophic pseudarthrosis with the longest duration in patients with two allergies (**Figure 24 C**). Overall, the study showed that number of allergies had more impact on atrophic pseudarthrosis compared with hypertrophic pseudarthrosis. Moreover, patients with atrophic pseudarthrosis showed more inhomogeneity in age, leucocytes, BMI and duration time between operation and revision correlated to the number of allergies compared to patients with hypertrophic pseudarthrosis.

4.5.3. Biomechanical characteristics

Following factors were analyzed for evaluation of biomechanical characteristics of aseptic pseudarthrosis: fracture type (open or closed), osteosynthesis type (plate, intramedullary pins, screw fixation, cerclage), and a possible loosening of the implant. The study revealed higher pseudarthrosis occurrence in closed fractures (118; 72.8 %) when compared with open fractures (44; 27.2 %) (**Figure 25 A**). Furthermore, a tendency of a correlation of pseudarthrosis development and the used osteosynthesis material was shown. Overall, there were more patients suffering from pseudarthrosis treated with plates (81; 50.0 %) than with intramedullary pins (55; 34.0 %) or screw fixation (20; 12.3 %) of the fracture (**Figure 25 B**). Pseudarthrosis resulting from fractures treated with cerclage showed the lowest percentage (6; 3.7 %) in the study. 38.3 % (62) of all patients had a loosening of the implant (**Figure 25 C**).

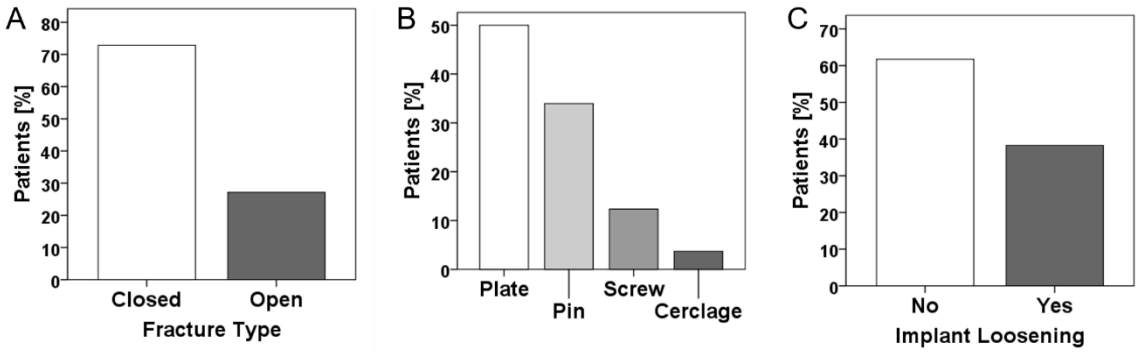

Figure 25: Frequency analysis of fracture-implant characteristics. A) More patients with pseudarthrosis had closed fractures than open fractures. B) Osteosynthesis with plates resulted in more pseudarthrosis than treatment with medullary pins, screws, or cerclage. B) In 38.3 % of the cases, a loosening of implant was involved in pseudarthrosis development.

However, an association was found between type of osteosynthesis and pseudarthrosis type ($\chi^2(1) \geq 2.999$, p=0.000285) (**Figure 26 A**). There were more patients with plates and

pins in the hypertrophic pseudarthrosis group compared with atrophic pseudarthrosis patients. Patients with screws suffered more from atrophic pseudarthrosis.

Comparing patients with hypertrophic and atrophic pseudarthrosis, no association between implant loosening and type of pseudarthrosis was found ($\chi^2(3) \geq 17.803$, p=0.622) (**Figure 26 B**).

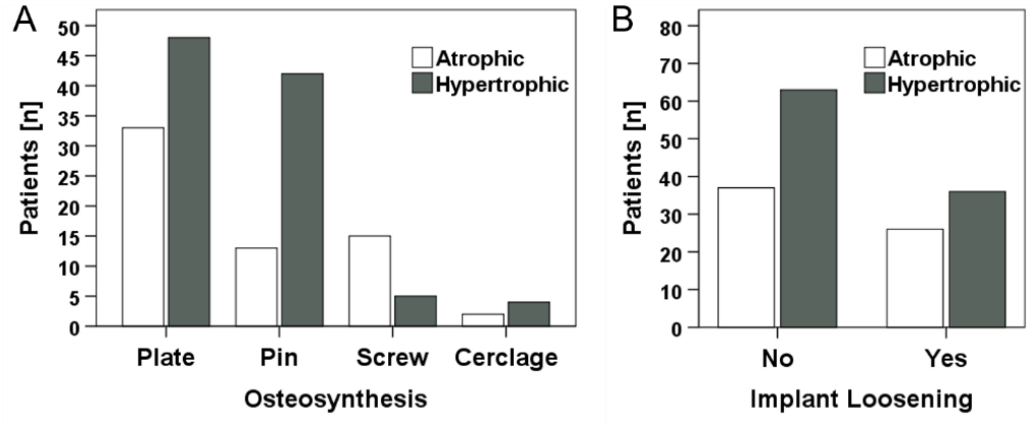

Figure 26: Association was found between osteosynthesis and type of pseudarthrosis. A) Hypertrophic pseudarthrosis patients had more plates and pins for osteosynthesis material compared with atrophic pseudarthrosis patients. Screw fixations were more seen in atrophic pseudarthrosis patients. ($\chi^2(1) \geq 2.999$, p=0.000285) B) There was no association between implant loosening and type of pseudarthrosis ($\chi^2(3) \geq 17.803$, p=0.622).

4.5.4. Obesity and medication use have impact on fracture healing

Obesity is associated with significantly increased rates of post-operative medical complications including pseudarthrosis. GARS is linked to metabolic conditions like diabetes mellitus. Therefore, evaluation of obesity and possible link to pseudarthrosis was assessed in this study. Patients are generally considered obese with a BMI over 30 kg/m². The range of 25-30 kg/m² is defined as overweight, 18.5-25 kg/m² as normal weight and <18.5 kg/m² is defined as underweight. [82, 166]

In our study, 58 patients (36.0 %) were normal weighted. Almost two-thirds of the participants in the study were overweighed with a BMI over 25. In total 100 patients (62.1 %) had overweight, distributed in 44 obese patients (27.3 %) and 56 overweighed patients (34.8 %). Only 3 of 162 patients (1.9 %) were underweighted.

Interestingly, BMI increased with increasing age in both groups, atrophic and hypertrophic pseudarthrosis (**Figure 27 A**). Allergic patients with an atrophic pseudarthrosis had a higher BMI than non-allergic patients, although not significantly.

There was no significant difference in the BMI of patients between atrophic and hypertrophic pseudarthrosis (**Figure 27 B**).

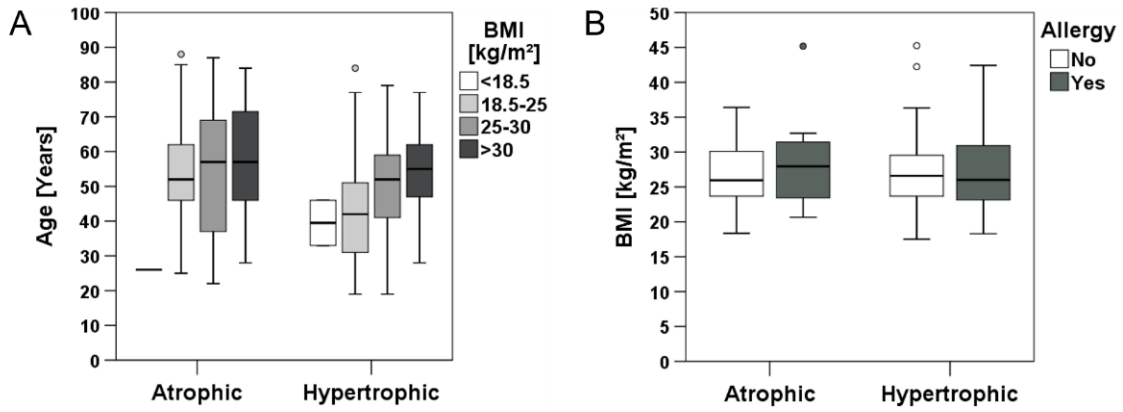

Figure 27: Obesity correlated with age in pseudarthrosis patients. A) BMI was higher in older patients with either atrophic non-union or hypertrophic non-union. Age of patients with atrophic pseudarthrosis was higher compared to patients with hypertrophic pseudarthrosis. B) Patients with an atrophic pseudarthrosis suffering from an allergy had a higher BMI compared to non-allergic patients, although not significantly. (Mann Whitney U test, *=p≤0.05)

Disease morbidity and medication use have generally not been identified as risk factors for pseudarthrosis [82]. Thus, this study included evaluation of several morbidities like diabetes mellitus (DM), nicotine abuse, cardiovascular diseases (CD) and a combination of those. Moreover, the medication of Non-steroidal anti-inflammatory drug (NSAID) was contemplated in this study.

By comparing patient morbidities and NSAID medication, no significant differences between patients with atrophic and hypertrophic pseudarthrosis were found. However, more than 40% of patients in both groups suffered from at least one of the morbidities which were evaluated in this study. Differences in type and numbers of the assessed morbidities and comorbidities were not different between patients with either atrophic or hypertrophic pseudarthrosis ($\chi^2(6) \geq 5.015$, p=0.566) (**Figure 28 A**).

Nevertheless, permanent NSAID intake was more frequent in patients with hypertrophic pseudarthrosis (27, 27.3 %) when compared with atrophic pseudarthrosis (13, 20.3 %). However, no association was found between NSAID intake and type of pseudarthrosis ($\chi^2(1) \geq 1.017$, p=0.313) (**Figure 28 B**).

Risk factors like medical drug use and obesity can lead to post-operative medical complications. Thus, evaluation of concomitant injuries was conducted to see if they lead to further risk of post-operative complications.

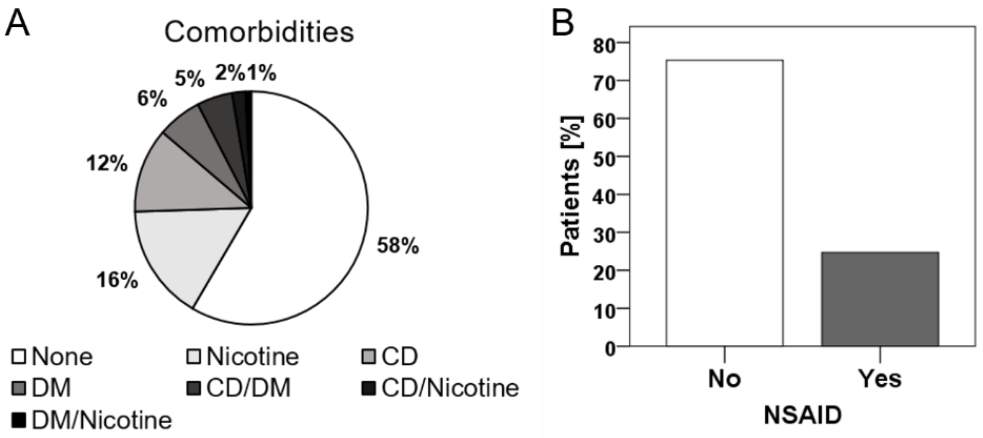

Figure 28: Evaluation of morbidities and medication use in pseudarthrosis patients. A) 58.9 % of the patients had no morbidity (96 patients). Of all considered morbidities, nicotine abuse was the highest (26; 16.0 %), followed by cardiovascular diseases (19; 11.7 %) (CD=cardiovascular disease, DM=diabetes mellitus). B) 40 (24.7 %) patients in this study took NSAIDs.

4.5.5. Concomitant injuries occur in younger patients

Little is known about the clinical importance of osteosynthetic concomitant injuries in polytraumatized patients and their influence on fracture healing. Therefore, this study investigated the impact of concomitant injuries on pseudarthrosis.

Overall, 53 (32.7 %) of all 162 patients exhibited concomitant injuries. Comparing the age of patients revealed that patients with concomitant injuries were younger compared with patients with one fracture. This was seen in both, atrophic and hypertrophic pseudarthrosis patients (**Figure 29 A**).

Interestingly, in female patients there was a decreasing tendency in the age of patients with allergies. In both cases, mono fracture and multiple injuries, age of non-allergic female patients was highest in non-allergic patients and lowest in patients with multiple allergies (**Figure 29 B**). This was not seen in male patients. More interestingly, the BMI of female patients with atrophic non-union was higher when no concomitant injuries were involved, although not significantly. In contrast, the reverse was seen in female

hypertrophic pseudarthrosis patients. Here, BMI was higher when patients had more than one injury, although not significantly (**Figure 29 C**).

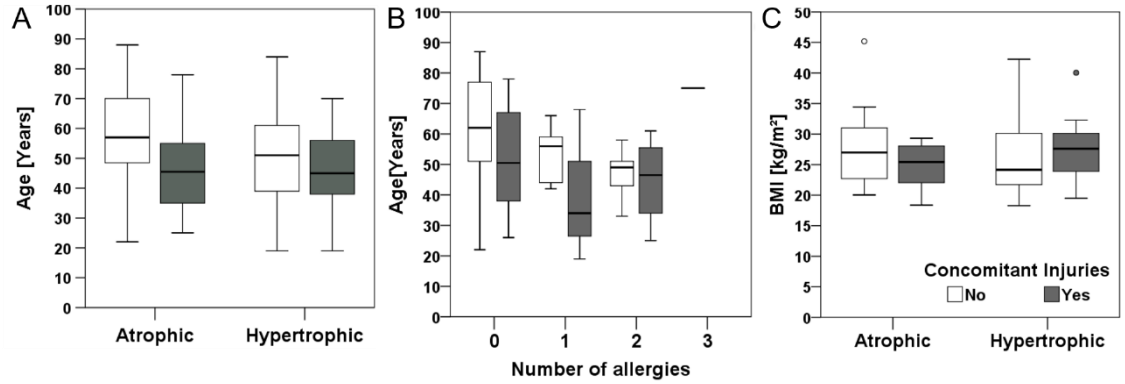

Figure 29: Concomitant injuries appeared more in younger patients. A) Age of patients with concomitant injuries was lower compared to patients with mono-fracture in both, atrophic pseudarthrosis and hypertrophic pseudarthrosis patients. B) Female patients with one fracture showed a decreasing tendency in age correlated to number of allergies. Interestingly, in female patients with concomitant injuries, age decreased first but increased again. Nevertheless, highest age was also seen at non-allergic patients. C) BMI of female patients with hypertrophic non-union and concomitant injuries was higher compared to patients with one injury. In female patients with atrophic pseudarthrosis, the reversed was seen. (Mann Whitney U test, *=p≤0.05)

4.6. Microbial infections in septic pseudarthrosis

The second retrospective clinical study evaluated the impact of microbial infections in pseudarthrosis. In total, 211 patients participated in this study (AZ 68/18). 85 (40.3 %) patients were female and 126 (59.7 %) males. The mean age of the patients was 51.93 ± 17.08 years.

4.6.1. Comparison of septic and aseptic pseudarthrosis

Descriptive data showed some differences between septic pseudarthrosis patients and patients with aseptic pseudarthrosis (**Table 4.2**). Of the total 211 patients, 43 (20.4 %) were diagnosed with septic pseudarthrosis and 168 (79.6 %) with aseptic pseudarthrosis. The mean age of the septic pseudarthrosis cohort was 52.91 ± 17.66 years (ranging from 23 to 95 years). This was not different to the mean age of aseptic pseudarthrosis patients (51.68 ± 16.97; ranging from 18 to 94 years).

Septic and aseptic pseudarthrosis patients showed same distribution of male and female patients and of patients with or without allergies. Additionally, ASA classification showed the same pattern in aseptic and septic pseudarthrosis. Patients were mostly classified with ASA class II, namely in 100 (59.5 %) aseptic patients and 26 (60.5 %) septic patients. Also, frequencies of patients with or without implant loosening was the same in aseptic and septic pseudarthrosis. No association was found between infection and type of osteosynthesis (medullary nail, cerclage, screw fixation, plate).

Table 4.2: Descriptive data showing demographics and fracture characteristics of aseptic and septic pseudarthrosis patients as frequencies in numbers [n] and percent [%].

		Aseptic Pseudarthrosis [n / %]	**Septic Pseudarthrosis** [n / %]
Patients	Total Number	168	43
Gender	Female	67 / 39.9	18 / 41.9
	Male	101 / 60.1	25 / 58.1
Allergies	No	100 / 59.5	29 / 67.4
	Yes	64 / 38.1	14 / 32.6
AO Localization	Humerus	24 / 14.3	3 / 7.0
	Radius/Ulna	42 / 25.0	3 / 7.0
	Femur	50 / 29.8	12 / 27.9
	Tibia/Fibula	52 / 31.0	25 / 58.1
ASA	1	13 / 7.7	2 / 4.7
	2	100 / 59.5	26 / 60.5
	3	39 / 23.2	12 / 27.9
BMI	<18.5	5 / 3.0	-
	18.5-25.0	58 / 34.5	13 / 31.7
	25.0-30.0	50 / 29.8	9 / 22.0
	>30.0	40 / 23.8	19 / 46.3
Concomitant Injuries	No	125 / 74.4	36 / 83.7
	Yes	43 / 25.6	7 / 16.3
Fracture	Closed	141 / 83.9	24 / 55.8
	Open	27 / 16.1	19 / 44.2
Implant Loosening	No	113 / 67.3	29 / 67.4
	Yes	55 / 32.7	14 / 32.6
Pseudarthrosis Type	Atroph	59 / 35.1	20 / 46.5
	Hypertroph	109 / 64.9	23 / 53.5

Distribution of fracture localizations was different in aseptic and septic pseudarthrosis patients. While almost two-thirds (25; 58.1 %) of the septic pseudarthrosis patients suffered from a tibia/fibula fracture followed by femur fractures with one-quarter (12; 27.9 %), fractures in patients with aseptic pseudarthrosis were more evenly spread in tibia/fibula, femur, and radius/ulna (52; 31.0 %, 50; 29.8 %, 42; 25.0 %; respectively). Moreover, in the cohort of septic pseudarthrosis patients, more patients were found with obesity compared to the aseptic pseudarthrosis patients and more patients suffered from an open fracture. Interestingly, patients with septic pseudarthrosis had lower rate of concomitant injuries compared to patients with aseptic pseudarthrosis. In addition, patients with septic pseudarthrosis had almost to the same percentage atrophic and hypertrophic pseudarthrosis while the aseptic pseudarthrosis were more hypertroph.

Pearson's chi-squared test showed an association between septic/aseptic pseudarthrosis and BMI. Patients with BMIs over 30 kg/m² were more prone to septic pseudarthrosis ($\chi^2(3) = 8.3129$, p=0,041) (**Figure 30 A**). Another association was found in patients with tibial fractures ($\chi^2(3) = 14.534$, p=0.002) (**Figure 30 B**). They were more likely to suffer from an infection compared with patients with fracture of the humerus, radius/ulna or femur. Patients with open fractures were also had more septic pseudarthrosis ($\chi^2(1) = 17.447$ p=0.000081) (**Figure 30 C**).

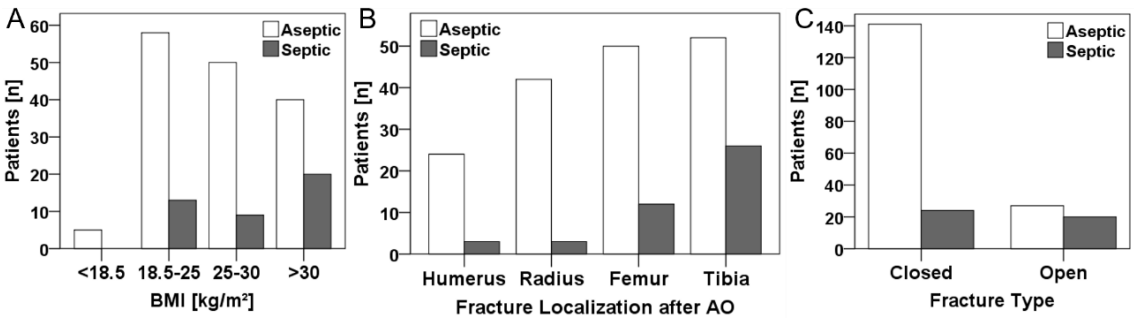

Figure 30: Patients with tibial fracture, high BMI and open fractures were more prone to septic pseudarthrosis. A) Association was found between BMI and aseptic/septic pseudarthrosis. Patients with an BMI over 30 were more susceptible to infections ($\chi^2(3)=8.3129$, p=0,041). B) Risk of infection was associated with fracture localization. Patients with tibial fractures were more prone to septic pseudarthrosis $\chi^2(3)=14.534$, p=0.002). C) Septic pseudarthrosis were highly associated with open fractures ($\chi^2(1) = 17.447$ p=0.000081).

Patients with septic pseudarthrosis had also more surgical revisions than patients with aseptic pseudarthrosis ($\chi^2(17) = 109.405$, $p=1.1589*10^{-16}$). According to these results, data was evaluated with more focus on the septic pseudarthrosis itself.

4.6.2. Number of surgical revisions of patients with septic pseudarthrosis

43 patients in this study suffered from septic pseudarthrosis. Numbers of surgical revision in this patient group ranged from one revision to 24 revisions. Majority of patients (23, 53.5 %) with septic pseudarthrosis needed 1-5 revision operations. 12 (27.9 %) patients had 6-10 surgical revisions, while 5 (11.6 %) had 11-15 and 3 (7.0 %) had more than 15 surgical revisions.

There were equal numbers of female and male patients with up to 5 revisions. There were more male patients with 6-10 revisions, 11-15 revisions and over 15 revisions compared with female patients. However, this was not significant. No association was found between gender and number of revisions ($X^2(3) = 1.408$, $p = 0.704$) (**Figure 31 A**).

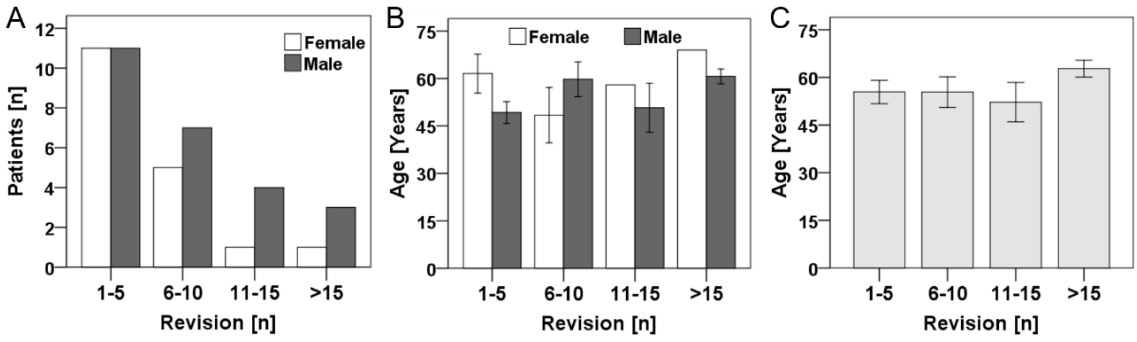

Figure 31: Numbers of surgical revisions were not associated with gender in septic pseudarthrosis. A) While there were more male patients with more than six revision operations compared with female patients, no association was found between gender and number of revisions ($X^2(3)> = 1.408$, $p = 0.704$). B) There was no significant difference in age between the two genders and the number of revision operations, although ages varied between and in groups. C) Patients age was higher in group with more than 15 surgical revisions, although not significantly. (Mann Whitney U test, *=p≤0.05)

Although age varied between the different numbers of revisions, there was no statistically significant difference between male and female patients (**Figure 31 B**). Patients with more than 15 surgical revisions were older compared to patients with less revisions, although not significantly (**Figure 31 C**). Subsequent data analysis was conducted to compare mono- and polymicrobial infections and their impact on septic pseudarthrosis development and outcome.

4.6.3. Comparison of mono- and polymicrobial infections with germ-changes in course of treatment

In total, 43 patients had microbial infections distributed over all surgical revisions. Infections were considered as polymicrobial infections (PMI) when there was initial proof of polymicrobial infections. Consecutively determined different pathogens during surgical treatment was regarded as germ-changes (GC). In total, 22 (51.2 %) patients were diagnosed with monomicrobial infections (MMI) and 6 (14.0 %) patients suffered from polymicrobial infections. In addition, in 15 patients (34.9 %) germ-changing was detected during surgical treatment. Most patients had infections after more than one revision surgery.

Overall, 111 infections were detected in those 43 patients and different pathogens were determined. Bacteria and microorganisms isolated from cultures covered a wide spectrum of species. Majority of the pathogens were different strains of *staphylococci* (59; 53.2 %) followed by *enterococci* (25, 22.5 %). Other infectious microorganisms were methicillin-resistant *staphylococci aureus* (MRSA) (5; 4.5 %), strains of *streptococci* (7; 6.3 %), gram-negative bacilli such as *pseudomonas aeruginosa* (12, 10.8 %) and other bacilli, mainly *candida albicans* (3; 2.7 %) (**Table 4.3**).

Table 4.3: Number and type of infectious pathogens in septic pseudarthrosis. In total, 111 infections with various microorganisms were detected in 43 patients. *Staphylococcus aureus* and *Enteroccci* were the most detected species.

Microorganism	Number [n]	Percent [%]
Staphylococcus Aureus	29	26.1
Staphylococcus Epidermis	18	16.2
Staphylococcus Coagulase-negative	7	6.3
Staphylococcus Capitis	3	2.7
Staphylococcus Hominis	2	1.8
MRSA	5	4.5
Streptococci	7	6.3
Enterococci	25	22.5
Gram-negative bacilli	12	10.8
Other microorganisms	3	2.7
Total	**111**	**100.0**

Looking deeper into the 59 staphylococci infections, half of the species were *staphylococci aureus* (29; 49.2 %), followed by *staphylococcus epidermis* (18, 30.5 %), *coagulase-negative staphylococcus* (7; 11.9 %), *staphylococcus capitis* (3; 5.1 %), and *staphylococcus hominis* (2; 3.3 %).

Descriptively, there was a difference in distribution of pathogens between MMI, PMI and GC pseudarthrosis patients. In septic pseudarthrosis patients with MMI, 22 infections were detected, of which 19 (86.4 %) were *staphylococci* infections. Looking at the pseudarthrosis patients with PMI, most identified pathogens were also *staphylococci* (11; 47.8 %) followed by *enterococci* (4; 17.4 %). In patients with change of germ-type within course of treatment, majority of detected pathogens were also *staphylococci* (30; 45.5 %) followed by *enterococci* (20; 30.3 %) as well as gram-negative bacteria (6; 9.1 %). Thus, patients with change of germs and PMI had more *enterococci* infections compared to patients with MMI. Moreover, patients with GC and PMI also had infections with strains of *streptococci* and gram-negative bacteria, while this was not seen in MMI non-union patients (**Figure 32**). However, Pearson's chi-squared tests showed no significant association between type of infection and type of infectious pathogen ($X^2(18)> = 22.733$, $p = 0.201$).

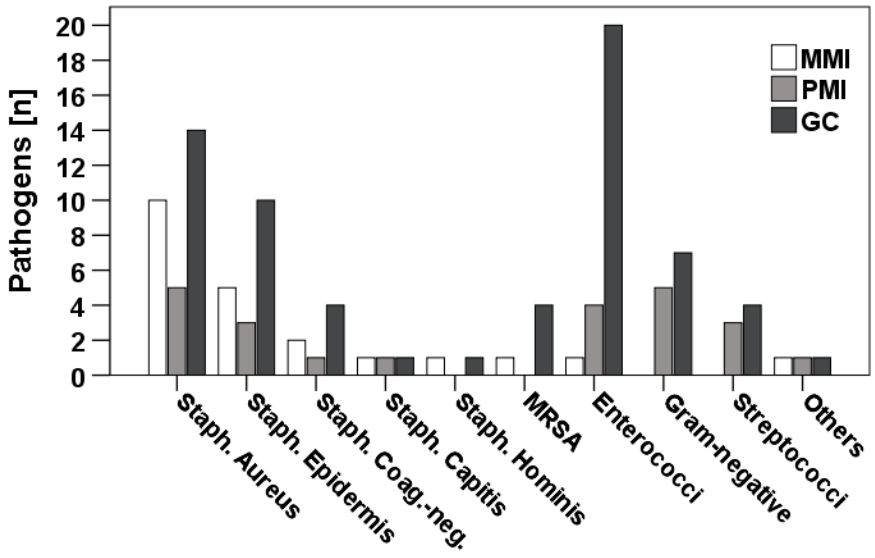

Figure 32: *Enterococci, gram-negative bacili* and *streptococci* were more evident in patients with PMI and GC compared to MMI patients. Septic pseudarthrosis patients with PMI and GC had more infections with enterococci. Moreover, gram-negative bacilli and streptococci infections were only detected in patients with PMI and GC. Main bacterial strains in MMI pseudarthrosis patients were different species of staphylococci. However, no significant association was found between type of pathogen and type of infection ($X^2(18)> = 22.733$, $p = 0.201$).

Looking at the number of surgical revisions of septic pseudarthrosis patients, differences between the infection types were found. PMI and GC pseudarthrosis patients had to undergo more surgical revisions compared with MMI patients. There was no patient with MMI with more than 10 revision surgeries; most MMI patients needed 1-5 revision surgeries until successful treatment of non-union. In the groups with 6-10 and 11-15 revisions, more patients were diagnosed with PMI and GC. Pearson's chi-squared tests showed that there is indeed an association between number of surgical revisions and type of microbial infection (mono-, polymicrobial or germ-changing) ($X^2(6)> = 25.383$, p=0.0003). (**Table 4.4**).

Table 4.4: Number of surgical revisions is higher in patients with polymicrobial infections and germ-changes compared to monomicrobial patients.

Surgical Revisions			
	Revision [n]	Frequency [n]	Percent [%]
MMI	1-5	17	77.3
	6-10	5	22.7
	11-15	-	-
	>15	-	-
	Total	22	100.0
PMI	1-5	4	66.7
	6-10	-	-
	11-15	2	33.3
	>15	-	-
	Total	6	100.0
Germ-Change	1-5	1	6.7
	6-10	8	53.3
	11-15	3	20.0
	>15	3	20.0
	Total	15	100.0

No association was found between comorbidities and microbial infection type (mono- or polymicrobial or germ-change) ($X^2(14)> = 14.599$, p=0.406). Also, no associations were found between gender ($X^2(2)> = 0.193$, p=0.908), osteosynthesis ($X^2(10)> = 15.387$, p=0.119), fracture type (open or closed) ($X^2(2)> = 1.666$, p=0.466), pseudarthrosis type (atroph or hypertroph) ($X^2(2)> = 3.803$, p=0.149), allergies ($X^2(2)> = 2.330$, p=0.0312), medication ($X^2(20)> = 18.203$, p=0.574), implant loosening ($X^2(2)> = 1.626$, p=0.444), ASA physical status classification ($X^2(4)> = 2.594$, p=0.628) or concomitant injuries

(X^2(2)> = 1.933, p=0.380) and type of microbial infection. Fracture localization classification after AO showed more tibial non-unions in patients with germ-changes (10; 66.7 %) within the course of treatment and in the PMI patients (4; 66.7 %) compared with MMI patients (11, 50.0%). In addition, patients with monomicrobial infections had more fractures at radius/ulna and femur compared with PMI patients and GC patients. However, there was no association found between fracture localization and infection type (X^2(6)> = 4.773, p=0.573). Although no association was found between BMI and type of microbial infection (X^2(4)> = 1.559, p=0.816), more patients with germ-changing (15; 53.3 %) and PMI (3; 50.0 %) had BMI over 30 compared MMI patients (8; 40.0 %).

Age of patients with germ-changes were slightly higher compared to patients with monomicrobial infections, although not significantly. However, patients with PMI were significantly older compared to MMI patients (Mann Whitney U test, p=0.033). BMI and leucocytes number were not different between pseudarthrosis patients with mono- and polymicrobial infections or germ-changes. CRP value was higher in patients with germ-changes within course of treatment compared with MMI and PMI patients, although not significantly (**Table 4.5**).

Table 4.5: Descriptive data of patients with septic pseudarthrosis.

Descriptives						
	Microbial Infection Type	**Mean**	**Std. Deviation**	**Std. Error**	**Minimum**	**Maximum**
Age [Years]	Mono	48.5	16.650	3.550	18	85
	Poly	63.3	10.764	4.394	55	84
	Germ-Change	54.3	20.290	5.239	19	93
BMI [kg/m²]	Mono	29.5	5.929	1.326	19.6	42.5
	Poly	31.0	8.930	3.646	22.3	46.5
	Germ-Change	31.8	8.719	2.251	22.2	46.9
Leucocytes [Tsd/µL]	Mono	7.8	2.095	0.457	5.2	13.5
	Poly	7.4	3.209	1.309	5.5	13.7
	Germ-Change	7.3	2.697	0.696	4.1	13.4
CRP [mg/L]	Mono	16.9	28.046	6.120	1.2	95.0
	Poly	11.2	13.415	5.477	0.6	36.5
	Germ-Change	42.5	57.502	14.847	0.7	197.3
Hospital Stay [Days]	Mono	27.3	25366	5.408	3.1	118.8
	Poly	27.8	27472	11.216	8.3	826
	Germ-Change	95.7	80.788	20.859	6.2	257.5

Overall, hospitalization stay in days was also significantly prolonged in septic pseudarthrosis patients with germ-changes compared to pseudarthrosis patients with MMI (Mann Whitney U test, p=0.001) and PMI (Mann Whitney U test, p=0.020).

4.7. Summary of results

Despite the diagnostic possibilities available today, pseudoarthrosis can only be diagnosed once they have already been established. Currently, it is not possible to predict the outcome of fracture healing in the early phase. However, early prediction would allow the treatment to be adapted, thus avoiding additional surgery and long periods of stress for the patient. Thus, this work aimed for analyzing risk factors for pseudarthrosis as well as finding biomarkers for early pseudarthrosis (**Figure 33**).

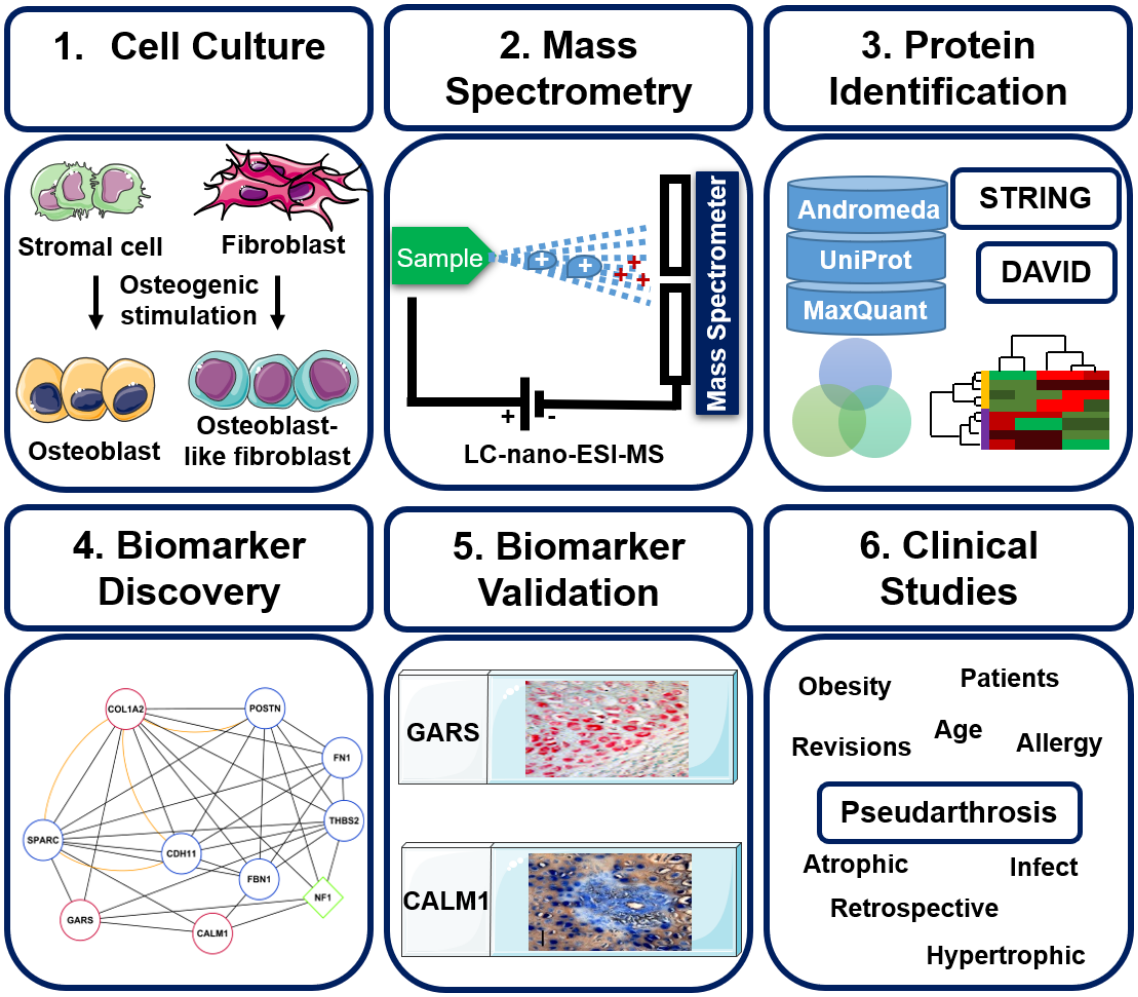

Figure 33: Discovery and evaluation of biomarker and risk factors for pseudarthrosis. This work elucidated protein-level differences between osteoblast-like fibroblasts and osteoblasts. It showed whether those differences result in discrepant tissue properties during bone healing leading to pseudarthrosis. Response of mesenchymal stromal cells and fibroblasts to osteoblast growth factors was therefore analyzed by mass spectrometric proteomics approach. Goal was the identification of a cellular marker for pseudarthrosis. Using bioinformatics tools, three proteins were discovered as possible makers for pseudarthrosis: CALM1, COL1A2, and GARS. Out of these three, CALM1 and GARS were further evaluated in human samples. Clinical studies revealed risk factors for pseudarthrosis.

In the current study, nano-LC-ESI-MS was applied to obtain deeper understanding of pseudarthrosis on cellular level and to find possible biomarker for pseudarthrosis prediction. Clinically, a revision of pseudarthrosis is required, and in many cases osteoblast growth factors like bone morphogenetic proteins (BMP) are applied to stimulate MSC differentiation into osteoblasts [7, 167, 168]. However, fibroblasts located abundantly in the site of pseudarthrosis respond to the same growth factors as osteoblasts and differentiate to osteoblast-like cells [169, 170] Biomarkers that predicts the response of pseudarthrosis treatment with growth factors would i) help in understanding the underlying pathomechanims leading to pseudarthrosis and ii) help in developing new, advanced treatment to improve patient's life and to decrease treatment costs. Therefore, this work was focusing on protein-level differences between osteogenic simulated MSCs and osteogenic stimulated fibroblasts. Thus, four different bone cell types were investigated using bottom-up proteomics: 1) mesenchymal stromal cells, 2) osteogenic stimulated MSCs, 3) fibroblasts, and 4) osteogenic stimulated fibroblasts.
Altogether, 193 identified proteins were common in all biological and technical replicates. Enrichment map network analysis showed that identified proteins can be found in extracellular matrix (ECM) components, proteinaceous ECM, blood vessels, platelet granules, wound healing, and vasculature development. Protein identification and network analysis also revealed three differentially expressed proteins under osteogenic conditions in fibroblasts: calmodulin 1 (CALM1), collagen type I alpha 2 (COL1A2), and glycyine-tRNA synthetase (GARS). Those findings were confirmed with RT-PCR. Of the three differentially expressed proteins, CALM1 and GARS were further analyzed as possible biomarkers in human aseptic pseudarthrosis samples. Fibrous and cartilage tissue was immuno-stained positive for CALM1 in human pseudarthrosis samples, while GARS-positive signals could be observed in mineralized tissue.

Evaluation of two retrospective clinical studies linked possible connection of pseudarthrosis formation to diseases and risk factors. Those diseases and risk factors are also linked to the two possible biomarkers. The focus of the first retrospective was the analysis of the possible connection of pseudarthrosis to allergies, morbidities, and other risk factors. In total, 162 patients with hypertrophic and atrophic aseptic pseudarthrosis were included in this study. Hypertrophic pseudarthrosis occurred more often in male patients. Atrophic pseudarthrosis was evenly seen in male and female patients. Moreover,

association between type of osteosynthesis material and type of pseudarthrosis was found. Hypertrophic pseudarthrosis occurred more after plating and intramedullary nailing. Atrophic pseudarthrosis was more prominent after screw fixation. Patients with hypertrophic pseudarthrosis used more often nonsteroidal anti-inflammatory drugs (NSAID) when compared to patients with atrophic pseudarthrosis. Besides, older patients were more obese compared with younger patients in both atrophic and hypertrophic pseudarthrosis patients. Allergies occurred more often in hypertrophic pseudarthrosis patients. Moreover, non-allergic patients with atrophic pseudarthrosis were older than patients with one or more allergies. In both, atrophic and hypertrophic pseudarthrosis patients, age was lower in patients with concomitant injuries compared with age of patients with mono-fractures.

The second study was evaluating the impact of microbial infections and especially polymicrobial infections on pseudarthrosis. In this study, septic and aseptic pseudarthrosis were compared. Interestingly, aseptic pseudarthrosis were more hypertrophic than atrophic, while septic pseudarthrosis were evenly classified as atrophic and hypertrophic. Fracture infection was associated with fracture of the tibia, BMI over 30 kg/m² and open fractures. Also, patients with septic pseudarthrosis had more surgical revisions compared with patients with aseptic pseudarthrosis. In total, 111 microbial infections were detected in 43 septic pseudarthrosis patients. 22 (51.2 %) patients had monomicrobial infections, 6 (14.0 %) patients suffered from polymicrobial infections and 15 (34.9 %) patients had germ-changes within course of pseudarthrosis treatment. Most patients had infections after more than one revision surgery. The three most prominent microbes in the infections were different strains of *staphylococci*, *enterococci*, and gram-negative bacilli. Interestingly, *enterococci*, *streptococci*, and gram-negative bacilli mainly occurred in PMI and GC pseudarthrosis patients. In addition, patients with polymicrobial infections and germ-changes had more surgical revisions compared with patients with monomicrobial infections.

5. Discussion

Bone regeneration after a fracture is an important subject among clinicians, researchers, and scientists. Pseudarthrosis or non-union is an incomplete fracture consolidation associated with secondary fracture healing [62, 171]. Clinically, a revision of pseudarthrosis is needed. Osteoblast growth factors like bone morphogenetic proteins (BMP) are often applied to stimulate MSC differentiation into osteoblasts [7, 167, 168]. However, fibroblasts located abundantly at the site of pseudarthrosis respond to the same growth factors as osteoblasts and differentiate to osteoblast-like cells. This can lead to increased fibrous tissue at the fracture site. Thus, normal bone growth is prevented [169, 170].

The hypothesis of this study was that protein-level differences between osteoblast-like fibroblasts and osteoblasts result in pseudarthrosis. Therefore, analysis of MSCs and fibroblasts response to BMP stimulation aimed to contribute in understanding of pseudarthrosis development. In addition, identification biomarkers for pseudarthrosis prediction and establishment of such markers were part of this thesis. By identifying such a biomarker, future pseudarthrosis treatment can be improved.

Whole proteome analysis of human hMSCs (SCC), fibroblasts (FC), MSC-derived osteoblasts (SCO), and osteoblast-like fibroblasts (FO) was carried out using nano-HPLC-ESI-MS. Quantitative and qualitative proteome analysis enabled the discovery of changes in expression levels of the four different cell types. Three biomarkers were significantly down-regulated in osteoblast-like fibroblasts when compared to MSC-derived osteoblasts. Those proteins were: calmodulin 1 (CALM1), collagen type 1 alpha 2 (COL1A2), and glycyine-tRNA synthetase (GARS). Further analysis of CALM1 and GARS in human pseudarthrosis samples showed promising results, indicating their valid status as biomarkers.

5.1. Osteoblast-like fibroblasts showed lower matrix mineralization

Human MSCs, derived from bone reaming debris, have a fibroblast-like morphology. In addition, they express certain cell surface markers, and they have the ability to differentiate into adipocytes, chondrocytes, and osteoblasts. Besides, MSCs share many characteristics with fibroblasts. Until today it is difficult to distinguish between MSCs and fibroblasts by their differentiation capacity [169, 170, 172]. In literature, contrary

reports are found referring to differentiating ability of fibroblasts. Denu et al. 2016 showed differentiation capabilities of fibroblasts [169], while Pittenger et al. 1999 and Cappellesso-Fleury et al. 2010 demonstrated the incapability of fibroblasts to differentiate into adipocytes, chondrocytes or osteoblasts [40, 173].

Clinically, atrophic pseudarthrosis are often treated with BMPs to enhance MSCs differentiation into osteoblasts. BMPs are osteoinductive agents which stimulate bone formation. However, BMP application in pseudarthrosis treatment is debatable. Fibroblasts, the abundant cell type in pseudarthrosis tissue, are also stimulated by BMPs. This leads to an accumulation of fibrous tissue on the pseudarthrosis site. Fibrous tissue negatively influences bone matrix mineralization by osteoblasts as well as bone resorption by osteoclasts. Moreover, several studies reported side effects like local infections, wound complications, and heterotopic bone formation after pseudarthrosis treatment with BMPs [5, 174].

Differentiation capacity of fibroblasts and MSCs derived from human patients was therefore evaluated in vitro. Both cell types were osteogenic stimulated. MSCs (SCC) and fibroblasts (FC) showed differential potential into osteoblasts (SCO) and osteoblast-like fibroblasts (FO). This was histologically confirmed by specific Von Kossa staining which showed matrix mineralization. Descriptively, osteoblast-like fibroblasts showed lower matrix mineralization compared to MSC-derived osteoblasts (**Figure 10**). Taken together, these results indicate that stimulation of fibroblasts found at the pseudarthrosis site enhances impaired bone healing. Thus, their use in pseudarthrosis treatment is debatable.

5.2. Mass spectrometry identified biomarker for pseudarthrosis prediction

Proteomics tools are valuable in the analysis of proteins in a particular sample. Proteins which are differentially expressed in related samples, such as healthy vs. diseased samples, can be identified. Proteins found only in a diseased sample, can be seen as potential biomarkers. Pathway analysis, functional cluster analysis and network reconstruction analysis provide functional information of proteins found in mass spectrometry approach [137, 175-177]. For the first time to my knowledge, proteome profiles of MSCs and fibroblasts before and after osteogenic stimulation were analyzed via mass spectrometric approach and compared to each other.

In this study, mass spectrometry (MS) based quantitative proteomics was used in combination with peptide pre-fractionation using nano-HPLC for the analysis of four different cell types (SSC, SCO, FC, FO). 193 identified proteins were common in all biological and technical replicates, out of 2470 proteins in total. Enrichment map network analysis showed that identified proteins can be found in extracellular matrix (ECM) components, proteinaceous ECM, blood vessels, platelet granules and vasculature development. Also, the 193 proteins were connected to wound healing and wound response (**Figure 11**). These results are in accordance to previous studies of the proteome profile of MSCs. Maurer et al. showed in 2011 that among the proteins of MSCs are cell surface markers and growth factors. Moreover, MSC proteins showed interaction with molecules of the ECM [178]. A study of Celebi in 2009 revealed that the majority of MSC proteins belonged to ion transport, metabolism, and signal pathways' categories [179].
Three potential markers to differentiate SCO and FO were identified utilizing differential protein expression analysis: collagen type I alpha 2 (COL1A2), calmodulin 1 (CALM1), and glycine-tRNA synthetase (GARS) (**Table 4.1**). Expression of COL1A2, CALM1, and GARS in osteoblast-like fibroblasts was lower compared to MSC-derived osteoblasts. Moreover, corresponding genes of the three markers were validated with RT-PCR. The results of proteomics and RT-PCR experiments emphasizes the hypothesis, that osteoblast-like fibroblasts are indeed different on protein-level compared to osteoblasts.

5.3. Validation of potential biomarker in human and murine pseudarthrotic tissue

COL1A2

Collagen type I alpha 2 (COL1A2) is a fibrillar forming protein and a member of type I collagens. Mutations in the COL1A2 are linked to osteogenesis imperfecta [180], a heritable skeletal disorder characterized by bone fragility, fractures at birth, multiple bone deformities and short stature [181, 182]. Network analysis revealed co-expression and co-localization of COL1A2 with CDH11 (cadherin-11), FBN1 (fibrillin-1), FN1 (fibronectin 1), NF1 (neurofibromin 1), POSTN (periostin), SPARC (secreted protein acidic and rich in cysteine, also known as osteonectin), and THBS2 (thrombospondin-2) (**Figure 13**). It showed direct connection of COL1A2 to proteins which are involved in bone formation, matrix mineralization and wound healing [47, 183, 184]. Gelse et al. showed in 2012 that

COL1A2 is a characteristic protein of fibrous tissue and can be ascribed to the fibrocartilaginous callus in fracture healing [185]. COL1A2 quantity was decreased in osteoblast-like fibroblasts compared to MSC-derived osteoblasts (**Table 4.1**). This reflects on the mineralized matrix formation which was descriptively lower in osteoblast-like fibroblasts compared to MSC-derived osteoblasts (**Figure 10**).

GARS

Glycine-tRNA synthetase (GARS) is an aminoacyl-tRNA synthetase that charges tRNAs with glycine [151, 153]. Aminoacyl-tRNA synthetase are essential for protein translation in cytoplasm and mitochondria [186, 187]. Mutations in GARS are connected to atrophy and weakness of hand muscles, to distal muscular atrophy and to Charcot-Marie-Tooth disease (CMTD) [188-190]. Those muscle disorders and weaknesses are associated with low bone mass and increased fracture risk [191-193]. GARS is also connected to neuropilin 1, an extracellular binding partner of GARS. Neuropilin 1 is a receptor for vascular endothelial growth factor (VEGF), which is essential for angiogenesis regulation [194]. The appearance of blood vessels in the fracture callus is a crucial event in bone fracture healing. Vascularization promotes bone repair and regeneration by supplying oxygen and nutrients to the fracture site [194-197]. Hence, downregulation of GARS in osteoblast-like fibroblast points to an impairment in fracture angiogenesis and vascularization. Thus, bone healing is deteriorated and pseudarthrosis can develop. This is in accordance with literature, where disturbed bone healing is associated with a reduction or lack in vascularization of the regenerative tissue [196-198]. This study described for the first time, to my knowledge, the impact of GARS on fracture healing respectively its involvement in pseudarthrosis development.

CALM1

The third identified biomarker was calmodulin 1 (CALM1). CALM1 is a calcium (Ca^{2+})-binding protein which mediates the control of enzymes, ion channels and other proteins [154]. Ca^{2+}/CALM cell signalling is ubiquitous in all levels of cell life cycle. In bone turnover, calcium signalling plays a key role. It regulates osteoblasts and osteoclasts. Studies show that Ca^{2+}/CALM are important for osteoclast development, function and apoptosis [199, 200]. Osteoblast differentiation is also regulated through calmodulin-dependent kinase II (CaMKII). CaMKII regulates osterix (Osx), a zinc-finger

transcription factor that is required for osteoblast differentiation and new bone formation [155, 201, 202]. Osteoblast activation relies on the extracellular signal-related kinase (ERK)/Mitogen-activated protein kinase (MAPK)-pathway and on the Wnt signalling pathway [45, 203, 204]. CALM1 is connected to the ERK/MAPK and the Wnt signalling pathways via interaction with Ras-GTPase-activating-like protein (IQGAP1) [205]. IQGAP1 is integrating signals regulating cell adhesion, actin cytoskeleton, and cell cycle [205, 206]. In the ERK/MAPK pathway, IQGAP1 serves as a scaffold for MAPK. It binds amongst others to ERK and modulates its function. Thus, efficient MAPK cascade propagation requires IQGAP1 [207, 208]. Sequence of IQGAP1 is similar to neurofibromin 1. This suggests that IQGAP1 is a tumour suppressor like neurofibromin 1 [209]. In the absence of neurofibromin 1, ERK/MAPK pathway is activated. This is seen in NF1 patients. Studies suggest that this MAPK activation inhibits osteogenic differentiation [210-212]. Collectively, the role of CALM1 in regulating ERK/MAPK pathway via IQGAP1 points out the importance of CALM1 in bone metabolism and fracture healing.

In addition, CALM1 and IQGAP1 are also involved in the Wnt signalling pathway through interaction of IQGAP1 with β-catenin, an essential regulator for cellular proliferation and cell-cell adhesion [47, 203, 213]. β-catenin is sequestered in a complex under unstimulated conditions and therefore excluded from the nucleus. The β-catenin-complex is targeted for degradation by casein kinase 1 (CK1) and glycogen synthase kinase 3-β (GSK-3β). Inhibition of β-catenin degradation is the result of Wnt stimulation. β-catenin accumulates, translocates to the nucleus and activates osteoblast gene expression [47, 206, 208, 214]. IQGAP1 binds β-catenin and increases nuclear localization and expression of its transcriptional targets like genes for osteoblast differentiation. Hence, CALM1 regulates ERK/MAPK and Wnt signalling pathway by altering the interaction of IQGAP1 and its targets [205, 206, 208, 215].

To my knowledge, this study investigates for the first time the impact of CALM1 on fracture healing and pseudarthrosis development. This study suggests that CALM1 is indeed significant for fracture healing. Hence, development of pseudarthrosis due to lower amount of CALM1 is a result of disturbed osteoblast and osteoclast differentiation. In human pseudarthrotic tissue CALM1 was detected in fibrous tissue, chondrocytes and cartilage (**Figure 19**; **Figure 20**; **Figure 21**).

Taken together, validation of the promising biomarkers COL1A2, GARS, and CALM1 confirmed the hypothesis. There are indeed differences in the proteome of osteoblast-like fibroblasts and osteoblasts. Immunohistochemical evaluation indicated that lower amount of GARS and CALM1 in the callus can result in delayed healing and pseudarthrosis development.

5.4. Characterization of aseptic pseudarthrosis

A retrospective clinical study was performed to evaluate if pseudarthrosis formation is linked to diseases and risk factors which are also connected to COL1A2, CALM1, and GARS. The study's focus lied particularly in the analysis of the possible connection of pseudarthrosis development to allergies, morbidities like metabolic disorders and other risk factors. Also, this study aimed at analyzing if systemic factors influence the fate of pseudarthrosis to become atrophic or hypertrophic.

Bone healing process and pseudarthrosis treatment depends on the type of pseudarthrosis. Clinically, pseudarthrosis can be classified as atrophic or hypertrophic type based on the Weber-Cech classification of 1976 [216]. Atrophic pseudarthrosis have no sign of callus and no signs of bony consolidation in the fracture gap. In hypertrophic pseudarthrosis there is callus formation around the fracture gap as well as calcification. But bony consolidation within the fracture zone is also not sufficient in hypertrophic pseudarthrosis [143, 159, 160]. Treatment of aseptic atrophic differs from treatment of hypertrophic pseudarthrosis. In hypertrophic type treatment, mechanical stability must be improved to achieve bony consolidation. The surgical procedure for the avital atrophic pseudarthrosis includes resection of fibrous and cartilaginous tissue. Moreover, use of bone grafts to enhance the biological potential is necessary in treatment of atrophic pseudarthrosis [216]. Therefore, identification of systemic factors that influence pseudarthrosis type formation in either atrophic or hypertrophic can help in the development of an improved treatment of pseudarthrosis.

5.4.1. Histological analysis showed differences in aseptic pseudarthroses

Histologically, atrophic, and hypertrophic pseudarthrosis samples show differences which suggest a different cellular background. Histological analysis in this study revealed lower cellular density in atrophic pseudarthrosis with only few mineralized tissue structures (**Figure 15**). Hypertrophic pseudarthrosis had more mineralized tissue

structures and a higher cellular density (**Figure 18**). Atrophic pseudarthrosis showed granulation tissue, suggesting vascularization (**Figure 17**). In both forms of pseudarthrosis, the main tissue types identified with histological analysis were fibrous, cartilaginous, fibrocartilaginous, and connective tissue. These findings agree with the study from Iwakura et al. in 2009. This study mainly fibrous tissue with various amounts of fibroblast-like cells in human aseptic hypertrophic pseudarthrosis samples [74]. Takahara et al. [217] reported in 2016 that aseptic atrophic pseudarthrosis tissue has in fact good vascularization, represented by small vessels and granulation tissue. In this study, the histological results also showed granulation tissue.

This work here only had a small sample size of two pseudarthrotic tissue sample for each type, atrophic and hypertrophic. Therefore, further studies with larger samples are needed for a more detailed histological analysis of aseptic human pseudarthrosis. Afterwards applied histomorphometry can reveal differences between atrophic and hypertrophic pseudarthrosis.

5.4.2. Impact of allergies on fracture healing

In 1972, Horton et al. discovered that osteoclastic bone resorption can be stimulated by activated peripheral blood leucocytes [218, 219]. In fracture healing, immune system and skeletal system are interacting through common proteins and enzymes, for example RANK (receptor activator of nuclear factor kappa B) and RANK Ligand (RANKL). RANK and RANKL play a role in the immune system as mediators of T-cell activation and dendritic function. They are also involved in regulation of osteoclastogenesis [219-221]. Immune cells such as macrophages are involved in all phases of bone repair after fracture. They have a major impact on the long-term outcome of bone repair [56, 222]. Regarding the impact of allergies, Ferencz et al. showed in 2006 a correlation between increased fracture risk and pollen-allergy in postmenopausal women. Several clinical studies support histamine involvement in bone resorption [223, 224]. However, Zura et al. reported in 2016 that allergies are apparently protective for pseudarthrosis development. Overall, 19.5 % of all patients in Zura's study suffered from an allergy. In comparison to non-allergic patients, pseudarthroses were less developed in patients with allergies [225, 226].

In this current retrospective study, 25.2 % of the patients with pseudarthrosis suffered from an allergy. This is comparable with the prevalence of allergies in patients in

Germany (2016: 28.1 %) [227]. There were no significant differences in the number of allergies between atrophic and hypertrophic pseudarthrosis. But more patients with hypertrophic pseudarthrosis suffered from allergies (30.2 % of patients with hypertrophic pseudarthrosis; 17.2 % of patients with atrophic pseudarthrosis). Nevertheless, the protective effect of allergies on pseudarthrosis development described by Zura needs to be further investigated and analyzed.

A well-known risk factor for delayed healing and pseudarthrosis development is the patient's age [82, 225]. The increase of fractures in the elderly correlates with age-related illnesses. Those illnesses can increase fall risk and fracture risk and pseudarthrosis development. Age-related illnesses include diabetes, Alzheimer's and Parkinson's disease, stroke, multiple sclerosis as well as systemic bone diseases such as osteoporosis, osteopenia, and sarcopenia [82, 228-230]. Physiological changes occur with aging which can influence fracture healing. Vascularization and angiogenesis are impaired in bone healing in the elderly. Besides, inflammatory response during fracture healing is disturbed due to alteration in immune response and increased pro-inflammatory status. Macrophages, T-cells and MSCs undergo age-related changes which can lead to impaired fracture healing [231]. This retrospective study revealed that allergy-free patients suffering from an atrophic non-union were significantly older compared to allergy-free hypertrophic non-union patients (**Figure 23**).

5.4.3. Biomechanical characteristics

The Gustilo-Anderson classification associated open fractures with a greater risk of pseudarthrosis due to disruption of the soft tissue [79, 232, 233]. Also, fracture hematoma is released through the fracture site of open fractures. This leads to the reduction of healing factors and to the enhancement of pseudarthrosis risk [234]. In this study 72.8 % of aseptic pseudarthrosis cases were seen in closed fractures. 27.2 % of the patients had open fractures. More hypertrophic pseudarthrosis were seen after open fractures. But no significant difference in the frequencies of atrophic and hypertrophic pseudarthrosis was observed.

Another widely accepted reason for development of pseudarthrosis is insufficient mechanical stability of the implants [83, 232]. For hypertrophic pseudarthrosis, mechanical instability is one of the main reasons for pseudarthrosis development [235]. In this current study, no association between implant loosening and pseudarthrosis type

was found. Implant loosening was identified by radiographic signs like breakage of implants, loosening zones around the implants and screw migration. Identifying implant loosening with radiographs alone is a limitation in this current study. Future studies should include more advanced diagnostic tools for characterization of the loosened status of orthopaedic implants. Such methods include magnetic resonance imaging (MRI) and computer tomography (CT).

An association was found between osteosynthesis and pseudarthrosis type. More patients with plates and intramedullary pins suffered from hypertrophic pseudarthrosis compared to atrophic pseudarthrosis patients. Patients with screws suffered more from atrophic pseudarthrosis (**Figure 26**). In literature, more hypertrophic pseudarthrosis after intramedullary nailing could be seen and more atrophic pseudarthrosis after plate or screw osteosynthesis [16, 55, 236]. Henderson reported that overly rigid fixation, for example with screws, lead to reduced motion at the fracture side. This led to decreased callus formation [236, 237]. On the other hand, inadequate immobilization is a risk factor for hypertrophic pseudarthrosis development. Osteosynthesis with intramedullary pins leads to an instability and an increased callus formation [238, 239].

5.4.4. Obesity and medication use have impact on fracture healing

Biological risk factors such as obesity, medication intake and morbidities can contribute to altered fracture healing in patients. Those risk factors are potentially increasing with age, another pseudarthrosis risk factor [82]. Obesity was associated with the risk of pseudarthrosis in several studies [82, 240, 241]. Cao suggested in 2011 that obesity could have a negative impact on bone metabolism by increasing pro-inflammatory cytokines levels and enhancing oxidative stress [242]. Other studies found no association between pseudarthrosis and obesity [80, 243, 244].

In this current study, almost two-thirds (62.1 %) of all pseudarthrosis patients were obese with a BMI over 25 kg/m². BMI increased with increasing age in both groups of pseudarthrosis type. In the atrophic pseudarthrosis cohort, allergic patients had a higher BMI than non-allergic patients (**Figure 27**). This is in accordance to other studies, where obesity was common among allergic patients [223].

Other comorbidities like smoking, diabetes and cardiovascular diseases were also documented to have a negative impact in bone healing. They also increase the risk of pseudarthrosis development [6, 88, 245]. In this current study more than 40 % of the

patients in both groups suffered from at least one morbidity. 18.4 % of all pseudarthrosis patients were smokers. 18.4% suffered from a cardiovascular disease and 11.6 % from diabetes mellitus. However, there were no differences between atrophic and hypertrophic pseudarthrosis.

Another risk factor for pseudarthrosis development is medication use. In this study, effect of NSAIDs (Nonsteroidal anti-inflammatory drugs) on pseudarthrosis was investigated. NSAIDs play an essential role in pain and inflammation control in posttraumatic conditions. Clinical and experimental data suggest that intake of NSAIDs can have a negative impact on fracture healing and may lead to pseudarthrosis development [246-249]. NSAID medication reduces prostaglandin production. Prostaglandins are needed in the inflammation phase of bone healing. They are essential for initiating the osteogenic response [250]. Prostaglandins influence osteoclast activity and on the anabolic effect by increasing numbers and differentiation of osteoblasts. Thus, prostaglandins are important for the balance of bone formation and resorption [99, 251]. Exact impact of NSAIDs on bone healing is not fully understood until today [251-253].

Only long-term NSAID intake was evaluated in this current study but not NSAIDs dosage. The rate of long-term NSAID intake was not statistically different between atrophic and hypertrophic pseudarthrosis cohorts (**Figure 28**). Thus, there was seemingly no influence of NSAID in development of non-union type under aseptic conditions. Regarding further shortcomings of this study, details of NSAID intake would be an area for future studies. Obtained information on the dosage and the duration time of NSAID use could be of relevance for analyzing impact of NSAID on pseudarthrosis development.

5.4.5. Polytrauma occur in younger patients

Impact of concomitant injuries (polytrauma) on bone healing remains to be poorly understood until today. The pathophysiological and immunological response to polytrauma has to be further investigated to improve treatment of multiple injured patients [254, 255]. Studies showed that patients with polytrauma had higher risk of malunion or pseudarthrosis development compared to patients with isolated fractures. Additional injuries of soft tissues, hemorrhage and chest led to local and systemic hypoxia which had negative impact on fracture healing [256]. Soft tissue injury impairs nutritional blood flow to the site of the injury. Thus, early fracture healing can be impaired by disrupting the local blood supply [91]. Chest trauma associated with fracture led to

decreased fracture healing in a rat animal model. This was due to disturbance of the inflammatory balance during early phase of bone healing. Recruitment of inflammatory cells and expression of cytokines at the fracture site was altered in rats with polytrauma [257]. Several studies led to conflicting results regarding the effect of hemorrhagic shock to fracture healing. Bundkirchen et al. showed in 2017 that hemorrhagic shock leads to delayed fracture healing or even to pseudarthrosis development. Starr et al. 2002 showed no effect of hemorrhagic shock [258, 259].

In this current study, there was no statistically significant difference between hypertrophic and atrophic pseudarthrosis in patients treated for one isolated fracture compared to patients with polytrauma. Concomitant injuries, which needed additional fracture fixation, appeared in 32.7 % and more often in younger patients (**Figure 29**). Reason might be high-energy trauma in youngsters. Further clinical studies need to clarify if the high rate of pseudarthrosis patients with concomitant injuries is based on systemic reasons. Those reasons include hemorrhage, chest trauma, soft tissue injury or simply additional fractures.

To summarize, there are different treatment strategies for aseptic atrophic and hypertrophic pseudarthrosis. Experimental studies have shown that an intrinsic healing potential in atrophic pseudarthrosis might be inhibited by systemic factors. This retrospective study aimed for an identification of risk factors that influence pseudarthrosis formation, either atrophic or hypertrophic. A significant higher rate of atrophic pseudarthrosis in nonallergic elderly patients was determined. In addition, more hypertrophic pseudarthrosis in nonallergic younger patients was seen. Further relevant risk factors which might influence pseudarthroses to become either atrophic or hypertrophic were not identified in this study. Considering the retrospective nature of this study, future prospective clinical trials with more advanced diagnostic tools can help in evaluating further role of systemic factors in pseudarthrosis development.

5.5. Microbial infections in septic pseudarthroses

Besides biological causes and mechanical instability, microbial infections of the bone itself, the soft tissue and/or of the fixation material are also important in the development of pseudarthroses. Typically, infections occur because bacteria or other microbes enter the body during the trauma. In addition, infections can come from bacteria entering the

body during surgery. Fracture treatment is complicated and even impaired in the presence of infections [167, 252, 260]. Postoperative outcomes are downgraded in the presence of microbial infections [261]. Successful fracture treatment needs the exact diagnosis of the infectious microbes. Moreover, risk factors of infection, such as immune compromise, malnutrition, and smoking as well as open fractures should be assessed in treatment of septic pseudarthrosis [167]. In this second retrospective study, potential risk factors and postoperative outcome factors of microbial and polymicrobial infections were analyzed. Besides, germ-changes within course of septic pseudarthrosis treatment were analyzed as well.

5.5.1. Comparison of aseptic and septic pseudarthrosis

Septic pseudarthroses were associated with open fractures, tibial fractures, and obesity in this retrospective study. This is in accordance with previous studies. Open fractures represent the most common cause of infected pseudarthrosis [77, 262-264]. Higher infection rates in open fractures result from concomitant soft tissue injuries. In an open fracture, either bone fragments stick out through skin or a wound penetrates down to the bone. In addition, nerves, tendons, and cartilage can be damaged. Normally, the skin acts as a barrier against contaminants and microbes. However, when the skin barrier is damaged, contamination with microorganisms can occur on the open fracture. Moreover, local tissue vascularization is impaired in open fractures. Treatment management for open fractures must therefore encompass prevention of infection, prevention of pseudarthrosis development and restoration of bone function. In previous studies, postoperative infection risks of open fractures are between 3 and 45 % [76, 262, 263]. Results of this current study is in alignment with literature. 42.6 % of all patients with infectious pseudarthrosis had open fractures (**Figure 30**).

Patients with the genetic disorder, type 1 neurofibromatosis (NF1) often suffer from dysplasia of the long bones, mostly of the tibia. Tibia bowing in NF1 patients increases risk of tibial fractures and pseudarthrosis development [265]. Tibia is subcutaneous. Therefore, tibia fractures often have a damaged periosteum, a key source of bone progenitor cells. Due to limited accessibility of bone progenitor cells, bone healing in tibia fractures is prone to complications like infections, delayed healing, and non-union development [210]. In the cohort with aseptic pseudarthrosis, 30 % of the patients had tibial fractures (**Table 4.2**). However, tibial fractures were associated with infections in

this retrospective study (**Figure 30**). Almost 60 % of the patients with septic pseudarthrosis had a tibial fracture (**Table 4.2**). These results are in line with previously published studies. Literature shows, that tibia is the most commonly involved bone in infectious pseudarthrosis [76, 84, 263, 266].

Infections were also associated with obesity in this retrospective study. This is also seen in literature (**Figure 30**). Previous studies showed that morbid obesity is a significant risk factor for systemic complications after trauma treatment. Patients with an BMI over 30 kg/m² have a greater rate of infection, more frequent need for revision surgeries and difficulties achieving fracture union [86, 243, 267]. Adipose tissue interacts with the immune system by secretion of adipokines. In obese patients with accumulated adipose tissue, the well-balanced system of immune cells and adipocytes is deteriorated. This leads to dysregulated immune response. However, the exact underlying mechanisms of obesity influence on infections are not fully established until today [268].

5.5.2. Comparison of mono-, polymicrobial infections and germ-changes

Until today, there is no data regarding the outcome of polymicrobial infections in septic pseudarthrosis patients compared to monomicrobial infections. But there are several studies describing polymicrobial infections in patients undergoing arthroplasty surgery [269, 270]. In 2016, a study of polymicrobial infections after total joint arthroplasty showed that number of surgical revisions is associated with polymicrobial infections [271]. Other studies were not able to correlate polymicrobial infections with revision surgeries [271, 272]. Data from this retrospective study showed, that pseudarthrosis patients with polymicrobial infections had more surgical revisions compared to pseudarthrosis patients with monomicrobial infections. Moreover, most patients had infections after more than one revision surgery (**Figure 31**).

Inflammatory markers like leucocytes and complement reactive protein (c-reactive protein, CRP) are indicators of infections. Thus, they have been investigated in fracture healing, trauma surgery and orthopedics [273-277]. CRP belongs to a group of plasma proteins which is part of the innate immune system. In response to interleukin-6 (IL-6) release after trauma and infection, CRP is secreted by macrophages and adipocytes [273, 274]. At the same time, IL-6 reduces production of fibronectin 1 (FN1). FN1 is a protein which is important for wound and bone healing, osteoblast mineralization and cell

adhesion [278]. Decrease of FN1 can lead to impaired bone healing [273]. Results of network analysis in this study showed, that FN1 is directly interacting with the two biomarkers CALM1 and COL1A2 (**Figure 13**). In the retrospective study, CRP values were higher in patients with germ-changes compared to monomicrobial and polymicrobial infected patients. However, this was not significant (**Table 4.5**). Bozhkova et al. showed in 2016 that elevated CRP levels are correlated to infections with different germs [279]. Moreover, other studies showed that polymicrobial infections are more likely prone to an unsuccessful outcome compared to monomicrobial infections [277, 279].

Another crucial part of septic pseudarthrosis treatment is the exact diagnosis of the infection causative microbes. The etiology of infection allows the selection of the best antimicrobial therapy [269, 280]. In most septic pseudarthrosis and prosthetic joint infections studies, *coagulase-negative staphylococci* and *staphylococcus aureus* species have been determined as the most commonly occurring infection causative microbe [80, 233, 269, 280, 281]. In this retrospective study, *staphylococci aureus* was also the most identified microbes in monomicrobial, polymicrobial and germ-change cases (**Table 4.3**). In addition, PMI and GC patients showed infections with *enterococci*, *streptococci*, and gram-negative bacteria in contrast to MMI.

In this retrospective study, potential risk factors and postoperative outcome factors different infection types (MMI, PMI, and GC) were analyzed. Moreover, septic, and aseptic pseudarthrosis were compared. Taken together, open fractures, tibial fractures as well as obesity were considered as risk factors for septic pseudarthrosis. In addition, the study clearly showed the deteriorated outcome of pseudarthrosis patients with polymicrobial infections and germ-changes within course of treatment. They had to undergo more surgical revisions and had prolonged hospital stays.

6. Conclusion

Despite the diagnostic options available today, pseudarthrosis can only be diagnosed when they have already been established. Currently, it is not possible to predict the outcome of a bone fracture in the early phase, e.g. during the initial surgery. Early prediction would allow for advanced treatment. Furthermore, early diagnosis can prevent pseudarthrosis development and, thereby, avoiding additional surgeries and long burden for the patient. A biomarker with the ability to predict type of pseudarthrosis or high-risk for pseudarthrosis development, will allow an early adaptive targeted treatment leading to a successful bone healing. Identification of novel biomarkers relies on the choice of technique. Several methods like genomics, metabolomics and proteomics are used to identify novel candidate makers to understand underlying disease mechanisms.

Previous studies showed that fibrous tissue influences bone fracture healing [265]. Aim of this study was to identify possible biomarkers within the hypothesis that protein-level differences between osteoblast-like fibroblasts and osteoblasts result in pseudarthrosis. Three promising proteins (calmodulin 1 (CALM1), collagen type 1 alpha 2 (COL1A2), and glycyine-tRNA synthetase (GARS)) were discovered by proteomics approach. CALM1 and GARS were further evaluated in human aseptic pseudarthrosis samples. Hence, CALM1 and GARS are indeed potential biomarker to decide the feasibility of fracture treatment with anabolic agents such as bone morphogenetic proteins (BMPs).

In addition, it is important to discriminate between aseptic atrophic and hypertrophic pseudarthrosis as treatment of the two types follows different strategies. The first retrospective study in this thesis aimed for identification of risk factors that influence pseudarthrosis formation, either atrophic or hypertrophic. Although one systemic factor was found, age combined with allergies, prospective clinical trials with more advanced diagnostic methods should be conducted to elucidate the role of systemic factors on type of pseudarthrosis. Another important factor for pseudarthrosis development is the impact of infections on bone healing, pseudarthrosis development and postoperative outcome. A second retrospective study revealed three risk factors for septic pseudarthrosis: open fractures, tibial fractures, and obesity. Moreover, elevated CRP level seems to be one potential indicator for polymicrobial infections. The study also showed that patients suffering from polymicrobial septic pseudarthrosis had a deteriorated outcome. However, both retrospective studies have potential shortcomings. Although, data of 162 patients with aseptic pseudarthrosis in the first study, and 44 patients with septic pseudarthrosis

in the second study were analysed, the number of patients remains low compared to other studies. In addition, retrospective studies can be biased because data was collected beforehand. Nevertheless, retrospective studies are useful as pilot studies, as they can help in hypothesis formulation and in identifying important risk factors. However, to make precise estimation of risk factors for pseudarthrosis development, either atrophic, hypertrophic, aseptic, or septic, prospective studies are required.

This work highlights the complex nature of bone healing and pseudarthrosis development. Understanding the underlying pathomechanisms leading to pseudarthrosis is important for treatment improvement. In addition, it showed the importance of patient-dependent factors and their influence in the healing process and pseudarthrosis development. Besides, this thesis showed that combination of proteomics approach, network analysis and retrospective studies could be used for improvement of disease treatment.

7. Implications and future prospects

Using interdisciplinary methods such as cell culture, proteomics, histology, and retrospective clinical studies revealed the potential role of CALM1 and GARS as biomarkers for pseudarthrosis. In addition, GARS and CALM1 have potential to discriminate between aseptic atrophic and hypertrophic non-union. This is of great importance as treatment of the two non-union types follow different strategies. Thus, further research with more samples is necessary to assess their potential role as biomarker. Despite the interesting results of this work, there are still scopes to examine. This current study also presented some limitations. For validation of GARS and CALM1 as biomarkers, it is necessary to compare findings with control samples. However, no human control samples were included here due to difficulties in obtaining such samples. However, additional studies must evaluate GARS and CALM1 in human control samples. In addition, all analyzed human samples were aseptic pseudarthrosis. No septic pseudarthrosis samples were used. Future experiments must therefore include not only human control samples but also septic pseudarthrosis samples. Furthermore, number of aseptic pseudarthrosis samples should be increased for a better statistic. Future experiments should consist of histological analysis of various samples (control, septic pseudarthrosis, aseptic pseudarthrosis) to elucidate tissue types which are unique for each class of pseudarthrosis. These experiments must include immunohistochemically staining of GARS and CALM1 with subsequent histomorphometric analysis. Moreover, blood sample analysis is recommended to detect values of GARS and CALM1. A correlation between biomarkers discrepancies in the tissue and their serum or whole blood level concentration can provide information about the healing status of surgically revised pseudarthrosis. The further validation of CALM1 and GARS as diagnostic tools in pseudarthrosis treatment is a challenging task for the future.

Because it was and is difficult to obtain control samples from human patients, samples from animal models could be utilized in further research. A suitable animal model for pseudarthrosis research is the $Nf1Prx1^{-/-}$ mouse model. This model closely recapitulates the development of pseudarthrosis in human patients with neurofibromatosis type 1 (NF1) [265, 282]. Neurofibromatosis type 1 (NF1) is an autosomal dominant genetic disease caused by mutation in the NF1 gene, which encodes the tumour suppressor neurofibromin (Nf1), an important component of the MAPK-pathway [265, 283, 284]. Patients with NF1 often have abnormalities of the skeleton. Those abnormalities include

tibia bowing and spontaneous fractures with the development of a congenital tibial pseudarthrosis. A key complication in congenital pseudarthrosis is the presence of accumulated fibrous tissue which prevents growth of functional bone tissue and provides inadequate mechanical support [284]. Therefore, this model is suitable to study not only development of pseudarthrosis but also for preclinical testing of candidate therapies [285]. In $Nf1Prx^{1-/-}$ mice, early osteoprogenitor cells are inactivated because those mice are lacking both Nf1 alleles in mesenchymal cells and their derivatives (osteoblasts, adipocytes, chondrocytes, muscle cells, endothelial cells of the skullcap and developing limb bud mesenchyme) [285]. Thus, osteoblast differentiation is inhibited, fibrous tissue formation is enhanced, and matrix mineralization is impaired in $Nf1Prx^{1-/-}$ mice [265, 282]. Indeed, pilot studies of pseudarthrosis biomarkers in a pseudarthrosis mouse model ($Nf1Prx1^{-/-}$) showed most promising results when compared to a wild type (WT) mouse model. Evaluation of CALM1 and GARS in the $Nf1Prx^{1-/-}$ mouse model showed impact of those two proteins on fracture healing and pseudarthrosis development. $Nf1Prx^{1-/-}$ -samples had lower staining intensity of the biomarkers compared to WT-mouse samples. The recapitulations of patient situation opened the door for further research questions in the future.

In addition, future clinical trials with more advanced diagnostic methods should be conducted to clarify the role of systemic factors and infections in pseudarthrosis development. The potential biomarkers must be evaluated on their analytical and clinical validity and their clinical utility. Interdisciplinary teamwork is required for those challenging tasks with the focus on biologist, biochemists, and clinicians.

8. Summary

Fracture healing is a complex physiological process, requiring long and complicated treatment. Delayed healing and pseudarthrosis occur in 5-10% of all fractures. In surgically challenging pseudarthrosis revisions, osteoinductive growth factors are often applied locally to stimulate the differentiation of mesenchymal stromal cells (MSC) into bone-forming osteoblasts, thereby accelerating fracture healing. However, fibroblasts are also stimulated by those growth factors. Particularly in the case of large-area defects, fibrous tissue can lead to pronounced pseudarthroses. Aim of the present study was therefore to find biomarkers that help to identify when the application of growth factors leads to increased fibroblast differentiation and thus worsens the course of bone healing. Biomarkers would allow early detection pseudoarthrosis development and thus a more targeted treatment. In addition to identifying such biomarkers, this work also used retrospective studies to identify patient-related risk factors that influence the type of pseudoarthrosis.

Differences in the proteomes of MSCs and fibroblasts before and after osteogenic stimulation were analyzed with mass spectrometry. Liquid chromatography-nano-electrospray ionization-mass spectrometry (LC-nano-ESI-MS) based quantitative proteomics, integrated with network analysis, was applied. Proteome analysis revealed three potential biomarkers, significantly down-regulated ($p<0.05$) in osteogenic stimulated fibroblasts compared to osteogenic stimulated MSCs. The promising proteins are alpha-2 type I collagen (COL1A2), calmodulin-1 (CALM1), and glycine tRNA synthetase (GARS). Corresponding gene network analysis showed connection of CALM1 and GARS with genes related to bone diseases and associated with pseudarthrosis formation. In the next steps, the successfully identified biomarkers must be tested further for their diagnostic potential and their role in fracture healing. Thus, future studies should include human serum analysis. A correlation between biomarkers discrepancies in the tissue and their serum level concentration could provide additional information about healing status of surgically revised pseudarthrosis.

In the second part of this study, two retrospective clinical studies were conducted to gain insight into systemic risk factors for pseudarthrosis. The results of this work show the importance of retrospective clinical studies to assess effectiveness of current surgical and pharmacological treatment approaches. Evaluation of individual patient characteristics can enable tailored and better pseudarthrosis treatment.

9. Zusammenfassung

Frakturheilung ist ein komplexer physiologischer Prozess, der lange und komplizierte Behandlungen erfordert. Verzögerte Heilung und Pseudarthrosen treten bei 5-10% aller Frakturen auf. Bei chirurgisch anspruchsvollen Pseudarthrose-Revisionen werden häufig Wachstumsfaktoren lokal eingesetzt, um die Differenzierung mesenchymaler Stromazellen (MSC) zu knochenbildenden Osteoblasten zu stimulieren und damit die Frakturheilung zu beschleunigen. Diese Wachstumsfaktoren stimulieren aber auch Fibroblasten. Vor allem bei großflächigen Defekten kann fibröses Gewebe zu ausgeprägten Pseudarthrosen führen. Ziel der vorliegenden Studie war daher die Identifizierung von Biomarkern, die helfen zu erkennen, wann die Zugabe von Wachstumsfaktoren zu vermehrter Fibroblasten Differenzierung führt und damit den Verlauf der Knochenheilung verschlechtert. Solche Biomarker würden eine Früherkennung der Pseudarthrose Entwicklung und damit gezieltere Behandlungen ermöglichen.

Mit Flüssigchromatographie-Nano-Elektrospray-Ionisation Massenspektrometrie (LC-Nano-ESI-MS), wurden Unterschiede im Proteom von MSCs und Fibroblasten vor und nach osteogener Stimulation analysiert. Dabei wurden drei potenzielle Biomarker entdeckt, die in osteogen stimulierten Fibroblasten im Vergleich zu osteogen stimulierten MSCs signifikant herunterreguliert waren ($p<0.05$): Alpha-2 Typ 1 Kollagen (COL1A2), Calmodulin-1 (CALM1) und Glycin tRNA Synthetase (GARS). Weitere Analysen zeigten eine Korrelation von CALM1 und GARS mit Genen, die mit Knochen-erkrankungen und mit der Bildung von Pseudoarthrose verbunden sind. Nachfolgend müssen die identifizierten Biomarker weiter auf ihr diagnostisches Potenzial und ihre Rolle bei der Frakturheilung getestet werden. Diese Studien sollten die Analyse von Humanserum beinhalten. Eine Korrelation zwischen Biomarker-Diskrepanzen im Gewebe und ihrer Konzentration im Serum könnte zusätzliche Informationen über den Heilungsstatus der chirurgisch revidierten Pseudarthrose liefern.

Weiterhin wurden retrospektive klinische Studien analysiert, um einen Einblick in systemische Risikofaktoren für Pseudarthrosen zu gewinnen. Die Ergebnisse zeigen die Bedeutung solcher Studien zur Beurteilung der Wirksamkeit aktueller chirurgischer und pharmakologischer Behandlungsansätze. Die Auswertung individueller Patienten-charakteristika kann eine maßgeschneiderte und bessere Pseudarthrose Behandlung ermöglichen.

10. Abbreviation List

Abbreviation	Term
[%]	Percentage
°C	Degree Celsius
ABC	Avidin-biotin complex
ACTB	Beta-actin
ALAS1	Delta-aminolevulinate synthase 1
ANOVA	Analysis of variance
AP	Alkaline phosphatase
B2M	Beta-2 microglobulin
BMI	Body mass index
BMP	Bone morphogenetic protein
BMU	Basic multicellular unit
BSP	Bone sialoprotein
CALM1	Calmodulin 1
CD	Cardiovascular diseases
CDH11	Cadherin-11
COL1A2	Collagen type 1 alpha 2
CT	Computer tomography
D	Day
DAVID	Database for Annotation, Visualization, and Integrated Discovery
DEG	Differentially expressed genes
DMEM	Dulbecco's modified eagle medium
DM	Diabetes mellitus
DNA	Deoxyribonucleic acid
dNTPs	Deoxynucleotides
e	Erythrocyte
ECM	Extracellular matrix
EDTA	Ethylenediaminetetraacetic acid
EF-2	Elongation factor 2
e.g.	for example, (*exempli gratia*)
ERK	Extracellular signal-regulated kinase
ESI-MS	Electrospray ionization mass spectrometry
FBN1	Fibrillin-1
FC	Fibroblasts served as control
FC	Fold change
FCS	Fetal calf serum
FDA	American Food and Drug Administration
FN1	Fibronectin 1
FO	Osteogenic stimulated fibroblasts
ft	Fibrous tissue
GAPDH	Glyceraldehyde 3-phosphate dehydrogenase

GARS	Glycine-tRNA-synthetase
GO	Gene ontology
Gt	Granulation tissue
HIER	Heat-induced epitope retrieval
HPLC	High performance liquid chromatography
HPRT	Hypoxanthine-guanine phosphoribosyltransferase
i.e.	that is (*id est*)
IBM	International business machines
IHC	Immunohistochemistry
KEGG	Kyoto Encyclopedia of Genes and Genomes
LH2	Procollagen-lysine,2-oxoglutarate 5-dioxygenase 2
Lox	Lysyl oxidase
LRP-5	Lipoprotein-receptor-related protein 5
MAPK	Mitogen activated protein kinase
M-CSF	Macrophage colony stimulating factor
MEPE	Matrix extracellular phosphoglycoprotein
mg	Milligram
ml	Millilitre
mm	Millimetre
M-MLV RT	Moloney Murine Leukemia Virus Reverse Transcriptase
MRI	Magnetic resonance imaging
MSC	Mesenchymal stem cell
mt	Mineralized tissue
NF1	Neurofibromatose type 1
Nf1	Neurofibromin 1
nm	Nanometre
NSAID	Non-steroidal anti-inflammatory drugs
Ob	Osteoblast
Oc	Osteoclast
OCN	Osteocalcin
ONC	Osteonectin
OPG	Osteoprotegerin
OPN	Osteopontin
Ot	Osteocyte
PDGF	Platelet-derived growth factor
PFA	Paraformaldehyde
PGK1	Phosphoglycerate kinase 1
PMI	Polymicrobial infections
PPIA	Peptidylprolyl isomerase A
RANKL	Receptor activator of nuclear factor kappa B ligand
RIPA2	Replication protein A2
ROS	Reactive oxygen species
RPL13a	Ribosomal protein L13a

RPL41	Ribosomal protein L41
RT	Room temperature
RT-PCR	Real-time polymerase chain reaction
Runx2	Runt related transcription factor 2
SCC	Mesenchymal stromal cells served as control
SCO	Osteogenic stimulated stromal cells
SEM	Standard error of mean
SOST	Sclerostin
Sparc	Secreted protein acidic and cysteine rich
SPSS	Statistical package for the social sciences
TBS	Tris-NaCl-Buffer
TGF-β	Transforming growth factor beta
THBS2	Thrombospondin-2
TNF	Tumor necrosis factor
Vegfa	Vascular endothelial growth factor alpha
WT	Wild type

11. Acknowledgment

This journey would not have been possible without the support of my family, professors and supervisors, and friends.

I would like to thank Prof Dr.rer.nat. Thaqif El Khassawna, my PhD supervisor, for giving me the opportunity to work in this interesting research field, for precious support, discussions, and the faith in my work. I have been extremely lucky to have a supervisor who cared so much about my work, and who responded to my questions and queries so promptly and with patience.

My sincere thanks also go to PD Dr.med. Markus Rupp, for being my co-supervisor, for your support, fruitful discussions and for the opportunity to analyze two retrospective clinical studies.

I also want to thank Dr.rer.nat. Sabine Schulz from the Analytical Chemistry Department (JLU Giessen) for the nano-HPLC-ESI-MS/MS analyses and M.Sc. Felix Schulze from the Department of Pediatrics of University Hospital Carl Gustav Carus (TU Dresden) for the genomics analyses.

I am thankful to Prof. Dr.rer.nat. Katrin Susanne Lips and for Univ.-Prof. Dr.med. Dr. h.c. Christian Heiß for the opportunity to work in the Institute of Experimental Trauma Surgery and for their support.

My research would have been impossible without the aid and support of my fellow lab members. I am profoundly grateful especially to Annette Stengel for her tremendous help with immunohistochemistry and histology, and to Olga Dakischew for her help with cell culture. I also want to thank Deeksha Malhan, PhD, for guidance with bioinformatics analyses, for the company in the lab/office and the fun discussions. Further, I would like to thank Tamina Denise Menges and Tobias Wagner for collecting patient's data for the second retrospective study.

Besides, I want to thank the whole "bone cracker"-team, Dr.rer.nat. Diaa-Eldin S Daghma, Dr.rer.nat. Fathi Hassan, Dr.biol.hom. Sabine Stötzel for their support, stimulating discussions and technical help. I also want to say thanks to all lab members (technical and non-technical staff members) of the Institute of Experimental Trauma Surgery for their help and support, especially Ida Oberst and Ivonne Bergen.

In addition, I want to thank the Institute for Physical Chemistry for the opportunity to finish this thesis during my stay there. I want to thank especially Dr. Marcus Rohnke for always supporting me.

I would extend countless thanks to my friends, for keeping me sane through the whole journey. Many thanks to Andreas for the endless discussions, game and movie nights.

私は人々が見つけることができる親友であることについて素晴らしいワンダーウーマンに感謝したい。私のために、楽しい日々のためにそこにいてくれてありがとう。ありがとう, 指揮官 Chrissi, 通信士官 Chrisi, 最高セキュリティ責任者 Sae。あなたのキャプテンであることは光栄です。

Finally, I want to thank my family. Danke Mama, Papa und Andi, dass ihr mich immer unterstützt habt. And finally, I want to thank my cats.

12. Thesis declaration

Hiermit erkläre ich, dass ich die vorliegende Arbeit selbständig und ohne unzulässige Hilfe oder Benutzung anderer als der angegebenen Hilfsmittel angefertigt habe. Alle Textstellen, die wörtlich oder sinngemäß aus veröffentlichten oder nichtveröffentlichten Schriften entnommen sind, und alle Angaben, die auf mündlichen Auskünften beruhen, sind als solche kenntlich gemacht. Bei den von mir durchgeführten und in der Dissertation erwähnten Untersuchungen habe ich die Grundsätze guter wissenschaftlicher Praxis, wie sie in der „Satzung der Justus-Liebig-Universität Gießen zur Sicherung guter wissenschaftlicher Praxis“ niedergelegt sind, eingehalten sowie ethische, datenschutzrechtliche und tierschutzrechtliche Grundsätze befolgt. Ich versichere, dass Dritte von mir weder unmittelbar noch mittelbar geldwerte Leistungen für Arbeiten erhalten haben, die im Zusammenhang mit dem Inhalt der vorgelegten Dissertation stehen, oder habe diese nachstehend spezifiziert. Die vorgelegte Arbeit wurde weder im Inland noch im Ausland in gleicher oder ähnlicher Form einer anderen Prüfungsbehörde zum Zweck einer Promotion oder eines anderen Prüfungsverfahrens vorgelegt. Alles aus anderen Quellen und von anderen Personen übernommene Material, das in der Arbeit verwendet wurde oder auf das direkt Bezug genommen wird, wurde als solches kenntlich gemacht. Insbesondere wurden alle Personen genannt, die direkt und indirekt an der Entstehung der vorliegenden Arbeit beteiligt waren. Mit der Überprüfung meiner Arbeit durch eine Plagiatserkennungssoftware bzw. ein internetbasiertes Softwareprogramm erkläre ich mich einverstanden.

Stefanie Kern
Giessen 2021

13. Literature

1. Giannoudis, P.V., E. Jones, and T.A. Einhorn, *Fracture healing and bone repair.* Injury, 2011. **42**(6): p. 549-50.
2. Zimmermann, G. and A. Moghaddam, *Trauma: Non-Union: New Trends.* 2010: p. 15-19.
3. Bartl, R., *Treatment of osteoporosis according to the "European Guidance 2008". Fracture-oriented--economical--cost-effective.* Internist (Berl), 2008. **49**(9): p. 1126-36.
4. Hak, D.J., et al., *Delayed union and nonunions: epidemiology, clinical issues, and financial aspects.* Injury, 2014. **45 Suppl 2**: p. S3-7.
5. Schlundt, C., et al., *Clinical and Research Approaches to Treat Non-union Fracture.* Curr Osteoporos Rep, 2018. **16**(2): p. 155-168.
6. Cunningham, B.P., et al., *Fracture healing: A review of clinical, imaging and laboratory diagnostic options.* Injury, 2017. **48 Suppl 1**: p. S69-S75.
7. Hausmann, M., et al., *Use of Bone Morphogenetic Proteins (BMPs) for the Treatment of Pseudarthroses - Efficiency and Therapy Failure.* Z Orthop Unfall, 2014. **152**(2): p. 144-51.
8. Sarahrudi, K., et al., *Elevated transforming growth factor-beta 1 (TGF-beta1) levels in human fracture healing.* Injury, 2011. **42**(8): p. 833-7.
9. Singh, A., et al., *Evaluation of serum alkaline phosphatase as a biomarker of healing process progression of simple diaphyseal fractures in adult patients.* International Research Journal of Biological Sciences, 2013. **2**(2): p. 40-43.
10. Kurdy, N.M., *Serology of abnormal fracture healing: the role of PIIINP, PICP, and BsALP.* J Orthop Trauma, 2000. **14**(1): p. 48-53.
11. Kottstorfer, J., et al., *The influence of non-osteogenic factors on the expression of M-CSF and VEGF during fracture healing.* Injury, 2013. **44**(7): p. 930-4.
12. Yamamoto, K., et al., *Direct conversion of human fibroblasts into functional osteoblasts by defined factors.* PNAS, 2015. **112**(19): p. 6152-6157.
13. Lee, D.Y., et al., *Disturbed osteoblastic differentiation of fibrous hamartoma cell from congenital pseudarthrosis of the tibia associated with neurofibromatosis type I.* Clin Orthop Surg, 2011. **3**(3): p. 230-7.
14. Tahaei, S.E., et al., *The reduced osteogenic potential of Nf1-deficient osteoprogenitors is EGFR-independent.* Bone, 2018. **106**: p. 103-111.
15. Han, X., A. Aslanian, and J.R. Yates, 3rd, *Mass spectrometry for proteomics.* Curr Opin Chem Biol, 2008. **12**(5): p. 483-90.
16. Megas, P., *Classification of non-union.* Injury, 2005. **36 Suppl 4**: p. S30-7.
17. Rupp, M., et al., *Do Systemic Factors Influence the Fate of Nonunions to Become Atrophic? A Retrospective Analysis of 162 Cases.* BioMed Research International, 2019. **2019**: p. 1-12.
18. Nauta, S.P., et al., *Clinical use of mass spectrometry (imaging) for hard tissue analysis in abnormal fracture healing.* Clin Chem Lab Med, 2020.
19. Datta, H.K., et al., *The cell biology of bone metabolism.* J Clin Pathol, 2008. **61**(5): p. 577-87.
20. Freemont, A.J., *Basic bone cell biology.* Int. J. Exp. Path. , 1993. **74**: p. 411-416.
21. Clarke, B., *Normal bone anatomy and physiology.* Clin J Am Soc Nephrol, 2008. **3** (3): p. S131-9.
22. OpenStaxCollege, *Anatomy & Physiology*. 2013, Texas: Rise University, OpenStax College.
23. Bayliss, L., D.J. Mahoney, and P. Monk, *Normal bone physiology, remodelling and its hormonal regulation.* Surgery (Oxford), 2012. **30**(2): p. 47-53.
24. Ascenzi, M.-G. and A.K. Roe, *The osteon: the micromechanical unit of compact bone.* Frontiers in Bioscience 2012. **17**: p. 1551-1581.

25. Ralston, S.H., *Bone structure and metabolism.* Medicine, 2013. **41**(10): p. 581-585.
26. Allen, M.R., J.M. Hock, and D.B. Burr, *Periosteum: biology, regulation, and response to osteoporosis therapies.* Bone, 2004. **35**(5): p. 1003-12.
27. Roberts, S.J., et al., *Uncovering the periosteum for skeletal regeneration: the stem cell that lies beneath.* Bone, 2015. **70**: p. 10-8.
28. Wang, Q., et al., *Artificial periosteum in bone defect repair—A review.* Chinese Chemical Letters, 2017. **28**(9): p. 1801-1807.
29. Baldwin, J.G., et al., *Periosteum tissue engineering in an orthotopic in vivo platform.* Biomaterials, 2017. **121**: p. 193-204.
30. License., T.w.i.l.u.t.C.C.A.U., *https://www.servier.de/medical-art/knochenstruktur*, in *To view a copy of this license, visit http://creativecommons.org/licenses/by/3.0/ or send a letter to Creative Commons, PO Box 1866, Mountain View, CA 94042, USA*.
31. Schwarcz, H.P., D. Abueidda, and I. Jasiuk, *The Ultrastructure of Bone and Its Relevance to Mechanical Properties.* Frontiers in Physics, 2017. **5**.
32. Le, B.Q., et al., *The Components of Bone and What They Can Teach Us about Regeneration.* Materials (Basel), 2017. **11**(1).
33. Ryser, M.D. and K.A. Murgas, *Bone remodeling as a spatial evolutionary game.* J Theor Biol, 2017. **418**: p. 16-26.
34. Raggatt, L.J. and N.C. Partridge, *Cellular and molecular mechanisms of bone remodeling.* J Biol Chem, 2010. **285**(33): p. 25103-8.
35. Sims, N.A. and T.J. Martin, *Coupling the activities of bone formation and resorption: a multitude of signals within the basic multicellular unit.* Bonekey Rep, 2014. **3**: p. 481.
36. Henriksen, K., et al., *Osteoclast activity and subtypes as a function of physiology and pathology--implications for future treatments of osteoporosis.* Endocr Rev, 2011. **32**(1): p. 31-63.
37. El Khassawna, T., et al., *Osteocyte Regulation of Receptor Activator of NF-kappaB Ligand/Osteoprotegerin in a Sheep Model of Osteoporosis.* Am J Pathol, 2017.
38. Charles, J.F. and A.O. Aliprantis, *Osteoclasts: more than 'bone eaters'.* Trends Mol Med, 2014. **20**(8): p. 449-59.
39. Greenblatt, M.B., J.N. Tsai, and M.N. Wein, *Bone Turnover Markers in the Diagnosis and Monitoring of Metabolic Bone Disease.* Clin Chem, 2016.
40. Pittenger, M.F., et al., *Multilineage Potential of Adult Human Mesenchymal Stem Cells.* Science, 1999. **284**: p. 143-147.
41. Ishii, M., et al., *Molecular markers distinguish bone marrow mesenchymal stem cells from fibroblasts.* Biochem Biophys Res Commun, 2005. **332**(1): p. 297-303.
42. G. Chamberlain, J.F., B. Ashton, J. Middleton, *Mesenchymal Stem Cells: Their Phenotype, Differentiation Capacity, Immunological Features, and Potential for Homing.* Stem Cells, 2007. **25**: p. 2739–2749.
43. Hofmann, A., et al., *Cell viability, osteoblast differentiation, and gene expression are altered in human osteoblasts from hypertrophic fracture non-unions.* Bone, 2008. **42**(5): p. 894-906.
44. Ge, C., et al., *Critical role of the extracellular signal-regulated kinase-MAPK pathway in osteoblast differentiation and skeletal development.* J Cell Biol, 2007. **176**(5): p. 709-18.
45. Matsushita, T. and S. Murakami, *The ERK MAPK Pathway in Bone and Cartilage Formation*, in *Protein Kinases*, D.G.D.S. Xavier, Editor. 2012, InTech. p. 381-398.
46. Eriksen, E.F., *Cellular mechanisms of bone remodeling.* Rev Endocr Metab Disord, 2010. **11**(4): p. 219-27.
47. Marie, P.J. and E. Hay, *Cadherins and Wnt signalling: a functional link controlling bone formation.* Bonekey Rep, 2013. **2**: p. 330.

48. Florencio-Silva, R., et al., *Biology of Bone Tissue: Structure, Function, and Factors That Influence Bone Cells.* Biomed Res Int, 2015. **2015**: p. 421746.
49. Rochefort, G.Y., C.L. Pallu S Fau - Benhamou, and C.L. Benhamou, *Osteocyte: the unrecognized side of bone tissue.* (1433-2965 (Electronic)).
50. Noble, B.S., *The osteocyte lineage.* Arch Biochem Biophys, 2008. **473**(2): p. 106-11.
51. Bonewald, L.F., *The amazing osteocyte.* J Bone Miner Res, 2011. **26**(2): p. 229-38.
52. van Oers, R.F., H. Wang, and R.G. Bacabac, *Osteocyte shape and mechanical loading.* Curr Osteoporos Rep, 2015. **13**(2): p. 61-6.
53. Neve, A., F.P. Corrado A Fau - Cantatore, and F.P. Cantatore, *Osteocytes: central conductors of bone biology in normal and pathological conditions.* (1748-1716 (Electronic)).
54. Morgan, E.F., A. De Giacomo, and L.C. Gerstenfeld, *Overview of skeletal repair (fracture healing and its assessment).* Methods Mol Biol, 2014. **1130**: p. 13-31.
55. Marsell, R. and T.A. Einhorn, *The biology of fracture healing.* Injury, 2011. **42**(6): p. 551-555.
56. Schlundt, C., et al., *Macrophages in bone fracture healing: Their essential role in endochondral ossification.* Bone, 2018. **106**: p. 78-89.
57. Einhorn, T.A., *The Cell and Molecular Biology of Fracture Healing.* Clinical orthopaedics and related research, 1998. **355S**: p. S7-S21.
58. Gerstenfeld, L.C., et al., *Three-dimensional Reconstruction of Fracture Callus Morphogenesis.* Journal of Histochemistry & Cytochemistry, 2006. **54**(11): p. 1215-1228.
59. Roberts, J.L., D.N. Paglia, and H. Drissi, *Transcriptional Mechanisms of Secondary Fracture Healing.* Curr Osteoporos Rep, 2018. **16**(2): p. 146-154.
60. Schmidt-Bleek, K., et al., *Initial immune reaction and angiogenesis in bone healing.* J Tissue Eng Regen Med, 2014. **8**(2): p. 120-30.
61. Schmidt-Bleek, K., et al., *Boon and Bane of Inflammation in Bone Tissue Regeneration and Its Link with Angiogenesis.* Tissue Eng Part B Rev, 2015. **21**(4): p. 354-64.
62. Loi, F., et al., *Inflammation, fracture and bone repair.* Bone, 2016. **86**: p. 119-30.
63. Schindeler, A., et al., *Bone remodeling during fracture repair: The cellular picture.* Semin Cell Dev Biol, 2008. **19**(5): p. 459-66.
64. Hankenson, K.D., K. Gagne, and M. Shaughnessy, *Extracellular signaling molecules to promote fracture healing and bone regeneration.* Adv Drug Deliv Rev, 2015. **94**: p. 3-12.
65. Hankenson, K.D., G. Zimmerman, and R. Marcucio, *Biological perspectives of delayed fracture healing.* Injury, 2014. **45 Suppl 2**: p. S8-S15.
66. Majidinia, M., A. Sadeghpour, and B. Yousefi, *The roles of signaling pathways in bone repair and regeneration.* J Cell Physiol, 2018. **233**(4): p. 2937-2948.
67. Hayrapetyan, A., J.A. Jansen, and J.J. van den Beucken, *Signaling pathways involved in osteogenesis and their application for bone regenerative medicine.* Tissue Eng Part B Rev, 2015. **21**(1): p. 75-87.
68. Yuan, J., F. Xin, and W. Jiang, *Underlying Signaling Pathways and Therapeutic Applications of Pulsed Electromagnetic Fields in Bone Repair.* Cell Physiol Biochem, 2018. **46**(4): p. 1581-1594.
69. Rybak, A.P., R.G. Bristow, and A. Kapoor, *Prostate cancer stem cells: deciphering the origins and pathways involved in prostate tumorigenesis and aggression.* Oncotarget, 2015. **6**(4): p. 1900-19.
70. Khassawna, T.E., *Cellular and Molecular Analysis of Fracture Healing in a Neurofibromatosis Type 1 Conditional Knockout Mice Model*, in *Biology*. 2013, Humboldt University Berlin.

71. Katsianou, M.A., et al., *Signaling mechanisms implicated in cranial sutures pathophysiology: Craniosynostosis.* BBA Clin, 2016. **6**: p. 165-176.
72. Panteli, M., et al., *Biological and molecular profile of fracture non-union tissue: current insights.* J Cell Mol Med, 2015. **19**(4): p. 685-713.
73. Frölke, J.P.M. and P. Patka, *Definition and classification of fracture non-unions.* Injury, 2007. **38**: p. S19-S22.
74. Iwakura, T., et al., *Human hypertrophic nonunion tissue contains mesenchymal progenitor cells with multilineage capacity in vitro.* J Orthop Res, 2009. **27**(2): p. 208-15.
75. Walsh, L.J., et al., *The impact of oral corticosteroid use on bone mineral density and vertebral fracture.* Am J Respir Crit Care Med, 2002. **166**(5): p. 691-5.
76. Henkelmann, R., et al., *Infection following fractures of the proximal tibia - a systematic review of incidence and outcome.* BMC Musculoskelet Disord, 2017. **18**(1): p. 481.
77. Shao, J., et al., *Incidence and risk factors for surgical site infection after open reduction and internal fixation of tibial plateau fracture: A systematic review and meta-analysis.* Int J Surg, 2017. **41**: p. 176-182.
78. G, D.A., D.S.P. Ss, and D.M. Cn, *Surgical site infections in orthopedic implant surgery and its risk factors: A prospective study in teaching hospital.* International Journal of Orthopaedics Sciences, 2017. **3**(3c): p. 169-172.
79. Santolini, E., R. West, and P.V. Giannoudis, *Risk factors for long bone fracture non-union: a stratification approach based on the level of the existing scientific evidence.* Injury, 2015. **46**: p. S8-S19.
80. Metsemakers, W.J., et al., *Risk factors for nonunion after intramedullary nailing of femoral shaft fractures: Remaining controversies.* Injury, 2015. **46**(8): p. 1601-7.
81. Napoli, N., et al., *Mechanisms of diabetes mellitus-induced bone fragility.* Nat Rev Endocrinol, 2016. **advance online publication**.
82. Zura, R., et al., *Biological Risk Factors for Nonunion of Bone Fracture.* JBJS Rev, 2016. **4**(1).
83. Everding, J., S. Rosslenbroich, and M.J. Raschke, *Pseudarthroses of the long bones.* Chirurg, 2017.
84. Mills, L.A., S.A. Aitken, and A. Simpson, *The risk of non-union per fracture: current myths and revised figures from a population of over 4 million adults.* Acta Orthop, 2017. **88**(4): p. 434-439.
85. Dishowitz, M.I., et al., *Systemic inhibition of canonical Notch signaling results in sustained callus inflammation and alters multiple phases of fracture healing.* PLoS One, 2013. **8**(7): p. e68726.
86. Wagner, E.R., et al., *Increasing Body Mass Index Is Associated with Worse Outcomes After Shoulder Arthroplasty.* J Bone Joint Surg Am, 2017. **99**(11): p. 929-937.
87. Willy, C., H. Rieger, and M. Stichling, *Prevention of postoperative infections : Risk factors and the current WHO guidelines in musculoskeletal surgery.* Unfallchirurg, 2017. **120**(6): p. 472-485.
88. Marin, C., et al., *The Impact of Type 2 Diabetes on Bone Fracture Healing.* Front Endocrinol (Lausanne), 2018. **9**: p. 6.
89. Jarvis, N.E., et al., *Surgery for the fractured clavicle: factors predicting nonunion.* J Shoulder Elbow Surg, 2018. **27**(5): p. e155-e159.
90. Giannoudis, P.V., T.A. Einhorn, and D. Marsh, *Fracture healing: The diamond concept.* Injury, 2007. **38**: p. S3-S6.
91. Schneider, P.S., E. Sandman, and P.A. Martineau, *Osteoimmunology: Effects of Standard Orthopaedic Interventions on Inflammatory Response and Early Fracture Healing.* J Am Acad Orthop Surg, 2018. **26**(10): p. 343-352.

92. Garcia-Gareta, E., M.J. Coathup, and G.W. Blunn, *Osteoinduction of bone grafting materials for bone repair and regeneration.* Bone, 2015. **81**: p. 112-121.
93. Vaibhav, B., et al., *Bone morphogenic protein and its application in trauma cases: a current concept update.* Injury, 2007. **38**(11): p. 1227-35.
94. Gautschi, O.P., S.P. Frey, and R. Zellweger, *Bone morphogenetic proteins in clinical applications.* ANZ J Surg, 2007. **77**(8): p. 626-31.
95. Giannoudis, P.V., et al., *The synergistic effect of autograft and BMP-7 in the treatment of atrophic nonunions.* Clin Orthop Relat Res, 2009. **467**(12): p. 3239-48.
96. Papanna, M.C., et al., *The use of bone morphogenic protein-7 (OP-1) in the management of resistant non-unions in the upper and lower limb.* Injury, 2012. **43**(7): p. 1135-40.
97. Moghaddam, A., et al., *Non-unions treated with bone morphogenic protein 7: introducing the quantitative measurement of human serum cytokine levels as promising tool in evaluation of adjunct non-union therapy.* J Inflamm (Lond), 2016. **13**: p. 3.
98. Cho, T.J., et al., *Biologic characteristics of fibrous hamartoma from congenital pseudarthrosis of the tibia associated with neurofibromatosis type 1.* J Bone Joint Surg Am, 2008. **90**(12): p. 2735-44.
99. Pountos, I., et al., *Fracture non-union: Can biomarkers predict outcome?* Injury, 2013. **44**(12): p. 1725-32.
100. Noor, Z., et al., *Mass spectrometry-based protein identification in proteomics-a review.* Brief Bioinform, 2020.
101. Tsai, T.H., et al., *LC-MS/MS-based serum proteomics for identification of candidate biomarkers for hepatocellular carcinoma.* Proteomics, 2015. **15**(13): p. 2369-81.
102. Park, M.A. and J.H. Callahan, *An Inductive Detector for Time-of-flight Mass Spectrometry.* Rapid Communicatios in Mass Spectrometry, 1994. **8**: p. 317-322.
103. Karpievitch, Y.V., et al., *Liquid Chromatography Mass Spectrometry-Based Proteomics: Biological and Technological Aspects.* Ann Appl Stat, 2010. **4**(4): p. 1797-1823.
104. Michalski, A., et al., *Mass Spectrometry-based Proteomics Using Q Exactive, a High-performance Benchtop Quadrupole Orbitrap Mass Spectrometer.* Molecular & Cellular Proteomics 2011. **10.9**.
105. Pol, J., et al., *Molecular mass spectrometry imaging in biomedical and life science research.* Histochem Cell Biol, 2010. **134**(5): p. 423-43.
106. Chen, C., et al., *Bioinformatics Methods for Mass Spectrometry-Based Proteomics Data Analysis.* Int J Mol Sci, 2020. **21**(8).
107. Wang, M., et al., *Label-free mass spectrometry-based protein quantification technologies in proteomic analysis.* Brief Funct Genomic Proteomic, 2008. **7**(5): p. 329-39.
108. McHugh, M.L., *Multiple comparison analysis testing in ANOVA.* Biochemia Medica, 2011. **21**(3): p. 203-209.
109. Zeng, Y., et al., *Quantitative proteomics and integrative network analysis identified novel genes and pathways related to osteoporosis.* J Proteomics, 2016. **142**: p. 45-52.
110. Harris, M.A., et al., *The Gene Ontology (GO) database and informatics resource.* Nucleic Acids Res, 2004. **32**(Database issue): p. D258-61.
111. Kanehisa, M., et al., *KEGG: new perspectives on genomes, pathways, diseases and drugs.* Nucleic Acids Res, 2017. **45**(D1): p. D353-D361.
112. Wenisch, S., et al., *Human reaming debris: a source of multipotent stem cells.* Bone, 2005. **36**(1): p. 74-83.
113. Trinkaus, K., et al., *Reaming debris: a source of vital cells! First results of human specimens.* Unfallchirurg, 2005. **108**(8): p. 650-6.

114. Lindl, T. and G. Gstraunthaler, *Zell- und Gewebekultur – Von den Grundlagen zur Laborbank*. Vol. 6. Auflage. 2008, Heidelberg: Spektrum Akademischer Verlag.
115. Schmitz, S., *Der Experimentator: Zellkultur*. Vol. 3. Auflage. 2011, Heidelberg: Spektrum Akademischer Verlag.
116. Crowley, L.C., et al., *Measuring Cell Death by Trypan Blue Uptake and Light Microscopy.* Cold Spring Harb Protoc, 2016. **2016**(7): p. pdb prot087155.
117. Niyaz, M., et al., *Isolation, culturing and characterization of rat adipose tissue derived mesenchymal stem cells: a simple technique.* Turk J Biol, 2012. **36** p. 658-664.
118. Fuentes, M., *Hemocytometer*. 2018, Hemocytometer blog.
119. Zhang, Y., et al., *Protein analysis by shotgun/bottom-up proteomics.* Chem Rev, 2013. **113**(4): p. 2343-94.
120. Schmidt, A., I. Forne, and A. Imho, *Bioinformatic analysis of proteomics data.* BMC Systems Biology, 2014. **8**(2): p. S3.
121. Bradford, M., *A rapid and sensitive method for the quantitation of microgram quantities of protein utilizing the principles of protein-dye binding.* Anal. Biochem., 1976. **72**: p. 248-254.
122. Zor, T. and Z. Selinger, *Linearization of the Bradford Protein Assay Increases Its Sensitivity: Theoretical and Experimental Studies.* Analytical Biochemistry, 1996. **236**: p. 302-308
123. Turiak, L., et al., *Digestion protocol for small protein amounts for nano-HPLC-MS(MS) analysis.* J Proteomics, 2011. **74**(7): p. 942-7.
124. Vandermarliere, E., M. Mueller, and L. Martens, *Getting intimate with trypsin, the leading protease in proteomics.* Mass Spectrom Rev, 2013. **32**(6): p. 453-65.
125. Fan, C., et al., *Dual matrix-based immobilized trypsin for complementary proteolytic digestion and fast proteomics analysis with higher protein sequence coverage.* Anal Chem, 2014. **86**(3): p. 1452-8.
126. Cleland, W.W., *Dithiothreitol, a New Protective Reagent for SH Groups*.* Biochemistry, 1964. **3**(4): p. 480-482.
127. Herbert, B., et al., *Reduction and alkylation of proteins in preparation of two-dimensional map analysis: Why, when, and how? .* Electrophoresis, 2001. **22**: p. 2046-2057.
128. Kim, Y.G., A.M. Lone, and A. Saghatelian, *Analysis of the proteolysis of bioactive peptides using a peptidomics approach.* Nat Protoc, 2013. **8**(9): p. 1730-42.
129. Erve, J.C., W. Demaio, and R.E. Talaat, *Rapid metabolite identification with sub parts-per-million mass accuracy from biological matrices by direct infusion nanoelectrospray ionization after clean-up on a ZipTip and LTQ/Orbitrap mass spectrometry.* Rapid Commun Mass Spectrom, 2008. **22**(19): p. 3015-26.
130. Lottspeich, F., J.W. Engels, and Z.L. Solodkoff, *Bioanalytik*. 2012: Spektrum Akademischer Verlag.
131. Astefanei, A., I. Dapic, and M. Camenzuli, *Different Stationary Phase Selectivities and Morphologies for Intact Protein Separations.* Chromatographia, 2017. **80**(5): p. 665-687.
132. Arens, N., S. Doll, and H.P. Mock, *The reproducibility of liquid chromatography separation technology and its potential impact on large scale plant metabolomics experiments.* J Chromatogr B Analyt Technol Biomed Life Sci, 2015. **991**: p. 41-5.
133. Cox, J., et al., *A practical guide to the MaxQuant computational platform for SILAC-based quantitative proteomics.* Nat Protoc, 2009. **4**(5): p. 698-705.
134. Cox, J., et al., *Andromeda: a peptide search engine integrated into the MaxQuant environment.* J Proteome Res, 2011. **10**(4): p. 1794-805.
135. The UniProt, C., *UniProt: the universal protein knowledgebase.* Nucleic Acids Res, 2017. **45**(D1): p. D158-D169.

136. Huang da, W., B.T. Sherman, and R.A. Lempicki, *Systematic and integrative analysis of large gene lists using DAVID bioinformatics resources.* Nat Protoc, 2009. **4**(1): p. 44-57.
137. Huang da, W., B.T. Sherman, and R.A. Lempicki, *Bioinformatics enrichment tools: paths toward the comprehensive functional analysis of large gene lists.* Nucleic Acids Res, 2009. **37**(1): p. 1-13.
138. Shannon, P., et al., *Cytoscape: A Software Environment for Integrated Models of Biomolecular Interaction Networks.* Genome Res, 2003. **13**(1): p. 2498-2504.
139. Nastou, K.C., et al., *The human plasma membrane peripherome: visualization and analysis of interactions.* Biomed Res Int, 2014. **2014**: p. 397145.
140. Schroeder, A., et al., *The RIN: an RNA integrity number for assigning integrity values to RNA measurements.* BMC Mol Biol, 2006. **7**: p. 3.
141. Chomczynski, P. and N. Sacchi, *Single-step method of RNA isolation by acid guanidinium thiocyanate-phenol-chloroform extraction.* Anal Biochem, 1987 **162**(1): p. 156-9.
142. Harrington, C.A., M. Winther, and M.M. Garred, *Use of bioanalyzer electropherograms for quality control and target evaluation in microarray expression profiling studies of ocular tissues.* J Ocul Biol Dis Infor, 2009. **2**(4): p. 243-249.
143. Rupp, M., et al., *Diaphyseal long bone nonunions - types, aetiology, economics, and treatment recommendations.* Int Orthop, 2017.
144. Kawamoto, T. and M. Shimizu, *A method for preparing 2- to 50-µm-thick fresh-frozen sections of large samples and undecalcified hard tissues.* Histochem Cell Biol 2000. **113**: p. 331–339.
145. Chan, J.K., *The wonderful colors of the hematoxylin-eosin stain in diagnostic surgical pathology.* Int J Surg Pathol, 2014. **22**(1): p. 12-32.
146. Rentsch, C., et al., *Comprehensive histological evaluation of bone implants.* Biomatter, 2014. **4**.
147. Torzewski, M., *Die Movat-Pentachromfärbung – eine farbenprächtige Darstellung verschiedener zellulärer und extrazellulärer Gewebskomponenten.* Mikroskopie, 2015. **2**(10): p. 204-208.
148. Ramos-Vara, J.A., *Technical Aspects of Immunohistochemistry.* Vet Pathol 2005. **42**: p. 405–426.
149. Ramos-Vara, J.A. and M.A. Miller, *When tissue antigens and antibodies get along: revisiting the technical aspects of immunohistochemistry--the red, brown, and blue technique.* Vet Pathol, 2014. **51**(1): p. 42-87.
150. Taylor, C.R. and L. Rudbeck, *Immunohistochemical Staining Methods*. 6th Edition ed. Educational guide. 2013: Dako Denmark A/S.
151. Park, S.G., P. Schimmel, and S. Kim, *Aminoacyl tRNA synthetases and their connections to disease.* Proc Natl Acad Sci U S A, 2008. **105**(32): p. 11043-9.
152. Park, M.C., et al., *Secreted human glycyl-tRNA synthetase implicated in defense against ERK-activated tumorigenesis.* PNAS, 2012. **109**(11): p. E640–E647.
153. Yao, P. and P.L. Fox, *Aminoacyl-tRNA synthetases in medicine and disease.* EMBO Mol Med, 2013. **5**(3): p. 332-43.
154. Chin, D. and A.R. Means, *Calmodulin: a prototypical calcium sensor.* Cell Biology, 2000. **10**: p. 322-328.
155. Zayzafoon, M., *Calcium/calmodulin signaling controls osteoblast growth and differentiation.* J Cell Biochem, 2006. **97**(1): p. 56-70.
156. Naz, H., et al., *Calcium/calmodulin-dependent protein kinase IV: A multifunctional enzyme and potential therapeutic target.* Prog Biophys Mol Biol, 2016. **121**(1): p. 54-65.
157. Flegal, K.M., B.K. Kit, and B.I. Graubard, *Body mass index categories in observational studies of weight and risk of death.* Am J Epidemiol, 2014. **180**(3): p. 288-96.

158. Martin-Calvo, N., L. Moreno-Galarraga, and M.A. Martinez-Gonzalez, *Association between Body Mass Index, Waist-to-Height Ratio and Adiposity in Children: A Systematic Review and Meta-Analysis.* Nutrients, 2016. **8**(8).
159. Calori, G.M., et al., *Non-unions.* Clinical Cases in Mineral and Bone Metabolism 2017. **14**(2): p. 186-188.
160. Calori, G.M., et al., *Classification of non-union: Need for a new scoring system?* Injury, 2008. **39**: p. S59-S63.
161. Kellam, J.F., et al., *Fracture and Dislocation Classification Compendium—2018.* Journal of Orthopaedic Trauma, 2018. **32**: p. S1-S10.
162. Haynes, S.R. and P.G.P. Lawler, *An assessment of the consistency of ASA physical status classification allocation.* Anaesthesia, 1995. **50**: p. 195-199.
163. Higashizawa, T. and Y. Koga, *Modified ASA Physical Status (7 grades) May Be More Practical In Recent Use For Preoperative Risk Assessment.* The Internet Journal of Anesthesiology, 2006. **15**(1): p. 1-5.
164. Kuhnisch, J., et al., *Multiscale, converging defects of macro-porosity, microstructure and matrix mineralization impact long bone fragility in NF1.* PLoS One, 2014. **9**(1): p. e86115.
165. Daghma, D.E.S., et al., *Computational segmentation of collagen fibers in bone matrix indicates bone quality in ovariectomized rat spine.* J Bone Miner Metab, 2017.
166. Oldroyd, A. and S. Dubey, *The association between bone mineral density and higher body mass index in men.* Int J Clin Pract, 2015. **69**(1): p. 145-7.
167. Nauth, A., et al., *Principles of Nonunion Management: State of the Art.* J Orthop Trauma 2018. **32**(3): p. 52-57.
168. Fayaz, H.C., et al., *The role of stem cells in fracture healing and nonunion.* Int Orthop, 2011. **35**(11): p. 1587-97.
169. Denu, R.A., et al., *Fibroblasts and Mesenchymal Stromal/Stem Cells Are Phenotypically Indistinguishable.* Acta Haematol, 2016. **136**(2): p. 85-97.
170. Haniffa, M.A., et al., *Mesenchymal stem cells: the fibroblasts' new clothes?* Haematologica, 2009. **94**(2): p. 258-63.
171. Gomez-Barrena, E., et al., *Bone fracture healing: cell therapy in delayed unions and nonunions.* Bone, 2015. **70**: p. 93-101.
172. Brohem, C.A., et al., *Comparison between fibroblasts and mesenchymal stem cells derived from dermal and adipose tissue.* Int J Cosmet Sci, 2013. **35**(5): p. 448-57.
173. Cappellesso-Fleury, S., et al., *Human fibroblasts share immunosuppressive properties with bone marrow mesenchymal stem cells.* J Clin Immunol, 2010. **30**(4): p. 607-19.
174. Kostenuik, P. and F.M. Mirza, *Fracture healing physiology and the quest for therapies for delayed healing and nonunion.* J Orthop Res, 2017. **35**(2): p. 213-223.
175. Warde-Farley, D., et al., *The GeneMANIA prediction server: biological network integration for gene prioritization and predicting gene function.* Nucleic Acids Res, 2010. **38**(Web Server issue): p. W214-20.
176. Lee, S.K., et al., *Profiling and semiquantitative analysis of the cell surface proteome in human mesenchymal stem cells.* Anal Bioanal Chem, 2013. **405**: p. 5501-5517.
177. Lee, J.-H. and J.-Y. Cho, *Proteomics approaches for the studies of bone metabolism.* BMB Reports, 2014. **47**(3): p. 141-148.
178. Maurer, M.H., *Proteomic definitions of mesenchymal stem cells.* Stem Cells Int, 2011. **2011**: p. 704256.
179. Celebi, B. and Y.M. Elcin, *Proteome Analysis of Rat Bone Marrow Mesenchymal Stem Cell Subcultures.* Journal of Proteome Research, 2009. **8**: p. 2164-2172.

180. Steiner, R.D., J. Adsit, and D. Basel. *COL1A1/2-Related Osteogenesis Imperfecta*. GeneReviews® 2005; Available from: https://www.ncbi.nlm.nih.gov/books/NBK1295/.
181. Ben Amor, I.M., F.H. Glorieux, and F. Rauch, *Genotype-phenotype correlations in autosomal dominant osteogenesis imperfecta.* J Osteoporos, 2011. **2011**: p. 540178.
182. Sato, A., et al., *Scoliosis in osteogenesis imperfecta caused by COL1A1/COL1A2 mutations - genotype-phenotype correlations and effect of bisphosphonate treatment.* Bone, 2016. **86**: p. 53-7.
183. Rocha, B., et al., *MALDI mass spectrometry imaging in rheumatic diseases.* Biochim Biophys Acta, 2017. **1865**(7): p. 784-794.
184. Alford, A.I., K.M. Kozloff, and K.D. Hankenson, *Extracellular matrix networks in bone remodeling.* Int J Biochem Cell Biol, 2015. **65**: p. 20-31.
185. Gelse, K., et al., *Molecular differentiation between osteophytic and articular cartilage--clues for a transient and permanent chondrocyte phenotype.* Osteoarthritis Cartilage, 2012. **20**(2): p. 162-71.
186. Boczonadi, V., M.J. Jennings, and R. Horvath, *The role of tRNA synthetases in neurological and neuromuscular disorders.* FEBS Lett, 2017.
187. Boczonadi, V., et al., *Mutations in glycyl-tRNA synthetase impair mitochondrial metabolism in neurons.* Hum Mol Genet, 2018. **27**(12): p. 2187-2204.
188. Sivakumar, K., et al., *Phenotypic spectrum of disorders associated with glycyl-tRNA synthetase mutations.* Brain, 2005. **128**(Pt 10): p. 2304-14.
189. Antonellis, A., et al., *Functional analyses of glycyl-tRNA synthetase mutations suggest a key role for tRNA-charging enzymes in peripheral axons.* J Neurosci, 2006. **26**(41): p. 10397-406.
190. Liao, Y.C., et al., *Two Novel De Novo GARS Mutations Cause Early-Onset Axonal Charcot-Marie-Tooth Disease.* PLoS One, 2015. **10**(8): p. e0133423.
191. Wasserman, H.M., et al., *Low bone mineral density and fractures are highly prevalent in pediatric patients with spinal muscular atrophy regardless of disease severity.* Neuromuscul Disord, 2017. **27**(4): p. 331-337.
192. Pouwels, S., et al., *Risk of fracture in patients with Charcot-Marie-Tooth disease.* Muscle Nerve, 2014. **50**(6): p. 919-24.
193. Veilleux, L.N. and F. Rauch, *Muscle-Bone Interactions in Pediatric Bone Diseases.* Curr Osteoporos Rep, 2017. **15**(5): p. 425-432.
194. Keramaris, N.C., et al., *Fracture vascularity and bone healing: A systematic review of the role of VEGF.* Injury, 2008. **39**: p. S45-S57.
195. Pacicca, D.M., et al., *Expression of angiogenic factors during distraction osteogenesis.* Bone, 2003. **33** p. 889-898.
196. Stegen, S., N. van Gastel, and G. Carmeliet, *Bringing new life to damaged bone: the importance of angiogenesis in bone repair and regeneration.* Bone, 2015. **70**: p. 19-27.
197. Lienau, J., et al., *Differential regulation of blood vessel formation between standard and delayed bone healing.* J Orthop Res, 2009. **27**(9): p. 1133-40.
198. Minkwitz, S., et al., *Longitudinal analysis of osteogenic and angiogenic signaling factors in healing models mimicking atrophic and hypertrophic non-unions in rats.* PLoS One, 2015. **10**(4): p. e0124217.
199. Williams, J.P., K. Micoli, and J.M. McDonald, *Calmodulin-an often-ignored signal in osteoclasts.* Ann N Y Acad Sci, 2010. **1192**: p. 358-64.
200. Masuyama, R., et al., *Calcium/calmodulin-signaling supports TRPV4 activation in osteoclasts and regulates bone mass.* J Bone Miner Res, 2012. **27**(8): p. 1708-21.
201. Zayzafoon, M., K. Fulzele, and J.M. McDonald, *Calmodulin and calmodulin-dependent kinase IIalpha regulate osteoblast differentiation by controlling c-fos expression.* J Biol Chem, 2005. **280**(8): p. 7049-59.

202. Choi, Y.H., et al., *Calmodulin-dependent kinase II regulates osteoblast differentiation through regulation of Osterix.* Biochem Biophys Res Commun, 2013. **432**(2): p. 248-55.
203. Baron, R. and M. Kneissel, *WNT signaling in bone homeostasis and disease: from human mutations to treatments.* Nat Med, 2013. **19**(2): p. 179-92.
204. Jin, H., et al., *Anti-DKK1 antibody promotes bone fracture healing through activation of beta-catenin signaling.* Bone, 2015. **71**: p. 63-75.
205. Li, Z. and D.B. Sacks, *Elucidation of the interaction of calmodulin with the IQ motifs of IQGAP1.* J Biol Chem, 2003. **278**(6): p. 4347-52.
206. Briggs, M.W. and D.B. Sacks, *IQGAP proteins are integral components of cytoskeletal regulation.* EMBO Rep, 2003. **4**(6): p. 571-4.
207. Roy, M., Z. Li, and D.B. Sacks, *IQGAP1 is a scaffold for mitogen-activated protein kinase signaling.* Mol Cell Biol, 2005. **25**(18): p. 7940-52.
208. White, C.D., M.D. Brown, and D.B. Sacks, *IQGAPs in cancer: a family of scaffold proteins underlying tumorigenesis.* FEBS Lett, 2009. **583**(12): p. 1817-24.
209. Bernards, A., *Neurofibromatosis type 1 and Ras-mediated signaling: filling in the GAPs.* Biochimica et Biophysica Acta 1995. **1242**: p. 43-59.
210. Schindeler, A., et al., *Models of tibial fracture healing in normal and Nf1-deficient mice.* J Orthop Res, 2008. **26**(8): p. 1053-60.
211. Shapira, S., et al., *The tumor suppressor neurofibromin confers sensitivity to apoptosis by Ras-dependent and Ras-independent pathways.* Cell Death Differ, 2007. **14**(5): p. 895-906.
212. Schindeler, A. and D.G. Little, *Ras-MAPK signaling in osteogenic differentiation: friend or foe?* J Bone Miner Res, 2006. **21**(9): p. 1331-8.
213. Chen, Y., et al., *Beta-Catenin Signaling Plays a Disparate Role in Different Phases of Fracture Repair: Implications for Therapy toImproveBoneHealing.* PLOS Medicine, 2007. **4**(7): p. 1216-1229.
214. Ghadakzadeh, S., et al., *beta-Catenin modulation in neurofibromatosis type 1 bone repair: therapeutic implications.* FASEB J, 2016. **30**(9): p. 3227-37.
215. Jang, D.J., B. Ban, and J.A. Lee, *Characterization of novel calmodulin binding domains within IQ motifs of IQGAP1.* Mol Cells, 2011. **32**(6): p. 511-8.
216. Froelke, J.P.M. and P. Patka, *Definition and classification of fracture non-unions.* Injury, Int. J. Care Injured 2007. **38S**: p. 19-22.
217. Takahara, S., et al., *Human pseudoarthrosis tissue contains cells with osteogenic potential.* Injury, 2016.
218. Horton, J.E., et al., *Bone resorbing activity in supernatant fluid from cultured human peripheral blood leukocytes. .* Science 1972. **177**: p. 793-795.
219. Ralston, S.H. and G. Schett, *Osteoimmunology.* Calcif Tissue Int, 2018. **102**(5): p. 501-502.
220. Rauner, M., et al., *Osteoimmunology-IMMUNOBONE : Regulation of bone by inflammation.* Z Rheumatol, 2018. **77**(Suppl 1): p. 12-15.
221. Takayanagi, H., *SnapShot: Osteoimmunology.* Cell Metab, 2015. **21**(3): p. 502 e1.
222. Walsh, M.C., et al., *Updating osteoimmunology: regulation of bone cells by innate and adaptive immunity. .* Nature Reviews Rheumatology, 2018. **14**: p. 146-156.
223. Ferencz, V., et al., *Increased bone fracture prevalence in postmenopausal women suffering from pollen-allergy.* Osteoporos Int, 2006. **17**(3): p. 484-91.
224. Biosse-Duplan, M., et al., *Histamine promotes osteoclastogenesis through the differential expression of histamine receptors on osteoclasts and osteoblasts.* Am J Pathol, 2009. **174**(4): p. 1426-34.
225. Zura, R., et al., *Bone fracture nonunion rate decreases with increasing age: A prospective inception cohort study.* Bone, 2017. **95**: p. 26-32.
226. Zura, R., et al., *Epidemiology of Fracture Nonunion in 18 Human Bones.* JAMA Surg, 2016. **151**(11): p. e162775.

227. Schmitz, R., R. Kuhnert, and M. Thamm, *12-Month prevalence of allergies in Germany.* 2017.
228. Puspitasari, M., et al., *Bone Metabolism and Fracture Risk in Diabetes Mellitus.* Journal of the ASEAN Federation of Endocrine Societies, 2017. **32**(2): p. 90-99.
229. Court-Brown, C.M., et al., *The epidemiology of open fractures in adults. A 15-year review.* Injury, 2012. **43**(6): p. 891-897.
230. Court-Brown, C.M. and M.M. McQueen, *Global Forum: Fractures in the Elderly.* J Bone Joint Surg Am, 2016. **98**(9): p. e36.
231. Clark, D., et al., *Effects of Aging on Fracture Healing.* Current osteoporosis reports, 2017. **15**(6): p. 601-608.
232. Nandra, R., L. Grover, and K. Porter, *Fracture non-union epidemiology and treatment.* Trauma, 2015. **18**(1): p. 3-11.
233. Gustilo, R.B. and J.T. Anderson, *Prevention of Infection in the Treatment of One Thousand and Twenty-five Open Fractures of Long Bones.* The Journal of Bone and Joint Surgery, 1976. **58-A**(4): p. 453-458.
234. Cross, W.W. and M.F. Swiontkowski, *Treatment principles in the management of open fractures. .* Indian Journal of Orthopaedics, 2008. **42**(4): p. 377–386.
235. Steinhausen, E., et al., *Non-unions. From diagnosis to healing.* Unfallchirurg, 2013. **116**(7): p. 633-47; quiz 648-9.
236. Henderson, C.E., et al., *2010 mid-America Orthopaedic Association Physician in Training Award: healing complications are common after locked plating for distal femur fractures.* Clin Orthop Relat Res, 2011. **469**(6): p. 1757-65.
237. Ebraheim, N.A., et al., *Nonunion of distal femoral fractures: a systematic review.* Orthop Surg, 2013. **5**(1): p. 46-50.
238. Koso, R.E., et al., *Healing, nonunion, and re-operation after internal fixation of diaphyseal and distal femoral fractures: a systematic review and meta-analysis.* Int Orthop, 2018.
239. Bosch, U., et al., *Diaphysäre Oberarmpseudarthrosen - operative und konservartive Behandlung.* Chirurg, 1999. **70**: p. 1202-1208.
240. Burrus, M.T., B.C. Werner, and S.R. Yarboro, *Obesity is associated with increased postoperative complications after operative management of tibial shaft fractures.* Injury, 2016. **47**(2): p. 465-70.
241. Liska, F., et al., *Smoking and obesity influence the risk of nonunion in lateral opening wedge, closing wedge and torsional distal femoral osteotomies.* Knee Surg Sports Traumatol Arthrosc, 2017.
242. Cao, J.J., *Effects of obesity on bone metabolism.* Journal of Orthopaedic Surgery and Research, 2011. **6**(30): p. 1-7.
243. Thorud, J.C., et al., *Effect of Obesity on Bone Healing After Foot and Ankle Long Bone Fractures.* J Foot Ankle Surg, 2017. **56**(2): p. 258-262.
244. Stewart, M.S., et al., *Effect of Obesity on Outcomes of Forefoot Surgery.* Foot Ankle Int, 2016. **37**(5): p. 483-7.
245. McKee, M.D., et al., *The Effect of Smoking on Clinical Outcome and Complication Rates Following Ilizarov Reconstruction.* J Orthop Trauma, 2003. **17**: p. 663–667.
246. Giannoudis, P., et al., *Nonunion of the femoral diaphysis: the influence of reaming and non-steroidal anti-inflammatory drugs.* Bone & Joint Journal, 2000. **82**(5): p. 655-658.
247. Bhandari, M., et al., *Predictors of reoperation following operative management of fractures of the tibial shaft.* Journal of orthopaedic trauma, 2003. **17**(5): p. 353-361.
248. Jeffcoach, D.R., et al., *Nonsteroidal anti-inflammatory drugs' impact on nonunion and infection rates in long-bone fractures.* Journal of Trauma and Acute Care Surgery, 2014. **76**(3): p. 779-783.
249. Marquez-Lara, A., et al., *Nonsteroidal anti-inflammatory drugs and bone-healing: a systematic review of research quality.* Jbjs reviews, 2016. **4**(3).

250. Kwong, F.N.K. and M.B. Harris, *Recent Developments in the Biology of Fracture Repair.* Journal of the American Academy of Orthopaedic Surgeons, 2008. **16**(11): p. 619-625.
251. Pountos, I., et al., *Do nonsteroidal anti-inflammatory drugs affect bone healing? A critical analysis.* ScientificWorldJournal, 2012. **2012**: p. 606404.
252. Jeffcoach, D.R., et al., *Nonsteroidal anti-inflammatory drugs' impact on nonunion and infection rates in long-bone fractures.* J Trauma Acute Care Surg, 2014. **76**(3): p. 779-83.
253. van Esch, R.W., M.M. Kool, and S. van As, *NSAIDs can have adverse effects on bone healing.* Med Hypotheses, 2013. **81**(2): p. 343-6.
254. Huber-Lang, M., et al., *Complement therapeutic strategies in trauma, hemorrhagic shock and systemic inflammation - closing Pandora's box?* Semin Immunol, 2016. **28**(3): p. 278-84.
255. Gebhard, F. and M. Huber-Lang, *Polytrauma-pathophysiology and management principles.* Langenbecks Arch Surg, 2008. **393**(6): p. 825-31.
256. Hildebrand, F., et al., *Is there an impact of concomitant injuries and timing of fixation of major fractures on fracture healing? A focused review of clinical and experimental evidence.* Journal of orthopaedic trauma, 2016. **30**(3): p. 104-112.
257. Recknagel, S., et al., *Systemic inflammation induced by a thoracic trauma alters the cellular composition of the early fracture callus.* J Trauma Acute Care Surg, 2013. **74**(2): p. 531-7.
258. Bundkirchen, K., et al., *Severe Hemorrhagic Shock Leads to a Delayed Fracture Healing and Decreased Bone Callus Strength in a Mouse Model.* Clin Orthop Relat Res, 2017. **475**(11): p. 2783-2794.
259. Starr, A.J., et al., *The Effect of Hemorrhagic Shock in a Caprine Tibial Fracture Model.* Journal of Orthopaedic Trauma, 2002. **16**(4): p. 250–256.
260. Rupp, M., C. Heiss, and V. Alt, *Septic nonunion in the left femoral shaft of a 22-year-old asylum seeker.* Dtsch Arztebl Int, 2018. **115**(58).
261. Wimmer, M.D., et al., *Polymicrobial infections reduce the cure rate in prosthetic joint infections: outcome analysis with two-stage exchange and follow-up≥ two years.* International orthopaedics, 2016. **40**(7): p. 1367-1373.
262. Haider, M.G., *Ways to prevent infection after open fracture of the lower limb.* Clujul Medical 2013. **86**(3): p. 240-244.
263. Momaya, A.M., et al., *Risk factors for infection after operative fixation of Tibial plateau fractures.* Injury, 2016. **47**(7): p. 1501-5.
264. Gaunder, C.L., et al., *Wound complications after open reduction and internal fixation of tibial plateau fractures in the elderly: a multicentre study.* Int Orthop, 2018.
265. El Khassawna, T., et al., *Deterioration of fracture healing in the mouse model of NF1 long bone dysplasia.* Bone, 2012. **51**(4): p. 651-60.
266. O'Halloran, K., et al., *Will My Tibial Fracture Heal? Predicting Nonunion at the Time of Definitive Fixation Based on Commonly Available Variables.* Clin Orthop Relat Res, 2016. **474**(6): p. 1385-95.
267. Weinlein, J.C., S. Deaderick, and R.F. Murphy, *Morbid Obesity Increases the Risk for Systemic Complications in Patients With Femoral Shaft Fractures.* J Orthop Trauma, 2015. **29**: p. e91–e95.
268. Huttunen, R. and J. Syrjanen, *Obesity and the risk and outcome of infection.* Int J Obes (Lond), 2013. **37**(3): p. 333-40.
269. Olszewski, D., et al., *Fate of Patients With a "Surprise" Positive Culture After Nonunion Surgery.* J Orthop Trauma, 2016. **30**: p. e19-e23.
270. Stucken, C., et al., *Preoperative diagnosis of infection in patients with nonunions.* J Bone Joint Surg Am, 2013. **95**(15): p. 1409-12.

271. Wimmer, M.D., et al., *Polymicrobial infections reduce the cure rate in prosthetic joint infections: outcome analysis with two-stage exchange and follow-up >/=two years.* Int Orthop, 2016. **40**(7): p. 1367-73.
272. Marculescu, C.E. and J.R. Cantey, *Polymicrobial prosthetic joint infections: risk factors and outcome.* Clin Orthop Relat Res, 2008. **466**(6): p. 1397-404.
273. Wright, E.H. and U. Khan, *Serum complement-reactive protein (CRP) trends following local and free-tissue reconstructions for traumatic injuries or chronic wounds of the lower limb.* J Plast Reconstr Aesthet Surg, 2010. **63**(9): p. 1519-22.
274. Tillett, W.S. and T. Francis, *Serological reactions in pneumonia with a non-protein somatic fraction of pneumococcus.* J Exp Med, 1930. **52**: p. 561-571.
275. Neumaier, M. and M.A. Scherer, *C-reactive protein levels for early detection of postoperative infection after fracture surgery in 787 patients.* Acta Orthop, 2008. **79**(3): p. 428-32.
276. Gelalis, I.D., et al., *Bacterial wound contamination during simple and complex spinal procedures. A prospective clinical study.* Spine J, 2011. **11**(11): p. 1042-8.
277. Wang, S., et al., *Evaluating the Use of Serum Inflammatory Markers for Preoperative Diagnosis of Infection in Patients with Nonunions.* Biomed Res Int, 2017. **2017**: p. 9146317.
278. Sproston, N.R. and J.J. Ashworth, *Role of C-Reactive Protein at Sites of Inflammation and Infection.* Front Immunol, 2018. **9**: p. 754.
279. Bozhkova, S., et al., *Failure of the first step of two-stage revision due to polymicrobial prosthetic joint infection of the hip.* J Orthop Traumatol, 2016. **17**(4): p. 369-376.
280. Lass, R., et al., *Bacterial adherence to different components of total hip prosthesis in patients with prosthetic joint infection.* Int Orthop, 2014. **38**(8): p. 1597-602.
281. Metsemakers, W.J., et al., *Infection after fracture fixation: Current surgical and microbiological concepts.* Injury, 2018. **49**(3): p. 511-522.
282. Kolanczyk, M. and D. Stevenson, *Neurofibromin in Skeletal Development*, in *Molecular Genetics of Pediatric Orthopaedic Disorders*, C.A. Wise and J.J. Rios, Editors. 2015, Springer New York.
283. Kuorilehto, T., et al., *NF1 Gene Expression in Mouse Fracture Healing and in Experimental Rat Pseudarthrosis.* Journal of Histochemistry & Cytochemistry, 2006. **54**(3): p. 363-370.
284. El-Hoss, J., et al., *A murine model of neurofibromatosis type 1 tibial pseudarthrosis featuring proliferative fibrous tissue and osteoclast-like cells.* J Bone Miner Res, 2012. **27**(1): p. 68-78.
285. Elefteriou, F., et al., *Skeletal abnormalities in neurofibromatosis type 1: approaches to therapeutic options.* Am J Med Genet A, 2009. **149A**(10): p. 2327-38.

Publications:

Surgical treatment outcome after serial debridement of infected nonunion – A retrostpective cohort study, Rupp M, **Kern S**, Walter N, Anastasopoulou L, Schnettler R, Heiss C, Alt V, March 2021)

Computed tomography for managing periprosthetic femoral fractures. Rupp M, **Kern S**, Ismat A, Ivo M, El Khassawna T, Szalay G, Heiss C, Biehl C (published in BMC Musculoskeletal Disorders, May 2019)

Computational Segmentation of Collagen Fibers in Bone Matrix indicates Bone Quality in Ovariectomized Rat Spine. Daghma DES, Malhan D, Simon P, Stötzel S, **Kern S**, Hassan F, Lips KS, Heiss C, El Khassawna T. (published in Journal of Bone and Mineral Metabolism, 2017)

A New Clinically Relevant T-Score Standard to Interpret Bone Status in a Sheep Model. Heiss C, **Kern S**, Malhan D, Böcker W, Engelhardt M, Daghma DES, Stoetzel S, Schmitt J, Ivo M, Kauschke V, Lips KS, Tushtev K, Rezwan K, El Khassawna T. (published in Medical Science Monitor, 2017)

Osteocyte Regulation of Receptor Activator of NF-κB Ligand/Osteoprotegerin in a Sheep Model of Osteoporosis. El Khassawna T, Merboth F, Malhan D, Böcker W, Daghma DES, Stoetzel S, **Kern S**, Hassan F, Rosenbaum D, Langenstein J, Bauer N, Schlagenhauf A, Rösen-Wolff A, Schulze F, Rupp M, Hose D, Secklinger A, Ignatius A, Wilke HJ, Lips KS, Heiss C. (published in American Journal of Pathology, 2017)

Postembedding Decalcification of Mineralized Tissue Sections Preserves the Integrity of Implanted Biomaterials and Minimizes Number of Experimental Animals. El Khassawna T, Daghma DES, Stoetzel S, Ray S, **Kern S**, Malhan D, Alt V, Thormann U, Henß A, Rohnke M, Stengel A, Hassan F, Maenz S, Jandt KD, Diefenbeck M, Schumacher M, Gelinsky M, Lips KS, Heiss C. (published in BioMed research international, 2017)

Parts of this doctoral thesis are published in:

Do systemic factors influence the fate of nonunions to become atrophic? - A retrospective analysis of 162 cases. Rupp M*, **Kern S***, Malhan D, El Khassawna T, Alt V, Heiss C, Raschke MJ. (*equal contribution, published in BioMed Research International, 2019)

Polymicrobial infections and microbial patterns in infected nonunions – A descriptive analysis of 42 cases. Rupp M, **Kern S,** Weber T, Menges T, Schnettler R, Heiss C, Alt V (published in BMC Infectious Diseases, 2020)

Manuscript in preparation:

Identification and characterization of potential new biomarker for pseudarthrosis.
Kern S, Malhan D, Schulz S, Spengler B, Heiss C, Rupp M, El Khassawna T

Poster and Presentations:

Talk: „3D-Druck: Ein patientengerechtes Vorgehen“, MAGIE Makerspace Gießen (Themenabend/Impuls „Medizintechnik und 3D-Druck“), 2018

Poster: “Identification and characterization of potential new biomarker for pseudarthrosis”, Deutscher Kongress für Orthopädie und Unfallchirurgie - DKOU, 2018

Poster: “Novel protein biomarkers for pseudarthrosis revealed by mass spectrometry”, 11th Annual GGL Conference, 2018

Poster: “Etablierung und Charakterisierung von Osteoporose Tiermodellen“, 1. Science Day Gießen, 2017

Poster: “Identification of novel biomarkers crucial for bone matrix mineralization in osteoporotic bone”, 10th Annual GGL Conference, 2017

Poster: „Do serological biomarkers reflect matrix mineralization in physiological and osteoporotic bone?”, 44th European Calcified Tissue Society Congress Salzburg, 2017

Poster: “Bioactive surface coating of bioinert oxide ceramics for stimulating bone anchoring”, 9th Annual GGL Conference, 2016

Talk: „Histological evaluation of the bone structure of diet, and diet/steroid-treated, ovariectomized sheep - a osteoporosis sheep model “, Deutscher Kongress für Orthopädie und Unfallchirurgie - DKOU, 2016